UNIVERSITY OF OKLAHOMA

GRADUATE COLLEGE

SIMULTANEOUS CRACKING OF PHENOLIC COMPOUNDS AND HYDROCARBONS OVER ZEOLITES

A DISSERTATION

SUBMITTED TO THE GRADUATE FACULTY

in partial fulfillment of the requirements for the

Degree of

DOCTOR OF PHILOSOPHY

By

ANH THE TO
Norman, Oklahoma
2014

SIMULTANEOUS CRACKING OF PHENOLIC COMPOUNDS AND HYDROCARBONS OVER ZEOLITES

A DISSERTATION APPROVED FOR THE
SCHOOL OF CHEMICAL, BIOLOGICAL AND MATERIALS ENGINEERING

BY

_____
Dr. Daniel Resasco, Chair

_____
Dr. Richard Mallinson

_____
Dr. Friederike Jentoft

_____
Dr. Walter Alvarez

_____
Dr. Daniel Glatzhofer

To my family, especially my father and late mother, for all of their loves and support during my education period in the past and career journey in the future.

Acknowledgements

I feel very privileged for finishing my Doctoral study at the University of Oklahoma. During this time I have had the opportunity to learn from different professors and fellow students about a wide variety of things; from technical topics to professional skills that are helpful for my future career path.

First I would like to acknowledge my advisor, Dr. Daniel E. Resasco, for giving me the opportunity to pursue a graduate program at OU and all of his valuable advises not only in the research, but also in the career development. He has mentored me not only on specific projects but also on being a better researcher and thinker. It is my great privilege to be his student.

I also feel very lucky to have Dr. Walter E. Alvarez from Phillips66 as a part of my committee. It helped me tremendously being able to discuss with him about how to apply research strategies to industrial processes.

I am grateful to have Dr. Richard G. Mallinson, Dr. Friederike C. Jentoft and Dr. Daniel T. Glatzhofer in my committee, who have given me valuable advices and suggestions that I have learned and benefited a lot from. I also appreciate Dr. Rolf E. Jentoft for his help with instrumentation troubleshooting and valuable discussions. And I would like to thank Dr. Steven P. Crossley and Dr. Tawan Sooknoi for their creative ideas in the research projects. Advises and instructions from Dr. Roberto Galiasso and Dr. Teerawit Prasomsri during my first year as a graduate student are also highly appreciated.

I would like to thank the funding from ConocoPhillips Fellowship and OCAST that made this project possible and all the help that I received from CBME's staff: Alan,

Terri, Vernita, and Donna. I have also learned, and obtained a lot of help from my senior and current coworkers of the group. Working and discussing with them have greatly extended my technical knowledge and cultural perspectives. Especially, I would like to acknowledge Yen Pham for her contribution in my research during her undergraduate study and prolongation of the research in her graduate study.

Finally, I would like to thank my father who gives a strong support so that I can focus completely on my study and career.

Table of Contents

List of Tables

List of Figures

Abstract

Co-processing bio-oils with hydrocarbons in conventional refinery processes has been considered as a promising strategy for upgrading and producing fuels from alternative sources. Co-feeding the phenolic fraction to the Fluid Catalytic Cracking (FCC) unit is an attractive but challenging pathway. Even though the high capacity and flexibility of the FCC process can boost the usage of bio-fuels, the strong adsorption and coke formation from the phenolic compounds might have a negative impact on the catalytic cracking of hydrocarbons. Therefore, in this research, we have conducted fundamental studies of the reaction of hydrocarbons, phenolic compounds, and their mixtures over zeolites under similar conditions to catalytic cracking process to understand the effect of the phenolic compounds on the reaction of hydrocarbons. The study has been carried out mainly using a micropulse reaction system in order to explore the reactivity of fresh catalysts.

The catalytic activity of HY zeolite is enhanced upon high temperature pretreatment due to the generation and synergism of the Lewis acid species with the original Brønsted acid sites to form a new type of site (synergistic site) that displays enhanced activity for both protolytic cracking and dehydrogenation reactions of paraffins. The activity enhancement caused by the synergistic sites is clearly evident for the monomolecular protolytic reaction, but it is not apparent in the conversion of olefins. Even though the synergistic sites were deactivated very quickly by strong adsorption of hydrocarbon species, they could be regenerated by a subsequent high temperature treatment. Furthermore, the preference for reaction pathways depends on the activation entropy of the transition state for each path. With n-hexane feed, the

enhancement of dehydrogenation is greater than for protolytic cracking, but the opposite trend was observed in the conversion of 2,3-dimethylbutane. The contributions of different reaction pathways of paraffins also depend on the reaction parameters. Monomolecular reaction is more favored at high reaction temperature, at low paraffin concentration, and at low conversion, where olefinic product's concentration is low; while bimolecular hydride transfer reaction is more favorable at high reaction temperatures with high paraffin and olefinic product concentrations. Also, branched paraffins with tertiary carbons are also better hydride donors than linear ones.

In the conversion of pure phenolic compounds (i.e. m-cresol and anisole), the zeolites capture the phenolic compounds significantly via molecular adsorption and condensation reactions forming oligomeric phenolic species (i.e. phenolic pools), which are still active for reaction at higher temperature to produce aromatics and light hydrocarbons. With increased reaction temperature, along with enhanced cracking to aromatics, the phenolic products were also captured to a less extent, which resulted in less carbonaceous deposition. The zeolite structure also has a strong effect on the formation and decomposition of the phenolic pool. For instance, small pore zeolite (i.e. HZSM-5) appears to be a better catalyst than HY in term of aromatic production, coke formation and catalyst stability.

Due to strong adsorption and coke formation tendency, co-feeding small amounts of m-cresol caused severe deactivation to the synergistic sites, and slightly deactivated the reaction at normal Brønsted acid sites due to competitive adsorption at low reactant concentrations. Interestingly, when the reactant concentration was increased or a better hydride donor reactant was used, the deactivation effect of m-

cresol diminished. Enhanced hydride transfer from the paraffin at higher reactant concentrations promoted desorption of the phenolic compounds and reduced coke formation leading to less deactivation. Co-feeding m-cresol also affected the contribution of different reaction pathways of paraffins. Competitive adsorption deactivated protolytic cracking and protolytic dehydrogenation paths. In addition, the phenolic pool, formed by condensation of phenolic compounds, acted as a hydride acceptor and competed with hydride transfer between hydrocarbons. In reverse, hydride transfer from hydrocarbons also promoted desorption of the phenolic compounds, suppressed the formation of the phenolic pool which resulted in less aromatics and coke formation.

The positive effect of hydride transfer towards catalyst deactivation was confirmed in the reaction of anisole with tetralin, a good hydride donor agent. In anisole conversion, catalyst deactivation is significant due to strong adsorption of phenolic compounds and coke formation. The latter is an irreversible process, whereas the former is reversible and can be minimized by incorporation of molecules such as tetralin with high H-transfer capacity. Co-feeding tetralin or other H-donors has a beneficial effect on anisole conversion and reduces coke formation. Other hydrocarbons with a weaker H-transfer capacity have lower (e.g., n-decane), negligible (e.g., benzene), or even detrimental effect on activity (e.g., propylene).

Chapter 1: Introduction

1.1 Biofuels upgrading via co-processing with hydrocarbons in refining processes

1.1.1 Motivation for biomass utilization as fuels

Transportation plays a key role in the growth of economic activities and the driving-age population. Specifically, transportation fuels have always accounted for a major fraction of energy and fuel demands, i.e. more than 50% of the world's consumption of liquid fuels since 2007 (Figure 1) [1] and 40% of U.S. energy consumption (Figure 2) [2]. While the projected liquid fuels demand is invariable in the U.S. [2], it is projected to grow to 111 million barrels per day in 2035 for the world consumption [1], where the demand mostly comes from the developing countries, such as China, India and Brazil, etc..

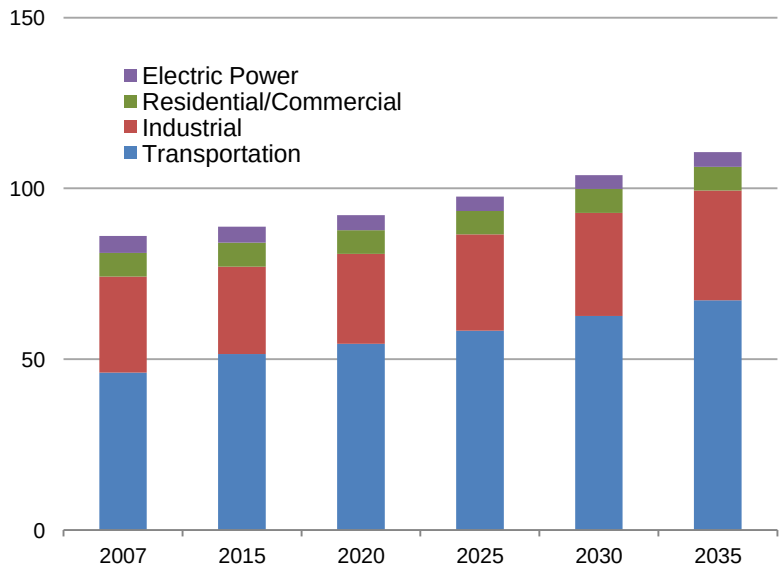

Figure 1. World liquid fuels consumption (in million barrels per day) by sector, 2007 – 2035. Reprinted from ref [1]

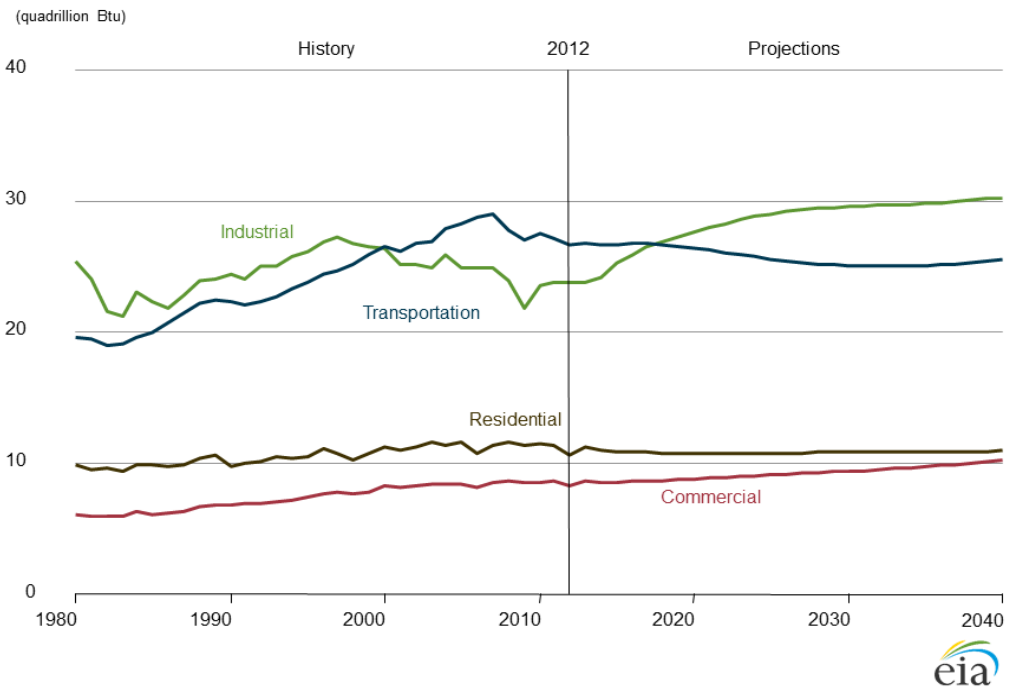

Figure 2. U.S. energy consumption (in quadrillion Btu) by sector, 1980-2040. Reprinted from ref [2]

Currently, most liquid fuels are produced from crude oil (Figure 3) [3]. As reported in the EIA International Energy Outlook 2013 [3], among 86.6 million barrels of liquid fuels were produced per day in 2010, in which 98% of those came from petroleum sources while only 2% came from biofuels, gas to liquids, and coal to liquids. Even though the growth in petroleum production is prospective due to contributions from the unconventional oil sources (such as extra heavy oil in Venezuela, bitumen in Canada and tight oil in the U.S.), many obstacles exist there. Due to difficulties in exploration, production and refining technology, together with the dependence of oil price on political situations, production of liquid fuel from conventional crude oils is volatile and not expected to satisfy the demand. Besides, usage of petroleum-derived liquid fuels raises concerns about environmental pollution as the production and combustion of fossil fuel add more CO_2 (which is a major greenhouse gas leading to

global warming), SO_x and NO_x gases (which cause acid rain) to the atmosphere. Hence, there is a strong motivation for research into alternatives for fossil fuels, especially fuels that come from renewable biomass sources [4-8]. Legislations have been proposed either in Europe [9] or the U.S [10] to mandate for certain amounts of renewable fuels to be used in the market. In Europe, energy legislation requires fuels containing at least 10% biofuels (in energy contents) by the end of 2020. While in the U.S., there is a mandate for production of 36 billion gallons of renewable fuel by 2022.

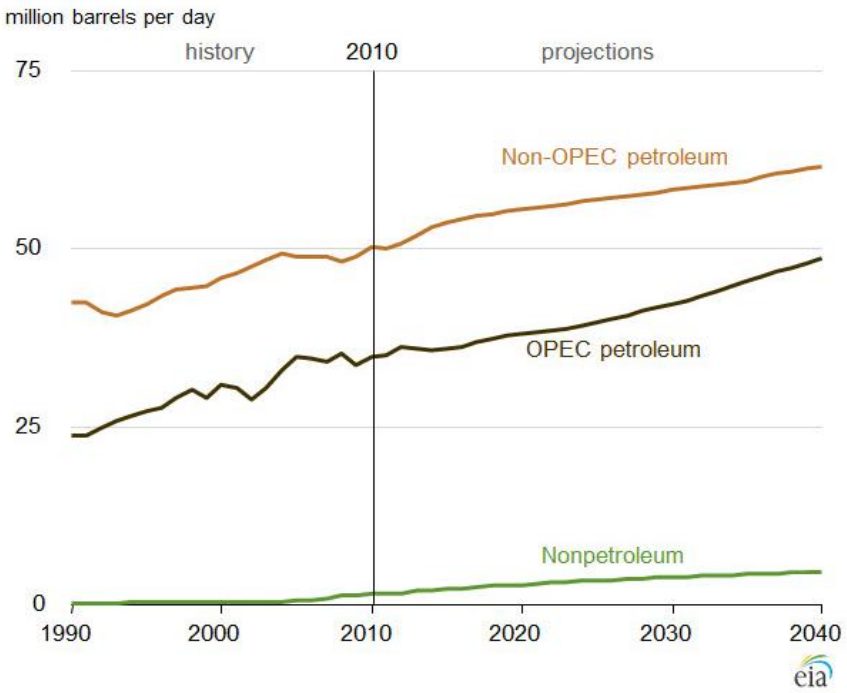

Figure 3. World liquid fuels production (in million barrels per day) by region and type, 1990-2040. Reprinted from ref [3]

Biomass is currently an attractive source for the production of fuels because of its abundance and sustainability. The total energy from agriculture and forest biomass resources in the U.S. can reach 3.8×10^9 barrels of oil energy equivalent [11, 12], which is half of the U.S. consumption. Even though combustion of biomass also produces CO_2, this biomass is produced in the photosynthesis process with consumption of

atmospheric CO_2, which results in no addition of CO_2 to the environment. Hence the energy obtained from biomass is a renewable energy. Besides that, the low S and N content in the biomass-derived fuels can also reduce air pollution when using as liquid fuels [4, 5, 13].

1.1.2 Bio-oil from biomass fast pyrolysis or torrefaction processes

The first generation of biomass-derived fuels is from fermentation of sugar and starch (for bioethanol) and esterification of vegetable oils (for biodiesel). However, due to competition with food production and the limitation in CO_2 reduction potential, production of these fuels is still small as compared to traditional petroleum refineries (i.e. less than $100MW_{th}$ as compared to few GW_{th}). The second generation of biofuels is obtained from lignocellulosic biomass feedstocks, which are abundant, cheap, and not competitive with food. Production of fuels from lignocellulosic biomass includes hydrolysis and fermentation to produce ethanol, gasification to produce syngas and further synthesis to produce methanol, or liquid fuels, and liquefaction by thermal treatment followed by upgrading to obtain liquid fuels. Biomass in nature has low energy density and is highly distributed with a variety of types and different structures. These adverse properties cause difficulties in large scale processing of biomass. Among many other processing methods, fast pyrolysis is the most suitable and cheapest solution to overcome the above hindrances. Pretreatment of biomass by fast pyrolysis produces a liquid (i.e. bio-oil) with increased energy density, which is suitable for transportation to central processing sites (i.e. refineries or power plants) for further conversion and upgrading. A fast pyrolysis plant can be operated at a suitable scale according to biomass production [4, 6, 14].

Biomass pyrolysis is a process where biomass feedstock is thermally degraded in the absence of oxygen. In a fast pyrolysis process, the heating rate is very high, i.e up to 200 K/s, and the reaction temperature is around 450 – 550 ^{o}C. Residence time of vapor products in the reactor is about a few seconds. After reaction, the vapor products are quickly cooled to a condensed liquid, incondensable gases, and char. Short residence times of the vapor products in the reactor prevents overcracking and polymerization of primary decomposition products to light gases and char, respectively. Hence, the yield of liquid fraction, which is the desired product, is high (60 – 70 wt% in dry feed basis) [4, 5, 15-21].

Table 1. Typical properties of wood pyrolysis and heavy fuel oil. Adapted from ref [6, 13, 22]

Properties	Pyrolysis oil	Heavy fuel oil
Moisture content (wt%)	15 – 30	0.1
pH	2.5	-
Specific gravity	1.2	0.94
Elemental composition (wt%)		
C	54 – 58	85
H	5.5 – 7.0	11
O	35 – 40	1.0
N	0 – 0.2	0.3
Ash	0 – 0.2	0.1
High heating value (MJ/kg)	16 – 19	40
Viscosity (at 50^{o}C) (cP)	40 – 100	180
Solids (wt%)	0.2 – 1	1

Pyrolysis oil (bio-oil) obtained from biomass fast pyrolysis is a dark brownish to blackish liquid, depending on the biomass feedstock and operating conditions [22, 23]. Some main properties of wood pyrolysis oil compared to fuel oil [6, 13, 22] are presented in the Table 1. The high water content from pyrolysis oil results from original moisture of the feedstock and dehydration reactions occurring during pyrolysis. Even though this property helps reduce the viscosity of the pyrolysis oil, which is beneficial for combustion, it causes many problems for using this oil for fuels, such as low heating value and possible phase separation. Pyrolysis oil also contains a large fraction of oxygenated compounds, which is represented by the high oxygen content. These compounds are still active and cause some property changes of the oil during storage (aging process) such as viscosity increase and phase separation. The high polarity of pyrolysis oil, due to the presence of oxygenated compounds, also causes immiscibility problems when they are mixed with hydrocarbons. The high acidity of pyrolysis oil, because of some acid components in the oil and high water content also make it very corrosive when it is stored, transported and processed. Pyrolysis oil contains over 200 compounds with different functional groups (i.e. acid, aldehyde, ketone, alcohol, ester, ether, phenolic) from the pyrolysis of different components in biomass (i.e. cellulose, hemicelluloses and lignin). Some main components in pyrolysis oil are levoglucosan, hydroxylacetaldehyde, acetol and acetic acid from cellulose and hemicellulose decomposition (mostly in water phase) and also phenolic compounds derived from lignin decomposition (mostly in organic phase), such as phenol, guaiacol, cresols, etc. [6, 17, 20, 21, 24]. Because of the poor properties of pyrolysis oil, it needs further upgrading to be used as fuel or blended in fuels. However, complexity in the

compositions of pyrolysis oil also cause difficulties in downstream catalytic upgrading because different components in pyrolysis oil have different activities and product formation. Hence, separation process should be included before catalytic upgrading.

Torrefaction is also a promising method for producing bio-fuels from biomass [25-27]. This process was originally applied in the biomass pretreatment step to increase the energy density of the biomass by increasing its C content, while decreasing O and H contents. The produced solid fuel from biomass torrefaction has high energy density, good stability and grindability for co-firing with coal in the boiler. Torrefaction, as originally defined [25], is also a thermochemical conversion process in which biomass is slowly heated to specified temperature ranges (200 – 300^{o}C) and retained there for a period of time to degrade its hemicelluloses. The products from decomposition of hemicelluloses are comprised of condensable gases (i.e. mainly acetic acid and water [28] with smaller quantities of methanol, formic acid, lactic acid, furfural and hydroxyacetone), and non-condensable gases (mainly CO_2 and CO). Extension of the torrefaction approach can also be applied to decompose different biomass components. Themogravimetric analysis (TGA) of different biomass components (i.e. hemicellulose, cellulose and lignin) [29, 30] showed that they were decomposed at different temperatures and some specific types of oxygenates were produced from each component. Hemicellulose decomposition occurs easily at low temperature (i.e. 220 – 315 ^{o}C) [29, 30], and produces mainly acetic acid and water with a small amount of other light oxygenates [28]. Pyrolysis of cellulose occurs at higher temperature ranges (i.e. 315 – 400 ^{o}C) [29, 30], and produces mainly levoglucosan via intramolecular condensation and sequential depolymerization of the glycosidic units [31]. Meanwhile,

pyrolysis of sugars, which have similar chemical structure to cellulose, produces mainly hydroxyacetaldehyde, and furanic compounds [6]. Among all, lignin was the most difficult decomposing component. Even though the decomposition starts at low temperatures (i.e. 200 ^{o}C), this happens slowly and products are still formed at up to 900 ^{o}C [29, 30]. Decomposition of lignin occurs primarily via depolymerization, forming phenolic monomers, such as guaiacol, catechol, isoeugenol, etc. [31, 32]. While the decomposition of these components occur primarily at different temperature ranges and form different types of products, their co-existence in biomass does not have any influence to each other's thermal conversion [29, 30]. These properties are very useful for a multi-stage torrefaction of the biomass. In this approach, the biomass can be torrefied (or pyrolyzed) at different temperature stages, in which decomposition of each component occurs primarily in each stage and form specific type of products. Consequently, separation of product group during pyrolysis of biomass can be achieved. The drawback of complexity in pyrolysis oil component can be improved and downstream catalytic upgrading of the bio-oil can be carried out more easily.

1.1.3 Bio-oil catalytic upgrading strategies

Various upgrading strategies have been studied to remove oxygen from pyrolysis oil, making it compatible for use as fuel or blending in fuels. The hydrodeoxygenation (HDO) of model oxygenated compounds in pyrolysis oil [33-38] and pyrolysis oil itself [39-42] has been studied extensively. Mercader et al. [39, 42] showed that HDO over ruthenium catalyst effectively reduces the O/C ratio, and increases the H/C ratio of the pyrolysis oil. Water phase oxygenates was observed to have higher HDO efficiency than oil phase oxygenates. HDO reaction of the water

phase oxygenates consumed more hydrogen and produced output that has higher H/C. Xu et al. [41] proposed two-step catalytic HDO in which the first mild HDO step was carried out over Ru/C catalyst at 300 ^{o}C, 10 MPa and the second step involved HDO at more severe conditions (400 ^{o}C, 13 MPa) using $NiMo/Al_2O_3$ catalyst. Significant oxygen removal was achieved and the final products include $C_{11} – C_{27}$ aliphatic hydrocarbons which are suitable for blending in liquid fuels. Nevertheless, high H_2 consumption and operating pressure are essential disadvantages of HDO processes which make them uncompetitive to traditional fuels in production cost. Furthermore, direct HDO of the whole pyrolysis oil might not be efficient since a significant amount of carbon was lost to light gases and coke. The total carbon yield of liquid products after HDO was only about 30% of the pyrolysis oil feed [39-42].

Small oxygenates in pyrolysis oil, such as acetone, acetic acid, small alcohols and aldehydes cannot be blended directly into fuels due to their high oxygen content in the molecules as well as short hydrocarbon chain length. However, they can be upgraded through aldol-condensation over mixed oxide [43] catalysts, ketonization of carboxylic acids over metal oxides [44-46] or zeolites [45, 47], etherification over Pd catalysts [48] to partially remove oxygen and increase carbon chain length of the molecules. The condensation products, which have high octane numbers, can be blended into gasoline fuel. Retention of carbon from the small oxygenates can also be achieved via alkylation with the phenolic compounds [49] which were obtained from thermal conversion of the lignin fraction.

The deoxygenation of oxygenated compounds by dehydration, decarbonylation and decarboxylation over acid sites of zeolites has also been studied as an upgrading

strategy for pyrolysis oil. Catalytic cracking of various model compounds has been studied extensively over different acidic catalysts, especially HZSM-5. Gayubo et al. [50-52] and Adjaye et al. [53, 54] studied transformation of oxygenates with different functional groups, including alcohols, phenols, aldehydes, ketones and acids. Their results showed that deoxygenation can be achieved with alcohols, ketones, acids, esters and some aldehydes, but phenolic compounds were very inactive. Severe catalyst deactivation was also observed because of thermal coke deposition of acetaldehyde, and phenolic compounds and catalytic coke formation from oligomerization and aromatic condensation [52]. The reaction of pyrolysis oil over HZSM-5 and other acidic catalysts was also studied by Gayubo et al. [55], and Adjaye et al. [56-58]. Adjaye et al. claimed that HZSM-5 is the most effective catalyst for the production of hydrocarbons from pyrolysis oil, and it is the most resistant to deactivation by coke formation. However, there was a significant amount of coke, tar and char formation, and the catalyst deactivation is also so severe that directly upgrading of pyrolysis oil through zeolites is not a straightforward task [59].

To overcome the drawback of complex composition of pyrolysis oil, the advantage of multi-stage pyrolysis or torrefaction can be applied. Specific product groups from thermal conversion of different biomass components can be separated by selecting the right temperature and residence time in the pyrolysis process. And cascading catalytic upgrading of each fraction can be carried out independently to efficiently achieve deoxygenation and carbon retention goals [49]. The overall scheme of biomass pyrolysis followed by selective catalytic upgrading of each fraction is shown in Figure 4. Retention of carbon in small oxygenates can be achieved via aldol

condensation [43], ketonization [44], etherification [48] and alkylation [49] reactions. Subsequently, deoxygenation [34, 60] of the large oxygenates can be achieved via HDO processes.

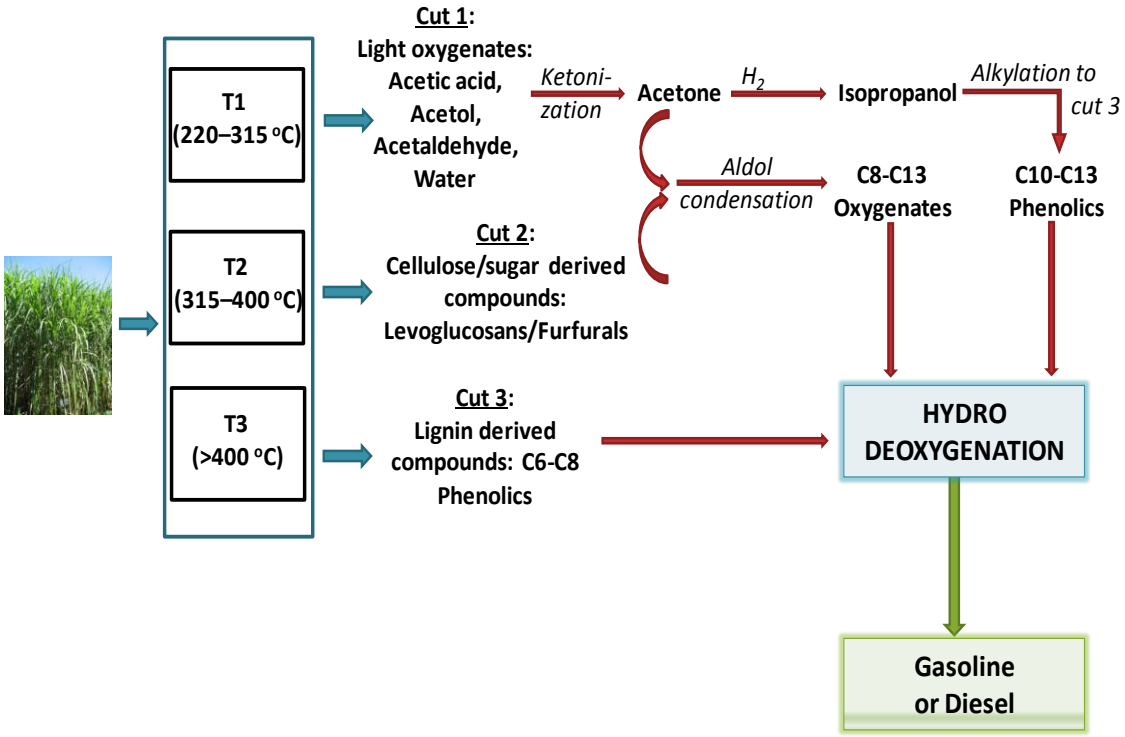

Figure 4. Multi-stage biomass torrefaction followed by cascading catalytic upgrading with final HDO step for fuel production

Co-processing of the pyrolysis oil with intermediate streams in the refinery units, for example in the Fluid Catalytic Cracking (FCC) unit [39, 42, 59, 61-64] or the hydro-treating or hydro-desulfurization (HDT or HDS) units [61, 62, 64-66], was considered as a potential strategy for processing pyrolysis oil, in the industrial standpoint. Mercader et al. [39, 42] and Fogassy et al. [59] co-processed HDO oil with both Long residue and Vacuum gas oil in the micro catalytic test (MAT) reactor over an FCC equilibrium catalyst (Ecat). Their results showed that a homogeneous mixture of 20 wt% of pyrolysis oil in the gasoil can be obtained and co-processed. The conversion

and product selectivity of the cracking reaction did not differ significantly as compared to the cracking of the gasoil feed. Slight increases of coke and dry gas were observed, but their yields reduced remarkably as compared to the cracking of the undiluted HDO oil, or as calculated by dilution ratio. Reactions of oxygenates with hydrocarbons in the gasoil feed can help reduce molecular adsorption, coke formation, and deactivation through hydrogen transfer and deoxygenation. Co-processing pyrolysis oil also uses existing infrastructure of the refinery, which can reduce the investment cost for bio-fuel production. Besides, with the current large processing capacity of the refining industry, large amounts of pyrolysis oil can be processed, so that rapid change in usage of bio-fuels as transportation can be achieved in the short term. This processing pathway was considered more competitive than fuels obtained from biomass gasification and biodiesels from vegetable oils [59, 62]. Co-processing pyrolysis oil can also diversify the feedstock for the refinery as the oil supplies are more stringent and expensive. However, miscibility of the pyrolysis oil with hydrocarbons was an important issue that needs to be considered when co-feeding the whole bio oil fraction. Preliminary phase separation or HDO of the pyrolysis oil might improve the miscibility problem. Other than that, cascading catalytic upgrading of different cuts from multi-stage biomass pyrolysis can also produce large oxygenates that are suitable for blending with hydrocarbons for co-processing in the refinery. The alternative scheme for biomass pyrolysis followed by catalytic upgrading and synergism with refinery is shown in Figure 5.

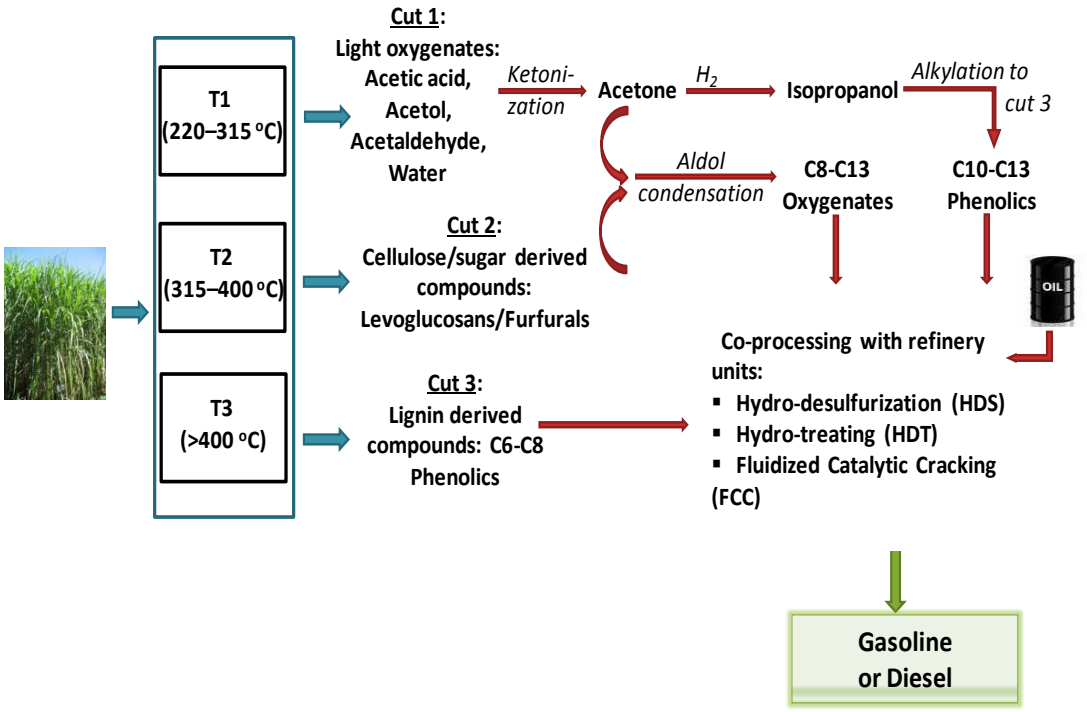

Figure 5. Multi-stage biomass torrefaction followed by cascading catalytic upgrading and co-processing with refinery units for fuel production

1.1.4 Coprocessing of pyrolysis oil in FCC unit

Since its first commercial startup in 1942, the FCC process has become the most important and fastest growing process in the refinery. More than 350 cat-crackers are operating worldwide, with the total capacity of 13.8 million barrels per day. This accounted for about 17% of the total worldwide refining capacity and one third of the total refining capacity of 16.5 million barrels per day in the U.S. in 1999 [67, 68]. The main purpose of a FCC unit in the refinery is to convert the high boiling point fractions of crude oil from distillation units or other processing units (i.e. delayed coker and hydrocracker) to lighter and more valuable products, such as naphtha for gasoline pooling, light cycle oil for diesel pooling, LPG, light gases, and coke. The catalytic cracking reaction occurs when the catalyst and hydrocarbon feed contacts at high temperature (i.e. over 500^{o}C) for a very short time (i.e. few seconds). The conversion

of hydrocarbons over zeolites undergoes a formation of carbenium ion (mostly) or carbonium ion at the acidic sites. Then, these carbocations react through beta scission cracking, isomerization, or hydride transfer and condensation to form different products [69-72]. Significant coke formation is an important characteristic of the FCC process. Short residence time of both reactant and catalyst in the fluidized riser, along with continuous catalyst regeneration were designed in conformity with strong coke formation of the reaction [67, 68]. FCC catalysts consist of active zeolites which mainly contribute to catalytic activity and selectivity of the catalyst, inert or active matrices to control physical properties (or sometimes catalytic properties of the catalyst) and additives [73]. The zeolites are mostly synthetic faujasite type zeolites (Y or ultra-stable Y) in rare earth or ammonium exchanged form. The matrices are made from synthetic components (amorphous silica, alumina or silica-alumina) or natural components (clay, thermally or chemically treated clay). Additives are used to enhance contaminant resistance of the catalysts (i.e. antimony (Sb), bismuth (Bi) and Tin (Sn) compounds), improve octane number of the naphtha fraction (ZSM-5 zeolite) or reduce toxic gas emissions (etc. metal oxides or Platinum). Depending on the feedstock and process objectives, the composition of different components in FCC catalysts can be varied significantly, from 10 – 50 wt% for the zeolite, 50 – 90 wt% for the matrix, and 0 – 10 wt% for the additives.

Because of its flexibility in operation, the FCC unit can process many variety of feedstock, such as gasoil and residue from atmospheric or vacuum distillation units, middle distillate fractions from delayed cokers or hydrocrackers, and bio-oil as well. Some studies [39, 42, 59, 61, 62, 64, 74] showed potential application of this unit in

processing pyrolysis oil. The co-processing of hydrotreated pyrolysis oil with Long residue and vacuum gasoil (VGO) was studied by Mercader et al. [39, 42] and Foggasy et.al [59], respectively. They found that co-processing produces more coke and dry gas, less LPG and similar gasoline, light cycle oil, and bottom yields, as compared to processing hydrocarbon feeds alone. Besides, co-processing also gave much lower yields of dry gas and coke as compared to direct processing of pyrolysis oil, and even lower than those calculated from the dilution ratio. Analysis of gasoline fraction showed that there were more branched paraffin and short benzene derivatives produced at the expense of linear paraffin comparing to the reaction of the pure feed. Formation of CO and CO_2 in the gas product, as well as the reduction of oxygen content in the products, showed that deoxygenation was achieved. Less H_2 production in pyrolysis oil co-feeding compared to reaction of gas oil showed that possibly more hydrogen transfer reaction occurs between hydrocarbons and oxygenates to remove oxygen in the feed.

Effects of adding oxygenates to the cracking reaction of hydrocarbons was studied with model compounds by Graca et al. [75-78]. In their studies, either phenol or guaiacol was co-fed with n-heptane or methylcyclohexane for cracking reactions over HY and HZSM-5 zeolites. Strong adsorption of phenolic species on the catalysts caused severe deactivation to the cracking reaction of methylcyclohexane and n-heptane. While coke formation from the cracking reaction was on Brønsted acid sites, phenol adsorbed on both Brønsted and Lewis sites and blocked the micropore. As phenol favorably adsorbed on strong acid sites, the deactivation effect was observed significantly at an early time on stream (TOS) and the deactivation was stronger in n-heptane cracking than methylcyclohexane cracking, as the former needed stronger acid

sites for cracking. The product selectivity changed slightly, but mostly because of the increased coke formation by phenols rather than the reaction of phenols with the hydrocarbon feeds. Only small alkylation products between phenol and small alkenes from n-heptane cracking were observed. Adsorption of guaiacol also caused severe deactivation to n-heptane cracking over HY and HZSM-5, with the more remarkable deactivation effect on HZSM-5. Guaiacol only reacted slightly to produce phenol, methane, and water, but did not affect product selectivity of n-heptane cracking. Graca et al. also studied co-feeding different oxygenates (including guaiacol, acetic acid, phenol and hydroxyacetone) with gasoil over FCC Equilibrium catalyst [63, 78]. They observed increased conversion of gasoline fraction when oxygenates were co-fed, but mostly because oxygenates and their products have the boiling point range in this fraction. Besides, they observed some aromatic products from dehydration and alkylation of both phenol and guaiacol in the gasoline fraction products. So, there might have been some hydrocarbon molecules in the gasoil feed that could transfer hydrogen with the phenolics to deoxygenate these molecules.

Among major types of oxygenated compounds in pyrolysis oil, the phenolic compounds have shown strong resistance to upgrading via HDO reaction because of their stable structure. Other than being produced from thermal conversion of the lignin fraction of the biomass, phenolic compounds are also major products from conversion pathways of small oxygenate. And they are also well miscible in hydrocarbons. Hence, co-feeding these phenolic compounds to catalytic cracking reaction of hydrocarbon is a promising strategy for valorization of bio-oil by enhancing aromatic production in the process.

1.2 Research objectives

Co-processing pyrolysis oil, especially the phenolic fraction, with hydrocarbon feed in FCC unit is a promising strategy for fuel production. However, due to the complexity and variety in nature of pyrolysis oils, even when separation techniques were applied, co-processing them with refinery intermediate streams raises many technical challenges that need to be further studied. Severe deactivation was observed in different pyrolysis oil upgrading reactions [52, 55-57], probably due to strong adsorption and coke formation of the oxygenated compounds, especially with the phenolic compounds. When they are co-processed in the refinery units, the deactivation effects of these compounds to the main reaction are very important and need to be studied. Active components in pyrolysis oil can undergo reaction with each other, or with hydrocarbon feedstock which will affect the overall product distribution. These interactions should be studied thoroughly in the fundamental levels with model compounds to understand the reactions taking place in the process. Furthermore, since oxygen removal is the main purpose for pyrolysis oil upgrading, when they are co-processed in the refinery units, the process operating conditions and catalysts might be modified in order to achieve this purpose efficiently without negative impact to the original process. Even though catalytic cracking reaction of hydrocarbons under FCC conditions have been studied extensively with different model compounds or the real feeds, the effects of co-feeding oxygenated compounds in the bio-oil to the reaction of hydrocarbon feeds and the reaction of oxygenated compounds themselves at similar conditions are still lacking. Hence, in this contribution, study of catalytic cracking of

hydrocarbons in the presence of oxygenated compounds that are present in pyrolysis oil, specifically the phenolic compounds will be reported.

In this research, conversions of paraffinic (i.e. hexane isomers) and naphthenic (i.e. tetralin) model compounds over protonated Y zeolites (HY), which is a main active component of the FCC catalyst, were studied. And the effects of co-feeding the phenolic compounds (i.e. m-cresol or anisole) to catalytic cracking of these hydrocarbons were evaluated. This research focuses on catalyst deactivation effect of these compounds to hydrocarbon cracking as well as their interaction with hydrocarbon feeds, which changed product distribution of the hydrocarbon reaction. Besides, conversions of pure phenolic compounds were also studied over the HY zeolite as well as the HZSM-5 zeolite (an important additive for aromatic production in FCC catalyst). In reverse, interaction with hydrocarbon which also affects production distribution of phenolic conversion will be presented.

1.3 Experimental

1.3.1 Introduction on Y and ZSM-5 zeolites

Zeolites are crystalline aluminosilicate material with the chemical composition of $M_{x/n}[(AlO_2)_x(SiO_2)_y].{}_zH_2O$. The charge compensating cation M (with valence n) in the natural zeolites can be alkali or alkali earth elements. However, it can be exchanged with other cations such as transition metals, rare earth metals or even protons (forming protonated or H-zeolite) to achieve specific catalytic properties. The primary structure units of zeolites are tetrahedrons of silicon (SiO_4) or aluminum (AlO_4). These units assemble to form secondary building units such as hexagonal prism, octahedrons,

truncated octahedrons, etc. in which the Si and Al atoms are located at the corner of the polyhedron and connected via an O atom. Assembling of the secondary building blocks forms s zeolite crystalline network [79].

The Y zeolite is a large-pore zeolite with the faujasite framework structure that has a very important application as solid-acid catalyst in the refining industry, especially the FCC catalyst. The building block units of the Y zeolite are the double 6-membered ring and the sodalite cage connecting together forming a large cavity with 12-membered ring windows (i.e. supercage). The connectivity of the supercage allows molecules to diffuse in three dimensions inside the crystal structure [80].

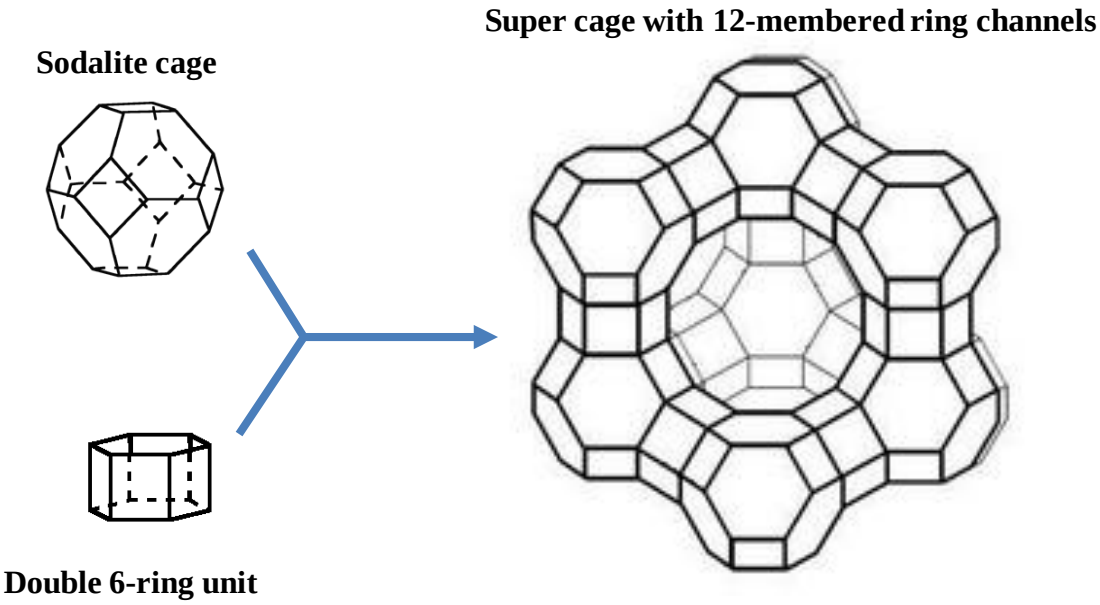

Figure 6. FAU zeolite building blocks

ZSM-5 is the second most used zeolite catalyst after zeolite Y with more than 50 processes that use ZSM-5 as the main catalytic component. In the FCC process, ZSM-5 is also used as a very important additive to enhance octane number of the gasoline fraction, as well as reduce the coke formation. The zeolite is constructed mainly from the 5-membered ring units that are organized as columns and connected to each other

forming the straight and sinusoidal channels with 10-membered ring windows. Even though these 2 channels only direct in 2-dimension, but since they are connected together, the molecules can also diffuse in 3-dimension inside the zeolite crystal [80].

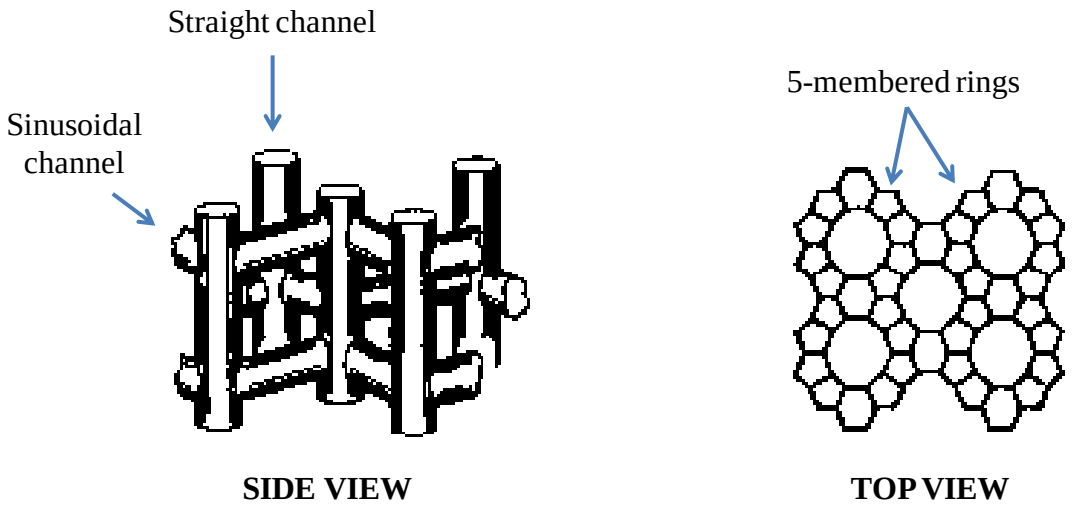

Figure 7. ZSM-5 zeolite channel structure

Because of their interesting properties, zeolites have been applied widely as catalysts and adsorbents in the industry, especially in refining and petrochemical industry. The first property is their ion exchange capability. Replacing Si by Al in the zeolite tetrahedral framework create a negative-charge imbalance which is compensated by a cation. These cations are mobile and can be replaced by other cations via ion exchanging and the nature of active site can be altered accordingly. When the cation is a proton, it can exhibit Brønsted acidity which has very important catalytic application. Other cations and extra-framework alumina (EFAl) species can also exhibit Lewis acidity. The second property is the shape and size of the zeolite pore structure which is in the range of molecular level. This property is very useful in separation and reaction applications. The reaction selectivity over zeolites results from of diffusivities of

reactants and products through the pore channels, and selectivity to transition states for different reaction pathways [81].

1.3.2 Reactor design and operation

In the FCC riser, residence time of the hydrocarbons and catalyst are as short as few seconds. Amount of coke formation and catalyst deactivation have been very important parameters for design process operation. Because for the catalytic cracking reaction over zeolites at high temperature, coke formation is rapid [67, 68]. When the phenolic compounds were co-fed with hydrocarbon, much more severe coke formation should be expected, because these phenolic compounds have very strong adsorption and coke formation tendency on zeolites [75-78]. Therefore, it is difficult to evaluate activity of the fresh catalyst to the cracking reaction of hydrocarbons and their mixture with phenolic compounds using traditional plug flow reactor operating continuously. Because for this type of reactor, product analysis can only be carried out at tens of minute or as soon as few minutes after the reaction started (for feed injection stability). At this point of time, coke formation is already significant, and the catalyst activity was measured when it was covered by coke. Hence, a unique reaction system (i.e. the micropulse reaction system) was designed and installed in order to evaluate the activity of the fresh catalyst.

The design of the reactor system is shown in Figure 8 below. The feed injection part includes a syringe pump to inject the liquid feed continuously into a heated injection port and a flow controller for Helium gas flow (He 2) to carry away the evaporated feed. Concentration of the reactant can be controlled by varying the feed injection and He flow rates. A stabilizer, which is a section of large tubing filled with

3mm diameter glass beads, is used for damping the fluctuation of reactant concentration in the gas flow. Two 6-port valves are placed in a heating box, connected to the reactor inlet, outlet, sample loop, and gas chromatograph (GC) to direct the flow and inject the pulse of reactants. The reactor includes a 1/4" quartz tube placed in the temperature controlled oven. The gas lines are made of 1/16" stainless steel tubes heated by heating tape to avoid condensation of the reactants and products. An HP-5890 GC, equipped with either an HP-5, HP-1 or HP-PLOT/Al_2O_3/"S" column and a flame ionization detector (FID), is used for product analysis. Other Helium gas flows are used as carrier gas for the reaction in the pulse experiment (He 1) and diluting gas (He 3) for product output before going to the GC.

The versatility of the reactor system is owing to the combination of the two 6-port valves. This reactor system can operate in two different modes: continuous flow or transient (or pulse) reaction by switching the two 6-port valves. Simplified flow diagram through the valve systems corresponding to two operation modes is shown in Figure 9. In a typical experiment, the catalyst is packed in the middle of the reactor by clean glass wool. The catalyst can be mixed with inert material (i.e. silica or 0.1-mm diameter glass beads). The top of the packed bed is filled with 1-mm diameter glass beads. The thermocouple was affixed in the middle of the furnace at the height corresponding to the center of the catalyst bed. Test measurements which were done to correlate the temperature of the furnace and the temperature inside the reactor tubes showed that the temperature difference was less than 5 ^{o}C. In the pulse experiment, initially the two 6-port valves are positioned (V1a and V2a positions, Figure 9a) such that reactant flow fills the sample loop. At the same time, the catalyst bed is always

under He flow. Then, when the 6-port valve V2 is switched (V2b position, Figure 9b), He 2 flow flushes the reactant in the sample loop to the reactor and the effluent goes directly to the GC for analysis. By changing the 6-port valve V1, the continuous flow experiment can be conducted. Initially the reactant flows through the reactor, the reaction takes place and the effluent fills the sample loop (Figure9c, V1b and V2a position). Then by switching the 6-port valve V2 (V2b position, Figure 9d), the He 2 flow flushes the reaction mixture in the sample loop to the GC for analysis.

Operation of the system in the pulse reaction mode is very useful for studying the activity of the fresh catalyst because it is not saturated by the reactant atmosphere and covered by coke. Reaction of a pulse series can also be conducted by repeating the pulse sequence to study deactivation behavior of the fresh catalyst. The size and concentration of reactant in a pulse can also be well controlled by varying feed injection and He 2 flow rates and the sample loop size. The combination between these 2 modes can be applied to study the reaction on deactivated catalysts by flowing a deactivating agent through the catalyst bed for a period of time and running a pulse experiment with the deactivated catalyst. Furthermore, sequential pulses of one compound after another are very interesting experiments that can be carried out on this system to study reaction of one compound with surface species formed by another compound. These advantages make this micro-pulse reaction system unique and helpful for many experimental purposes, especially to study the catalytic cracking reaction. More details about the experiment procedure and conditions will be described in later chapters depending on the study.

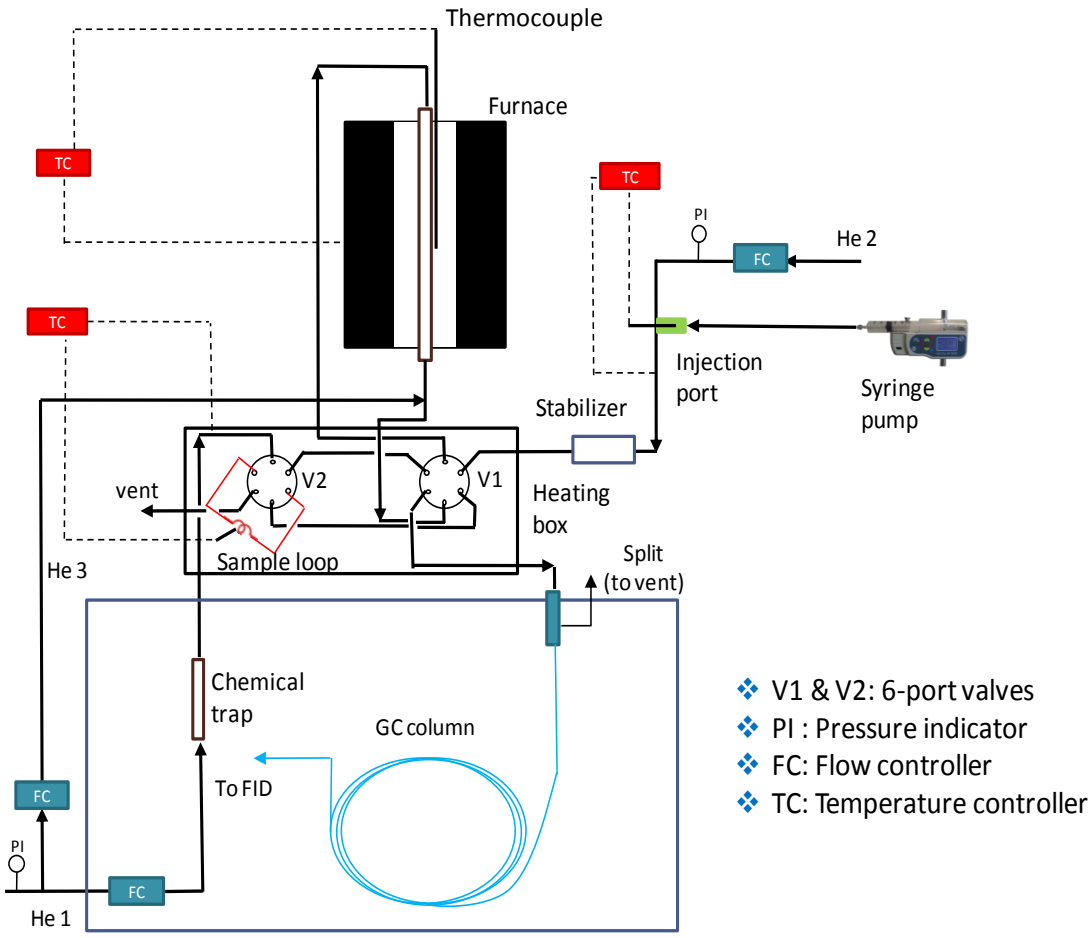

Figure 8. Design of the micropulse reaction system.

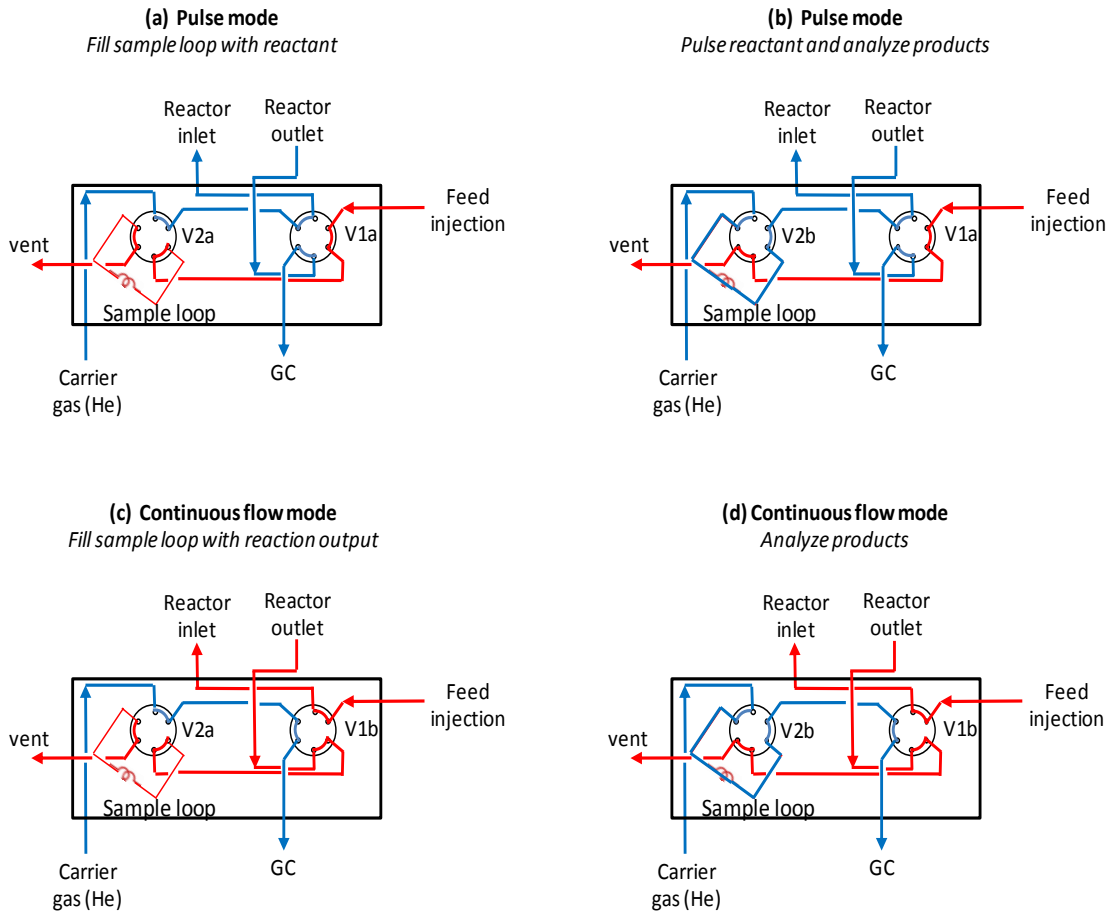

Figure 9. Six-port valve's positions and flow configurations in the pulse and continuous flow modes

1.3.3 Catalyst characterization techniques

Density and strength of the acid sites, especially the Brønsted acid site (BAS), are very important in catalytic activity of the zeolites. Therefore, many techniques have been developed for characterizing zeolite acidity. In this study, temperature-programmed desorption (TPD) of adsorbed isopropylamine (IPA) was used to quantify the density of the BAS because this site has been shown to adsorb and catalyze the dissociation of IPA to propylene and ammonia stoichiometrically. A specified amount of catalyst was used for the analysis. After pretreatment, the catalyst was cooled to 100

°C under 20 sccm of He and exposed to ten consecutive 2 μL pulses of liquid IPA. After flushing under He for 12 h at 100 °C to remove weakly adsorbed IPA, a 10 °C/min linear heating ramp was started up to 600 °C. The desorbed products were analyzed and quantified on a Microvision Plus MS, scanning over a 1–60 m/z range at a speed of 26 cycles/min. To quantify the BAS density, the propylene signal (m/z = 41) was calibrated with 100 μL propylene pulses [82].

Analysis of the carbonaceous deposits remaining on the catalyst after reaction was done by temperature programmed oxidation (TPO). The same reactor tube containing the spent catalyst was connected to the TPO system, equipped with a Cirrus mass spectrometer (MS) to measure the evolution of CO_2 (m/z = 44) during the TPO ramp. To oxidize the carbonaceous deposits, a stream of 20 sccm of He/O_2 (5% volume O_2) was used. Following reaction and after the furnace temperature was stable at 50 ^oC, the reactor was heated linearly with a 10 ^oC/min ramp up to 700 ^oC and held at this temperature until the CO_2 signal reached the baseline. For quantification, the CO_2 signal (m/z=44) was calibrated with 100 μl pulses of pure CO_2.

Temperature programmed decomposition (TPDe) of the carbonaceous deposits on the spent catalyst was also carried out to study the activity of the phenolic pool formed after m-cresol reaction. A Microvision Plus MS, scanning over a 1 – 200 m/z range at a speed of 15 cycles/min, was connected to the reactor outlet to detect product evolution during pulses of m-cresol through the catalyst bed and TPDe of the spent catalyst after that. After 10 pulses of m-cresol (1.5 μmol m-cresol/pulse each) over 50 mg catalyst-bed at 400 ^oC (or 500 ^oC), the catalyst was flushed for 20 minutes to remove all weakly adsorbed species. Then, a 5 ^oC/min linear heating ramp was

initiated; when reaching the target temperature (500 – 600 ^{o}C) it was held constant until all signals reached the baseline. In order to quantify the evolution rate of major products upon TPDe , pulses of toluene, benzene and methane with known amount were sent through an inert bed to the MS for calibration.

Chapter 2: Generation of synergistic sites by thermal treatment of HY zeolite. Evidence from the reaction of hexane isomers

2.1 Introduction

The catalytic cracking of hydrocarbons over zeolites is one of the most important chemical reactions involved in the refining of crude oil for the production of fuels and chemicals. Depending on the reaction conditions, cracking may occur via bimolecular or monomolecular pathways [72, 83]. In the bimolecular mechanism, the initiation step involves hydrocarbon protonation on an acid site to produce a carbocation. Subsequent hydride transfer from another alkane molecule triggers a chain propagation that leads to different cracking products via carbenium-ion-like transition states and β-scission steps. The resulting products are smaller olefins and the regenerated active site. The monomolecular mechanism includes protolytic cracking and dehydrogenation, which can occur through the formation of carbonium ions without the participation of a hydride transfer [84]. The contribution of each of the possible pathways to the final product distribution greatly depends on the relative rates of hydride transfer (bimolecular pathway) and initiation (monomolecular pathway) [85]. For instance, at high temperatures and low reactant partial pressures, the product distribution is governed by the monomolecular pathway; in contrast, at lower temperatures and higher olefin concentrations, the products of the bimolecular pathway become dominant.

In the commercial operation of a FCC unit, the reaction is carried out at intermediate temperatures and moderate hydrocarbon partial pressures. In addition to the protolytic cracking, thermal cracking and dehydrogenation also occur, producing

olefins that further enhance the extent of bimolecular reactions and influence the product distribution. In the commercial operation, the extent to which the various reaction steps contribute to the product distribution is further complicated by the varying nature of the active sites. The catalytic activity of each acid site in a pristine zeolite is thought to be constant, with the overall activity varying linearly with the number of tetrahedral aluminum sites in the zeolite [86, 87]. However, thermal [88-90] or hydrothermal [91-95] pretreatment of the zeolite can enhance paraffin conversion. Different explanations have been proposed for the observed activity enhancement. Al-majnouni et al. [89] and Yun et al. [90] have proposed that thermal pretreatments of a HZSM-5 zeolite can result in the dehydroxylation of Brønsted acid sites (BAS), generating redox sites with enhanced activity for propane and isobutane conversion. Formation of Lewis acid sites (LAS) by dehydroxylation of the BAS is believed to increase paraffin adsorption enthalpies, which causes a decrease in apparent activation energies for paraffin cracking [91]. Many authors have claimed that the interaction between the thus-produced LAS and a neighboring BAS generates a very strong acid, resulting in increased activity [88, 93-97]. Mirodatos et al. [93] proposed that the direct interaction between the LAS and an acidic OH group reduces the O–H bond strength, resulting in enhanced proton lability and higher acid strength. Moreover, Lago et al. [94] found that the enhanced activity was correlated to the number of paired-framework Al sites. Hence, they proposed that as one BAS in the pair was dehydroxylated to a LAS, it became electron withdrawing and enhanced the acid strength of the adjacent BAS. Recent theoretical studies [96, 97] supported the proposed mechanism of enhanced acidity via synergism between the Lewis species with the acidic OH group.

In particular, the deprotonation energy, a measure of the acid strength, was found to decrease to a greater extent when the LAS were adjacent to the BAS than for other configurations.

In this work, we have investigated the generation of synergistic sites during thermal pretreatment of HY zeolites and its effect on the cracking of different hexane isomers in a micropulse reaction system. This system has enabled us to evaluate the catalyst activity and the evolution of product distribution over the fresh catalyst at very short time on stream, when coke formation is negligible. Significant enhancement in activity and changes in product selectivities upon high temperature pretreatment imply the generation of new sites (synergistic sites) that not only have a higher cracking activity than normal BAS but also interact differently with the protolytic cracking or dehydrogenation transition states, which causes significant changes in selectivity.

2.2 Experimental

2.2.1 Materials

Several C_6 hydrocarbons were used in this study: n-Hexane (n-C6, 99% pure), 3-methyl pentane (3MP, 99%+), and 2-methyl-2-pentene (2M2P) (98%) from Sigma Aldrich; 2,3-dimethylbutane (23DMB, 99%+) from Tokyo Chemicals Inc.; and propylene from Airgas. These hydrocarbons were used for the reaction without further purification. Isopropylamine (99.5%+) from Aldrich was used for acid site quantification. The zeolites used as catalysts, including CBV780 (dealuminated HY zeolite with Si/Al = 40) and CBV600 (HY zeolite with Si/Al = 2.6), were obtained from

Zeolyst International. The catalysts were pelletized to 90–250 μm particles before reaction.

2.2.2 Catalyst characterization

Thermogravimetric analysis (TGA) on a Netzsch STA-449 F1 Jupiter TG coupled to a Netzsch QMS430C mass spectrometer (MS) was used to quantify water losses during zeolite activation. To avoid condensation, the transfer lines between the TGA and the MS were heated to 200 °C. Approximately 30 mg of CBV780 zeolite was used in each measurement. Argon carrier gas flowed at 50 sccm while the temperature was increased in a 10°C/min linear heating ramp from 30°C to different final temperatures (450, 600, and 1000 °C).

Temperature-programmed desorption (TPD) of adsorbed isopropylamine (IPA) was used to quantify the density of BAS [82]. In each TPD measurement, 50 mg of catalyst was used after pretreatments that mirrored those employed before reaction. After pretreatment, the catalyst was cooled to 100 °C under 20 sccm of He and exposed to ten consecutive 2 μL pulses of IPA. After flushing under He for 12 h at 100 °C to remove weakly adsorbed IPA, a 10 °C/min linear heating ramp was started up to 600 °C. The desorbed products were analyzed and quantified on a Microvision Plus MS, scanning over a 1–60 m/z range at a speed of 26 cycles/min. To quantify the BAS density, the propylene signal (m/z = 41) was calibrated with 100 μL propylene pulses.

2.2.3 Catalytic measurements

Conversion of different hydrocarbons (HC) in He carrier gas over HY zeolites was evaluated on a micropulse reactor. For the runs with hexane isomers as well as with propylene, 100 mg of catalyst was pretreated under 200 sccm He flow at different

temperatures (from 450 to 600 °C) and different periods of time (from 1 to 20 h). After each pretreatment, the He flow rate was lowered to 20 sccm and a pulse of the hydrocarbon reactant diluted in He (0.5 μmol HC/pulse, 3.7 mol % of HC in He) was sent over the catalyst bed. During the 1 h period between each pulse, the catalyst was exposed to continuous flow of He. The products were analyzed on-line by using an HP5890 GC, equipped with an HP-PLOT/Al_2O_3/"S" column and a flame ionization detector (FID) directly connected to the reactor outlet.

Due to the much higher reactivity of C6 olefins, the runs with 2M2P were conducted on 2 mg of catalyst diluted with glass beads to obtain a 2 cm long bed. Also, the He carrier gas flow rate for this reaction was increased to 150 sccm. The pulse size was increased to 6 μmol (3.7 mol % of 2M2P in He).

To quantify the extent of noncatalytic thermal conversion, pulses of each of the reactants were injected over an inert bed (acid-washed glass beads, 100 μm in diameter) under the same reaction conditions as used with the catalysts. In all cases, the contribution of thermal conversion was lower than 0.1% and was subtracted from the total conversion in each of the conversion values reported below. Each experiment was carried out in duplicate. The differences were always less than 10% and in most cases less than 2%. Therefore, each of the reported values is the average of the two measurements. Products were identified and quantified by using mixtures of reference compounds of calibrated concentrations.

For the continuous-flow reaction measurements, the catalyst was pretreated in He under the same conditions as those used in the pulse experiments. Then, a continuous flow of reactants was sent over the 100 mg catalyst bed at the specified

reaction temperature. The carrier gas (20 sccm) and reactant (0.25 mL/h) flow rates were adjusted to obtain a hydrocarbon concentration of 3.7 mol % in He. To monitor the evolution of H_2 production during these runs, a Microvision Plus MS was connected to the reactor outlet. To eliminate the contribution of H_2 formed during the fragmentation of the hydrocarbon feed, analysis of the continuous flow of reactants through an inert bed (acid-washed glass beads) was conducted under the same conditions. Thus, the H_2 evolution data reported in section 2.3.3 was obtained after subtracting the signal from this blank run.

2.2.4 Reaction rate calculations

Rate of nC6 reaction in a pulse was calculated as following:

$$r = X * N(A) / (W * \tau) \quad (\text{mol } g^{-1} s^{-1})$$

in which X : nC6 conversion

N(A) : pulse size of nC6 (0.5 μmol)

W : catalyst amount (g)

τ : residence time of the pulse (s)

The reaction rate of nC6 having contribution of the synergistic sites after high-temperature pretreatments can be expressed as:

$$r(HTT) = r(B) + r(syn)$$

in which r(B) : specific reaction rate (per gram) over normal BAS

r(syn): rate enhancement due to synergistic sites

2.3 Results

2.3.1 Catalyst characterization

The water evolution profiles from the CBV780 zeolite during the different thermal treatments are compared in Figure 10. The removal of physisorbed water in the low temperature range (60 – 170 °C) was practically the same in all three cases, so these data are not shown for the sake of clarity. As the treatment temperature increased, a considerable water release was observed in the mass spectrum above 450 °C, which corresponds to a mass loss of about 1.5 wt % observed in TGA. This evolution depends more strongly on temperature than on the extent of the treatment. That is, the evolution after 5 h at 450 °C (run III) was much less than that after 2 h at 600 °C (run II). This high-temperature water removal could be due either to strongly adsorbed water or a dehydroxylation reaction. This, in turn, could occur on BAS, extra-framework Al (EFAL) species, or silanol groups [98, 99].

The density of BAS for the catalyst pretreated at 600 and 450 °C was quantified from the propylene peak appearing at 350 °C in the TPD profile (Figure 11, peak a) [82]. The resulting values were practically identical (0.076 and 0.072 mmol propylene/g zeolite, respectively), which indicates that the water removal observed in the TGA experiments was not due to dehydroxylation of BAS. The observed 1.5 wt % water loss corresponds to about 0.8 mmol H_2O/g zeolite, more than ten times the total density of BAS and more than 100 times the observed decrease. On the other hand, the density of weak acid sites that adsorb IPA non- dissociatively and show a desorption peak at around 200 °C decreased when the pretreatment temperature was increased from

450 to 600 °C (Figure 11, peak b). These sites may be related to LAS or silanol groups [100, 101].

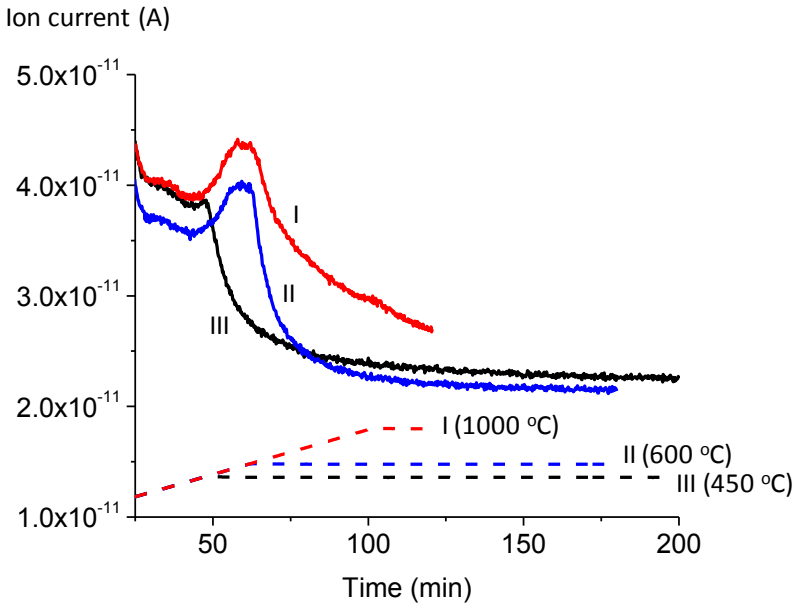

Figure 10. Evolution of water (m/z = 18, solid lines) from CBV780 zeolite during different thermal treatment profiles (dashed lines). A linear ramp of 10 °C/min was followed by an isothermal hold period at (I) 1000, (II) 600, and (III) 450 °C

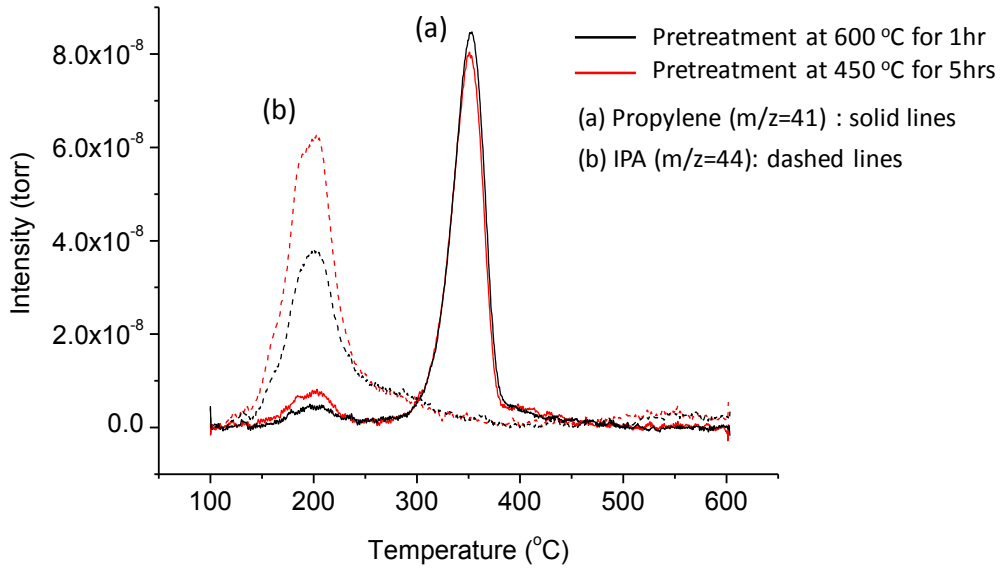

Figure 11. TPD profile of propylene (solid lines) and IPA (dashed lines) from IPA-TPD experiment of CBV780 zeolite with different thermal pretreatment conditions

2.3.2 Conversion of hexanes after different pretreatment conditions in a pulse reactor

The conversion of three different hexane isomers over CBV780 zeolite at 500 °C (n-C6) or 450 °C (3MP and 23DMB) was evaluated in the pulse reactor after different pretreatments. In these experiments, the catalyst was pretreated at different temperatures (450–600 °C) for different periods of time (1–5 h). Other reaction parameters, including carrier gas flow rate for the reaction (20 sccm) and the pretreatment (200 sccm), catalyst amount (100 mg), and size of HC pulse (0.5 μmol, 3.7 mol % HC in He), were kept constant.

As shown in Figure 12, the activity of the fresh catalyst (as seen in the first pulse) was strongly affected by the pretreatment conditions. The first-pulse conversions for all hexane isomers increased significantly when the pretreatment temperature increased from 450 to 600 °C. The enhancement in activity by high-temperature treatments (HTT) was remarkable because, as mentioned above, there was no significant change in the density of the BAS of the zeolite. This result indicates that the pretreatment of the zeolite at high temperatures generates a new active site with a very high cracking activity, which is evident with n-paraffins and iso-paraffins.

Interestingly, as shown in Figure 13, the activity enhancement of the CBV780 zeolite pretreated at high temperature diminished dramatically with subsequent hydrocarbon pulses. Moreover, the observed conversion on the high-temperature-treated (HTT) zeolite approached the conversion level of the low-temperature-treated (LTT) zeolite, which does not show any deactivation, but rather shows an increase in conversion with each subsequent pulse. As illustrated in Figure 13 a–c, similar trends were observed for all three hexane isomers. That is, regardless of the initial

pretreatment and initial activity they all reached the same conversion level for each reactant. The conversion for the initial pulses over the catalyst pretreated at 600 °C was higher than the constant conversion level, but then it decreased with increasing pulse number to a constant conversion level. By contrast, the initial conversion over the catalyst pretreated at 450 °C was lower than the constant level, but then it increased with increasing pulse number to the same value. Also, the results in Figure 13 show that the branched C6 isomers were much more active and more sensitive to the catalyst pretreatment temperature than n-C6. Interestingly, the intermediate catalyst pretreatment (500 °C for 5 h) showed activity enhancement only for the reaction with branched hexanes but not with n-C6. Similarly, the pretreatment at 600 °C for 1 h had a much more significant effect on conversion of branched isomers than it did on n-C6 (Figures 12 and 13).

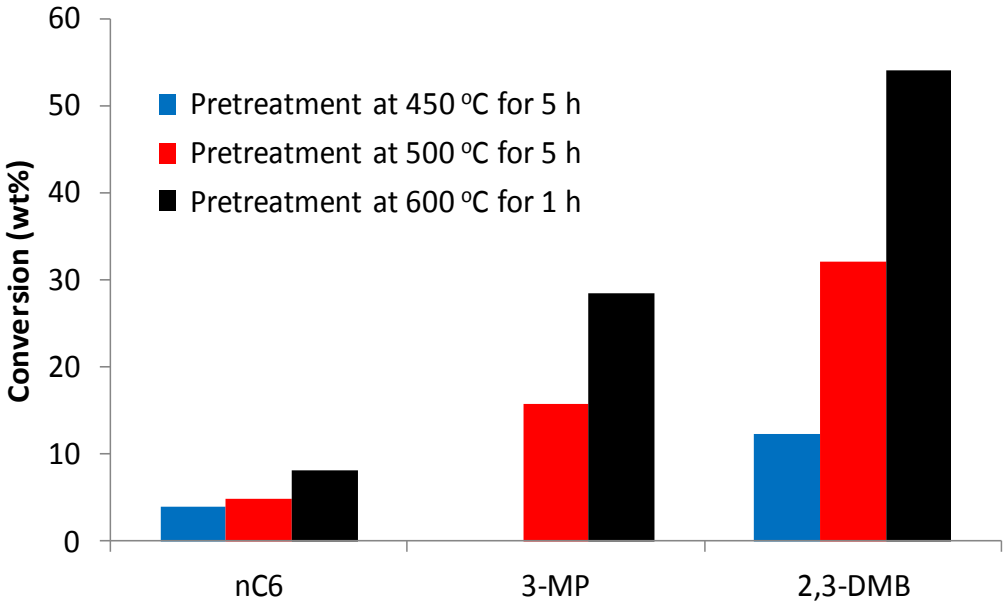

Figure 12. First-pulse conversion for n-C6 (500 °C), 3MP (450 °C) and 23DMB (450 °C) over CBV780 zeolite pretreated under different conditions

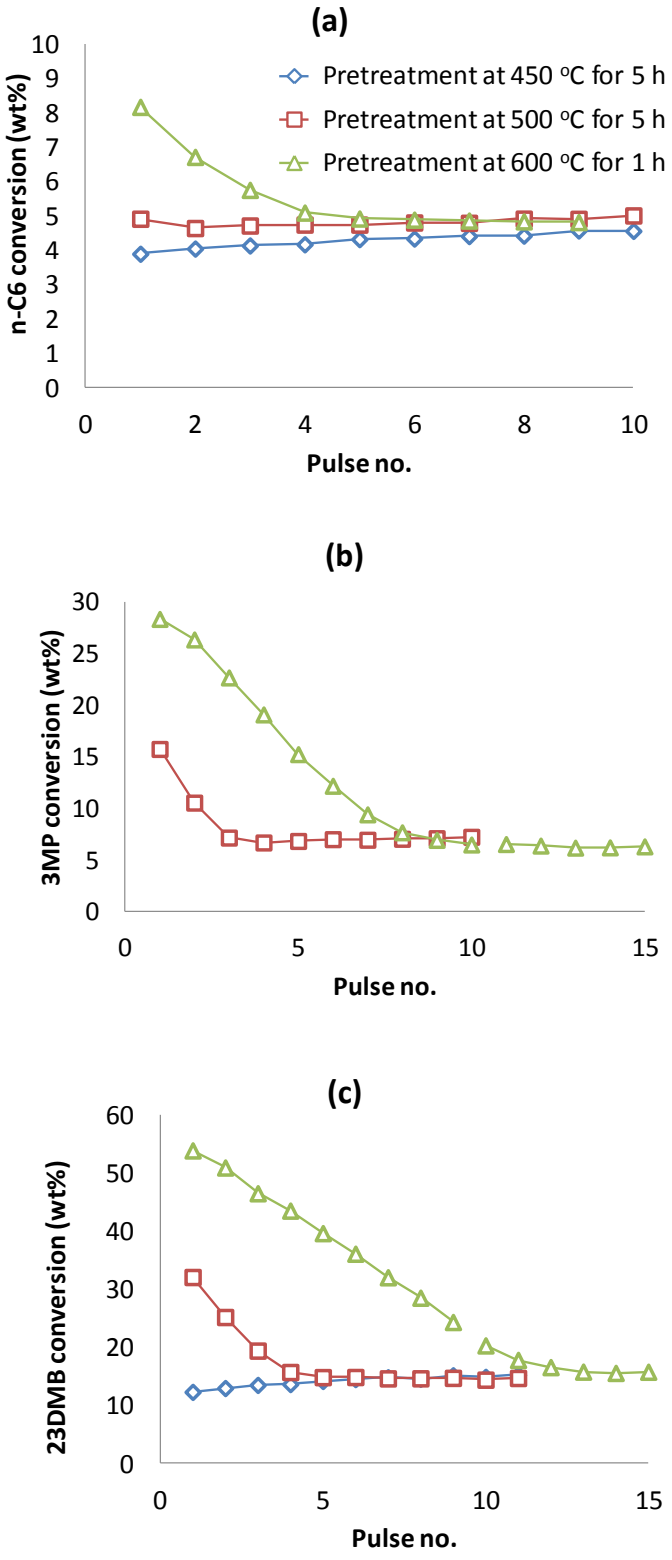

Figure 13. Conversion evolution with pulse number for (a) n-C6 (500 °C), (b) 3MP (450 °C, and (c) 23DMB (450 °C) over CBV780 zeolite pretreated under different conditions

Figure 14 shows the influence of catalyst pretreatment time on the activity of two HY zeolites with different Si/Al ratios. It is clear that the activity enhancement is not only a function of the pretreatment temperature, as shown above, but also a function of the duration of pretreatment. At a given temperature (e.g., 500 °C), the activity enhancement increases with the length of the pretreatment. For CBV780 zeolite, after about 15 h at 500 °C, longer pretreatments had very small incremental effects on cracking activity. The effect of pretreatment temperature is clearly much more pronounced than the effect of pretreatment length. For instance, pretreating the catalyst for only 1 h at 600 °C resulted in a stronger enhancement in activity than pretreating for 20 h at 500 °C (Figure 13a). It is important to note that the activity enhancement was not only evident with the dealuminated zeolite (CBV780, Si/Al = 40) but also with the high-alumina zeolite (CBV600, Si/Al = 2.6), as shown in Figure 14b.

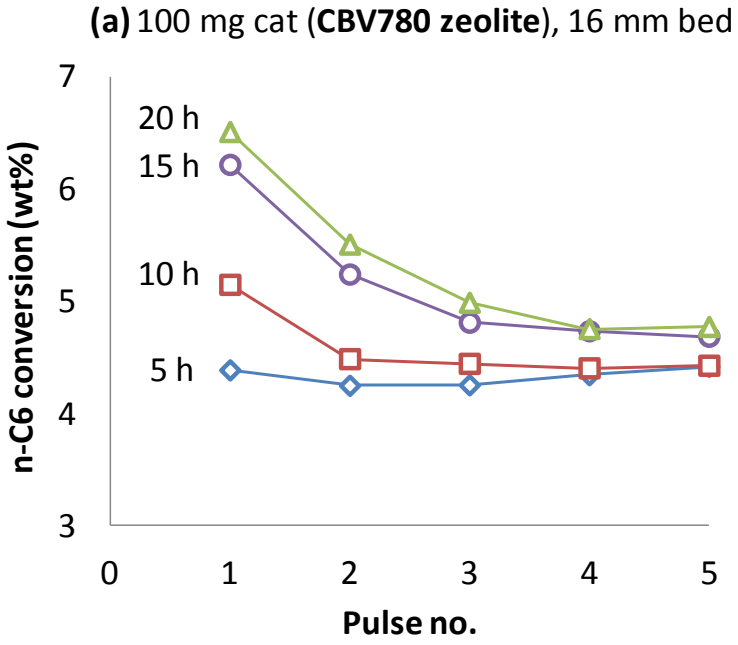

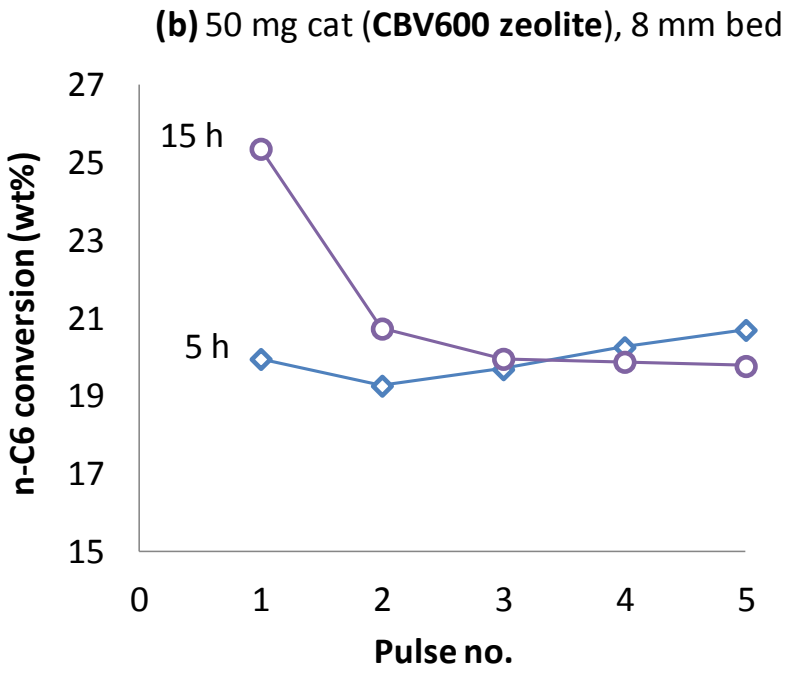

Figure 14. Conversion change with pulse number for n-C6 at 500 ^{o}C over (a) CBV780 and (b) CBV600 zeolites pretreated at 500 ^{o}C for different durations

The extent of activity enhancement on the two zeolites deserves some discussion. Although the relative enhancement is stronger for CBV780 than for CBV600, the absolute increase in activity was more pronounced for the high-alumina zeolite. That is, when the pretreatment time increased from 5 to 15 h, the initial n-C6 conversion increased by about 50% for CBV780 zeolite (low acid density) and only 25% for the CBV600 zeolite (high acid density), relative to the stable conversion. This result suggests that instead of an increase in the intrinsic activity of all the BAS in the zeolite, a finite number of new active sites is generated by the HTT. However, the absolute increase in conversion was higher for the CBV600 than for the CBV780 zeolite. That is, one can conclude that the density of the newly created sites is related to the density of BAS.

As shown in the Figure 14, for n-C6 reaction over CBV780 and CBV600 zeolites pretreated at 500 ^{o}C for 15 hrs, the conversion at the 5th pulse can be considered as the reaction over normal BAS only (e.g., r(B)), while the conversion at the 1st pulse has significant contribution of the synergistic sites (e.g., r(HTT)). Hence, rate enhancement due to synergistic sites generated at high temperature treatment at the 1st pulse can be calculated as following: r(syn) = r(HTT) – r(B)

As shown in table 2, the initial rate of n-C6 conversion for the CBV780 zeolite at 500 °C after pretreatment at 500 °C for 15 h, r(HTT), can be calculated as 3.97×10^{-7} mol g^{-1} s^{-1}. Similarly, the r(B) for this catalyst is 3.08×10^{-7} mol g^{-1} s^{-1}. Consequently, the difference is the contribution of the synergistic sites, r(syn) = 0.89×10^{-7} mol g^{-1} s^{-1}. A similar calculation done for the results obtained with the CBV600 zeolite shows that the r(syn) for this catalyst is 1.28×10^{-6} mol g^{-1} s^{-1}, an increase that is 12 times larger than that for CBV780. This result is comparable to the increase in the density of BAS in the CBV600 relative to the CBV780. Therefore, it is reasonable to conclude that the number of newly created sites is roughly proportional to the number of BAS.

Table 2. Calculated reaction rates for n-C6 conversion over CBV780 and CBV600 zeolites pretreated at 500 ^{o}C for 15 hrs

Catalyst	CBV780 (HY, Si/Al = 40)		CBV600 (HY, Si/Al = 2.6)	
Pulse number	1	5	1	5
X	0.062	0.048	0.250	0.200
W (g)	0.1	0.1	0.05	0.05
τ (s)	0.8	0.8	0.4	0.4
r (mol g^{-1} s^{-1})	3.97×10^{-7}	3.08×10^{-7}	6.41×10^{-6}	5.13×10^{-6}
r(syn)	0.89×10^{-7}		1.28×10^{-6}	

It is important to note that the HTT not only modifies the activity level, but also has an effect on the distribution of cracking products. For example, Figure 15 shows the evolution of reaction products from n-C6 cracking over the CBV780 zeolite. After five pulses the effect of pretreatment on product distribution disappears, but some important differences are evident between the samples pretreated at 500 and 600 °C, as clearly observed during the initial pulses.

Cracked products (C2–C5 olefins and C1–C5 paraffins) were the major yield from n-C6 cracking, while small amounts of hexenes (C6=) and light aromatics (i.e., benzene, toluene, xylenes and ethylbenzene) were also produced. Isomerization products (C6) were not observed in the reaction of n-C6. For the sample pretreated at 600 °C the initial selectivity to paraffinic products, particularly ethane (C2) and propane (C3), was drastically lower, but the selectivity to olefinic and aromatic products increased. Among olefinic products, only propene (C3=) selectivity decreased, while ethene (C2=) and butenes (C4=) increased, resulting in an overall increase in olefinic products. However, in parallel with the trends observed in activity, the selectivity variations disappeared after several reactant pulses were injected over the catalyst.

Similar behavior and product selectivity changes with increasing pulse numbers were observed in the experiments conducted with branched hexane feeds. Thus, for the sake of clarity, Figures 16 and 17 only show the variation of product selectivity with pulse number for the reaction of 3MP and 23DMB, respectively, over the CBV780 zeolite pretreated at 600 °C.

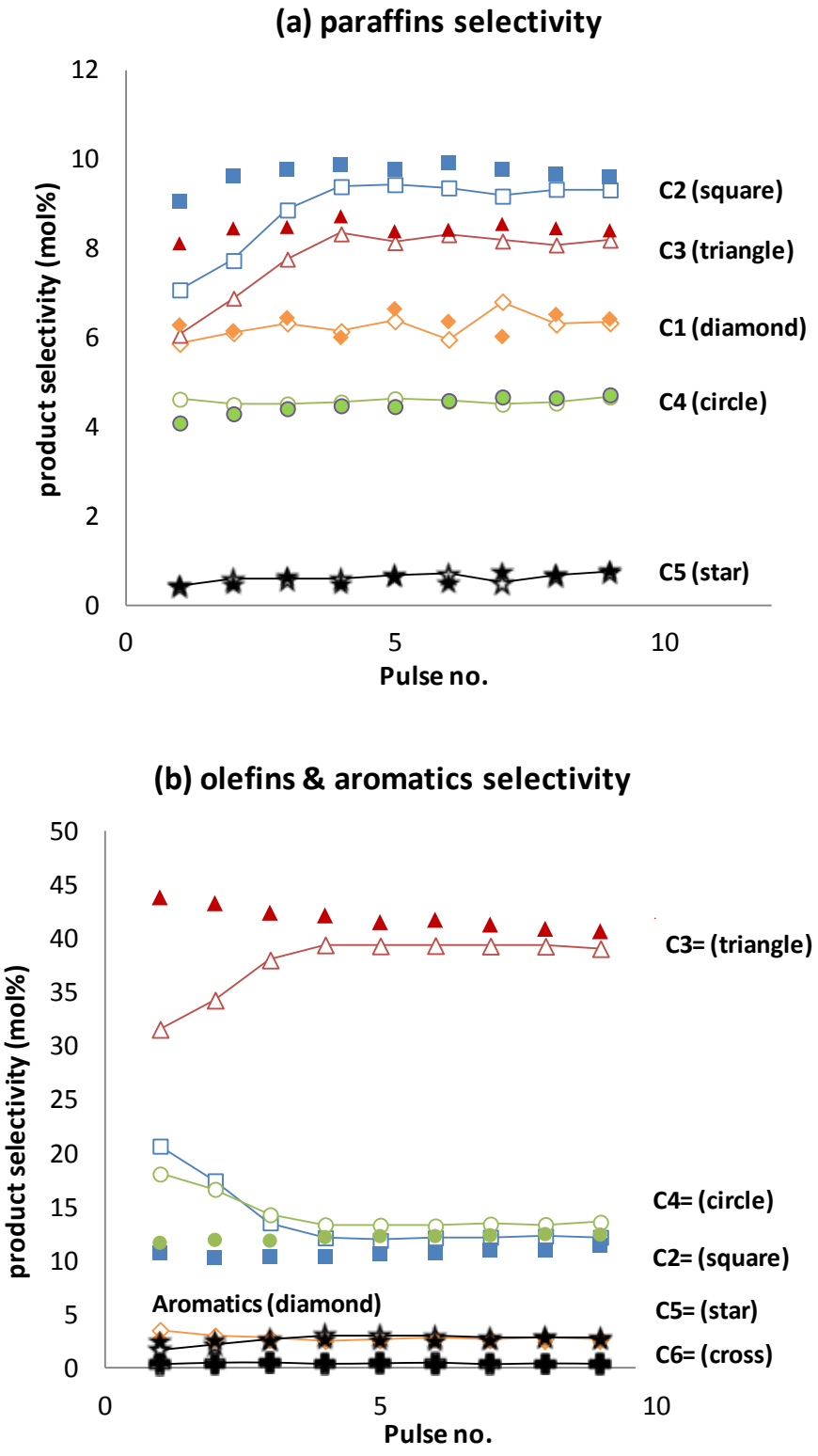

Figure 15. Product selectivity change with pulse number in n-C6 reaction at 500 ^{o}C over CBV780 zeolite pretreated at 500 ^{o}C for 5 h (solid symbol), and at 600 ^{o}C for 1 h (opened symbol + line)

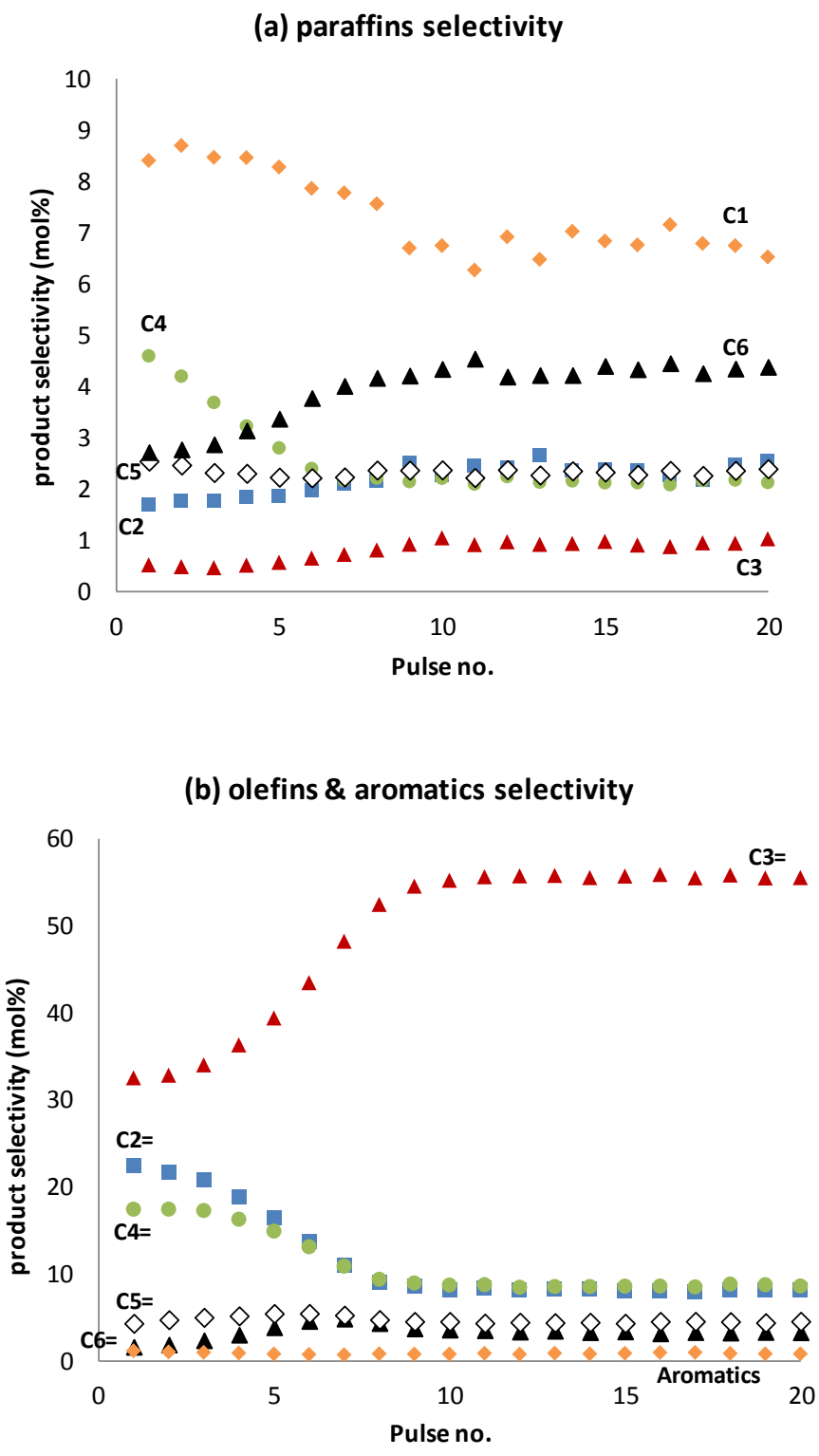

Figure 16. Product selectivity change with pulse number in 3MP reaction at 450 ^{o}C over CBV780 zeolite pretreated at 600 ^{o}C for 1 h

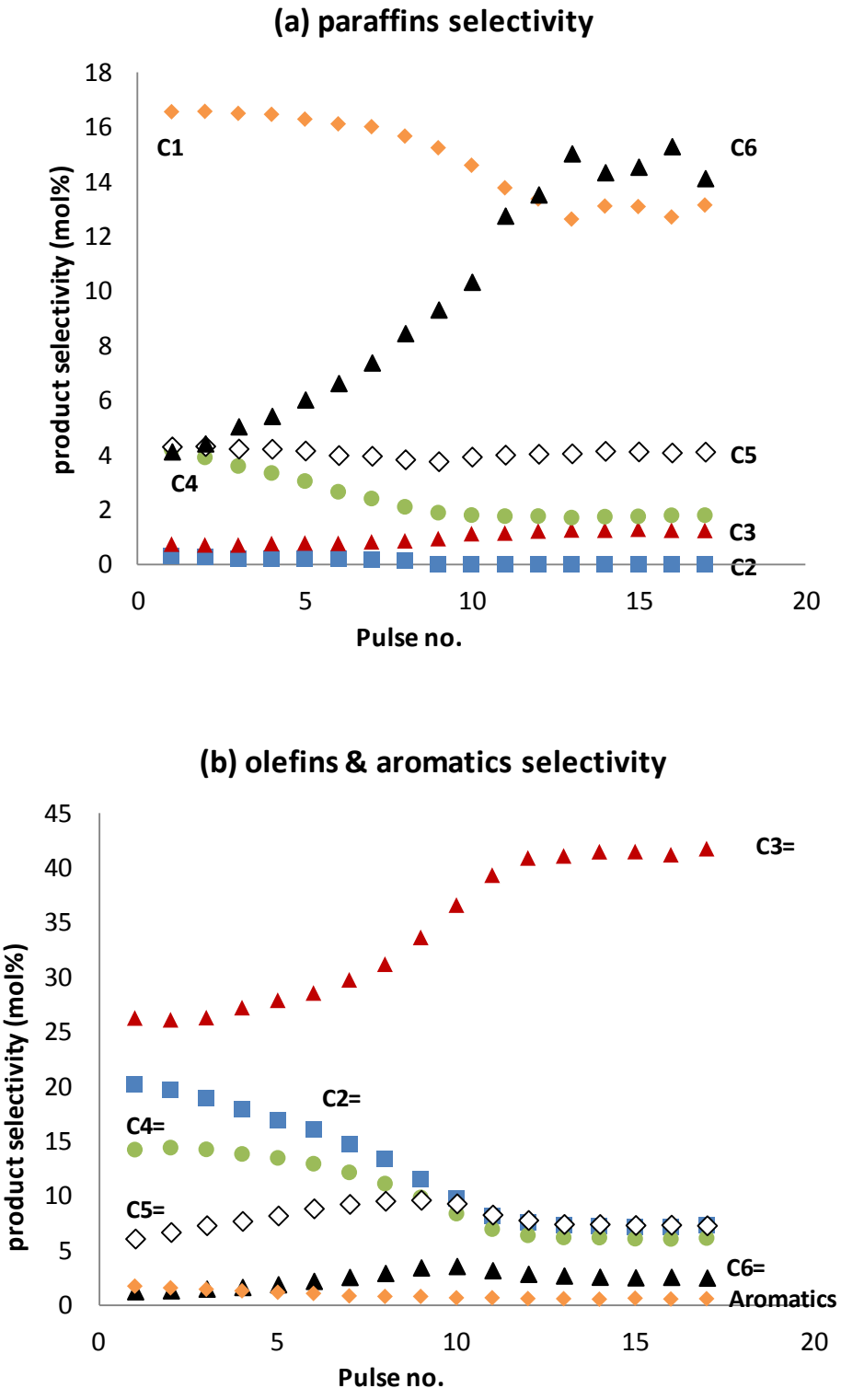

Figure 17. Product selectivity change with pulse number in 23DMB reaction at 450°C over CBV780 zeolite pretreated at 600°C for 1 h

The results for the 3MP and 23DMB reactions show similar trends but contrary to those with n-C6. The reactions of 23DMB and 3MP mainly yielded isomerization products, which was the expected result. The ability of the reactants to transfer hydrides facilitates the isomerization pathway, and the tertiary carbons in 23DMB and 3MP are known to be much better hydride donors than the secondary carbons in n-C6. The isomerization of the hexyl carbenium ions followed by hydride transfer from the reactants leads to the formation of hexane isomers [102]. The analysis of changes in product selectivity with pulse number for the branched C6s becomes more complicated because of the contribution of isomerization products and their cracked secondary products. However, some trends are clear. For example, the amount of C6 products decreased significantly in the first few pulses of the HTT catalyst, while selectivity to methane (C1) and butanes (C4) increased considerably. At the same time, the selectivity to pentenes (C5=) and hexenes (C6=) went through a maximum with pulse number; C2= and C4= decreased with the number of pulses injected, while C3= increased.

As a result of product selectivity change with catalyst pretreatment conditions, olefinicity of the cracking products was also changed. To quantify the olefinicity of the cracking products after the different pretreatments we can analyze the variation of the olefin to paraffin (O/P) molar ratio in the C1–C5 products (i.e., not including isomerization products). The variation of the O/P ratio as a function of pulse number is shown in Figure 18 for the reaction of n-C6 and 23DMB after different pretreatment conditions. The trends for 3MP (not shown) were very similar to those of 23DMB. The opposing trends for the linear and branched paraffins are evident. Although the O/P

ratio decreased as activity enhancement diminished for the case of n-C6, it increased for the reaction of branched isomers. The HTT led to an increased O/P ratio for the n-C6 cracking but a decreased ratio for the branched hydrocarbons. However, with both reactants, when comparing the 600 °C treated catalyst with the 500 °C one, the decreased selectivity toward C3= was compensated for by production of additional C2= and C4=. Thus, the total selectivity to olefinic products either did not change (in the 3MP reaction) or slightly increased (in the n-C6 and 23DMB reactions). In fact, the selectivity to paraffinic products caused the difference in O/P between linear and branched hexanes. Although the selectivity to paraffins decreased (mostly to C2 and C3) in the n-C6 cracking, it increased (mostly to C1 and C4) in the cracking of the branched hydrocarbons (3MP and 23DMB).

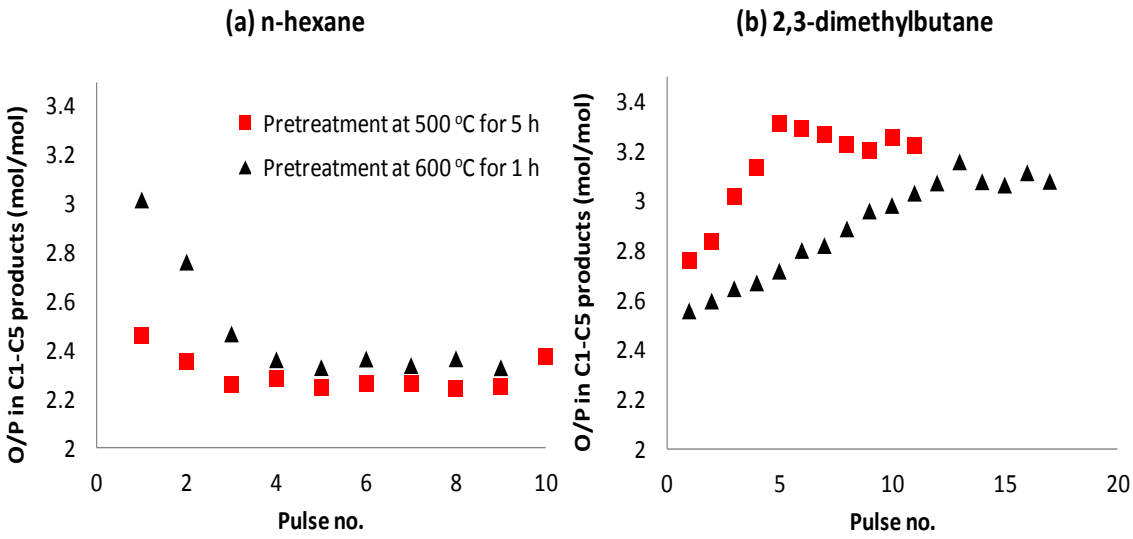

Figure 18. Variation of olefins/paraffins ratio (O/P) in cracked products (C1–C5) with pulse number in (a) n-C6 reactant (500 °C), and (b) 23DMB reactant (450 °C) over CBV780 zeolite pretreated at two different conditions

These results demonstrate that the catalyst pretreatment severity not only can enhance the activity, but also has a significant effect on product distribution. Of course, it can be argued that removal of adsorbed water at high pretreatment temperature might activate more BAS and result in higher conversions, leading to changes in product selectivity. Therefore, it is important to investigate the changes in product distribution caused by changes in conversion due to the thermal pretreatment compared to those changes obtained by simply varying the amount of catalyst exposed to the reactant pulse. This comparison is made in Figures 19 and 20 for n-C6 and 23DMB reactions respectively, which shows the variation of product selectivity with conversion over the fresh CBV780 zeolite catalyst (i.e., 1^{st} pulse) under different severity pretreatments and with conversions over normal BAS (i.e., 5^{th} pulse) when changing the catalyst amount. It is clear that the observed changes in product distribution resulting from varying the pretreatment severity are not due to changes in conversion. For instance, the product distribution hardly changed for the n-C6 runs when the conversion was increased by increasing the amount of catalyst (Figure 19I). Hence, the reaction pathways were not affected by the number of normal BAS in the system. In contrast, when the conversion was increased by increasing the extent of pretreatment (Figure 19II), the variations were significant (i.e., considerable decrease in C2 and C4, C3= decreased while C2= and C4= increased significantly). In consequence, the O/P ratio in the products increased considerably with the conversion when catalyst pretreatment severity was increased. Similarly, for the branched alkane the only change with conversion was further cracking of C6 isomers forming more C3= when the catalyst amount was increased. And slight increase in C4 and C5 products might also indicate more contribution from hydride

transfer when BAS density was increased (Figure 20I). But the opposite result was observed when the conversion was varied by pretreatment (Figure 20II). Besides some similar change in product selectivity with n-C6 reaction, significant increase in C1 was also observed. The contrasting trends indicate that the activity enhancement caused by high-temperature pretreatments results in changes in the reaction pathway and supports the hypothesis of the generation of new active sites instead of just increasing the number of conventional BAS.

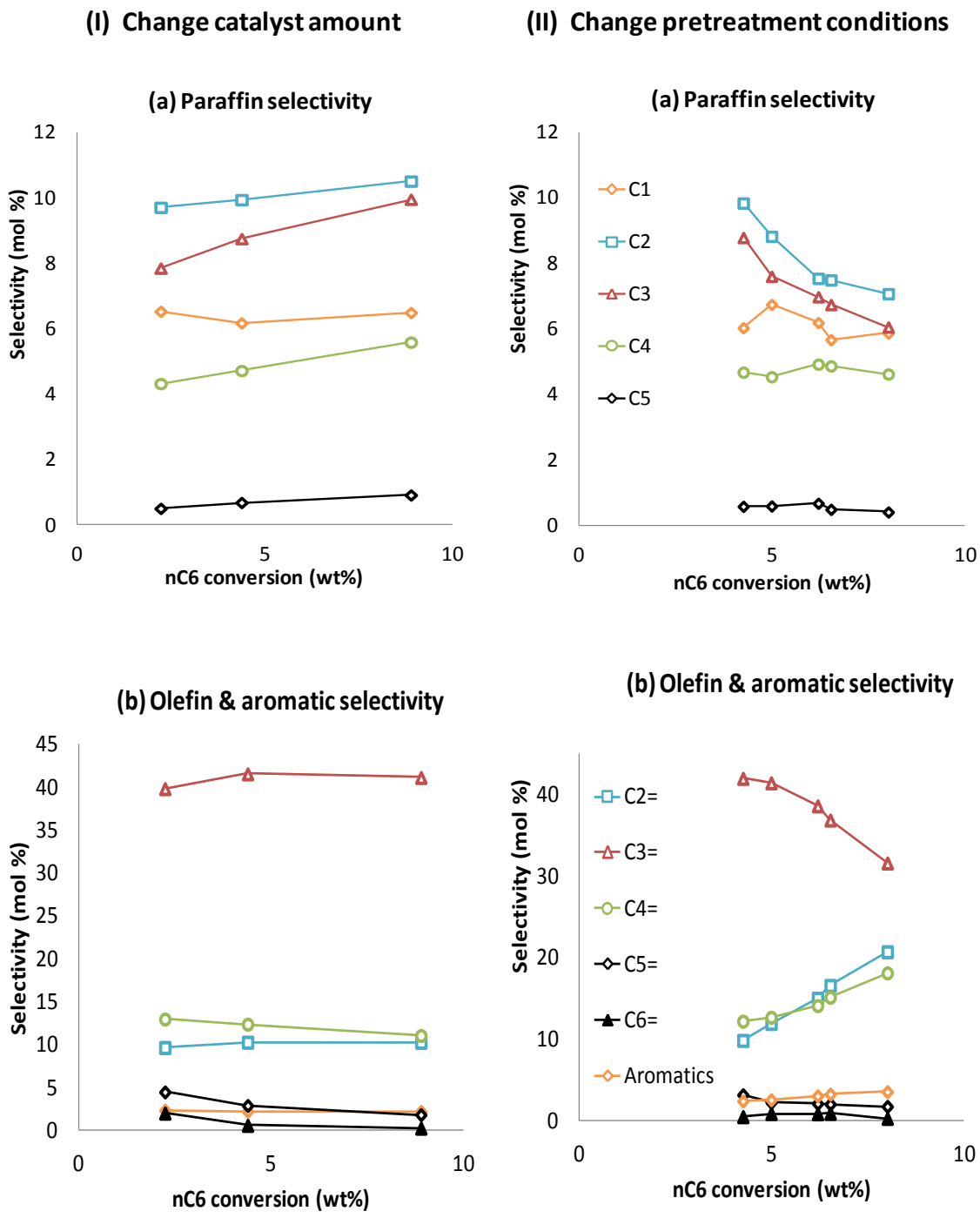

Figure 19. Change of product selectivity with feed conversion in n-C6 reaction at 500 ^{o}C over CBV780 zeolite. Difference between varying the catalyst amount vs. varying the pretreatment condition

(I) : product selectivity change by varying catalyst amount (50 – 200 mg), data at the 5th pulse

(II) : product selectivity change by varying pretreatment conditions, data at the 1st pulse (100 mg catalyst)

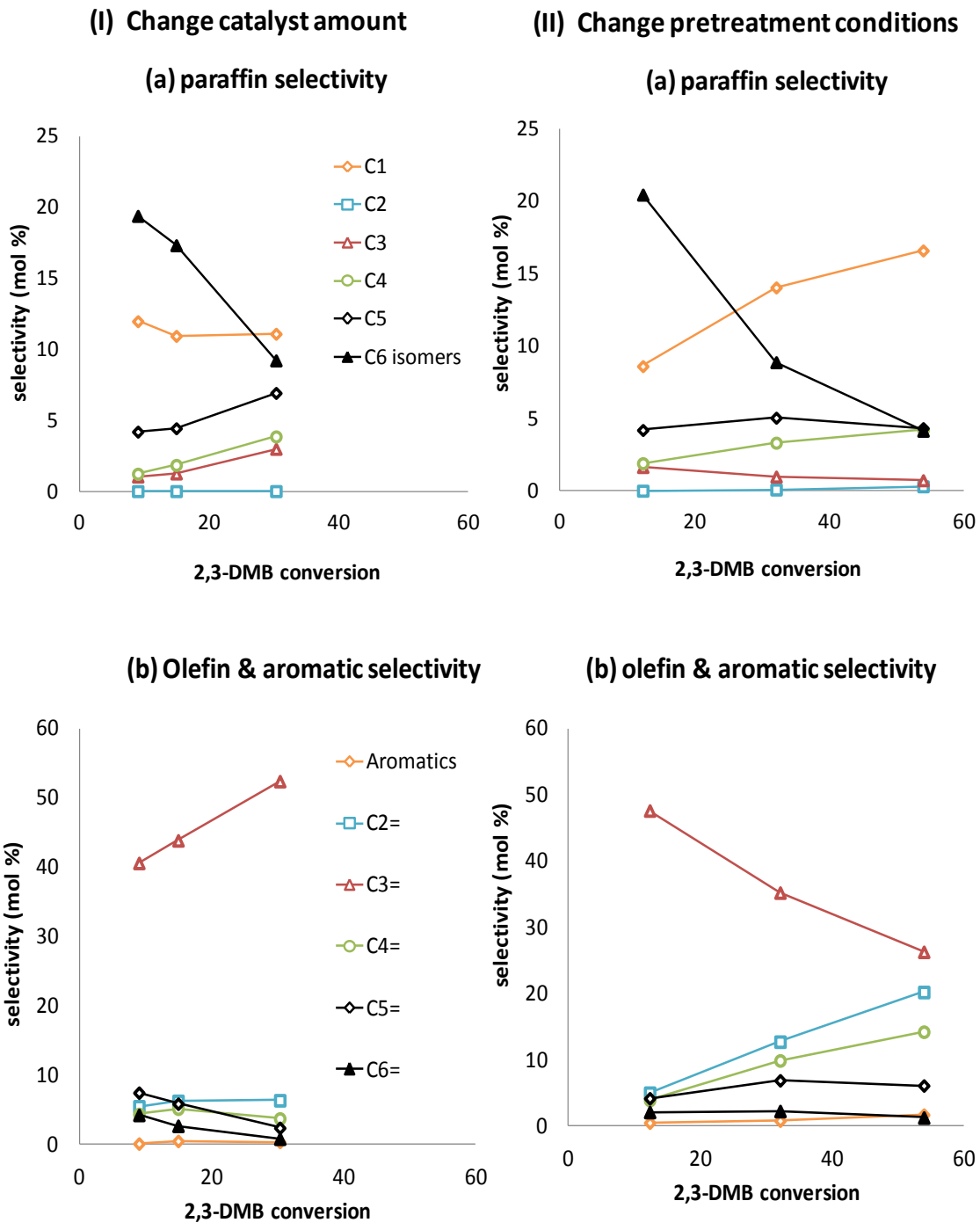

Figure 20. Change of product selectivity with feed conversion in 23DMB reaction at 450 ^{o}C over CBV780 zeolite. Difference between varying the catalyst amount vs. varying the pretreatment condition

(I) : product selectivity change by varying catalyst amount (50 – 200 mg), data at the 5th pulse

(II) : product selectivity change by varying pretreatment conditions, data at the 1st pulse (100 mg catalyst)

2.3.3 Conversion of hexanes after different pretreatment conditions in a continuous flow reactor

In addition to the studies in the pulse reactor, the cracking reaction of the various hexane isomers was investigated in the continuous-flow reactor. Special attention was paid to the formation of H_2 and CH_4 during cracking. After each thermal pretreatment, the catalyst was kept under a flow of pure He at the selected reaction temperature. When the baseline was stable, the pure He flow was switched to the mixture of 3.7 mol % reactant in He, and the evolution of H_2 and CH_4 was monitored by online MS. Because the fragmentation of hexanes in the MS also yields H_2 and many hydrocarbon fragments (data not shown), the H_2 (m/z = 2) intensity measured under catalytic reaction conditions was corrected by subtracting the H_2 (m/z = 2) intensity obtained when the feed was passed over an inert bed under the same conditions. A similar correction was applied for the CH_3 (m/z = 15) fragment. The corrected H_2 and CH_3 intensities for continuous-flow reactions of n-C6 and 23DMB over CBV780 zeolite pretreated at different conditions are shown as a function of time on stream in Figure 21. Significant amounts of H_2 were observed during the reaction of n-C6 over the CBV780 zeolite pretreated at 600 °C, but almost no H_2 formation occurred on the CBV780 zeolite pretreated at 450 °C (Figure 21a). Dehydrogenation of the feed clearly occurs over the HTT catalyst during the first 30 min of flow. In contrast, the hydrocarbon fragment practically did not change between HTT and LTT pretreatment conditions (Figure 21b). With 23DMB as a feed, the HTT catalyst showed significant evolution of both H_2 and CH_3– fragments (Figures 21c and 21d). The increased CH_3 intensity can be correlated to the initial high conversion and selectivity to methane, as

observed in the pulse experiment over the HTT catalyst; at the same time, the first sharp peak of H_2 intensity is most likely due to H_2 produced from the monomolecular dehydrogenation of the feed, which is similar to the n-C6 reaction.

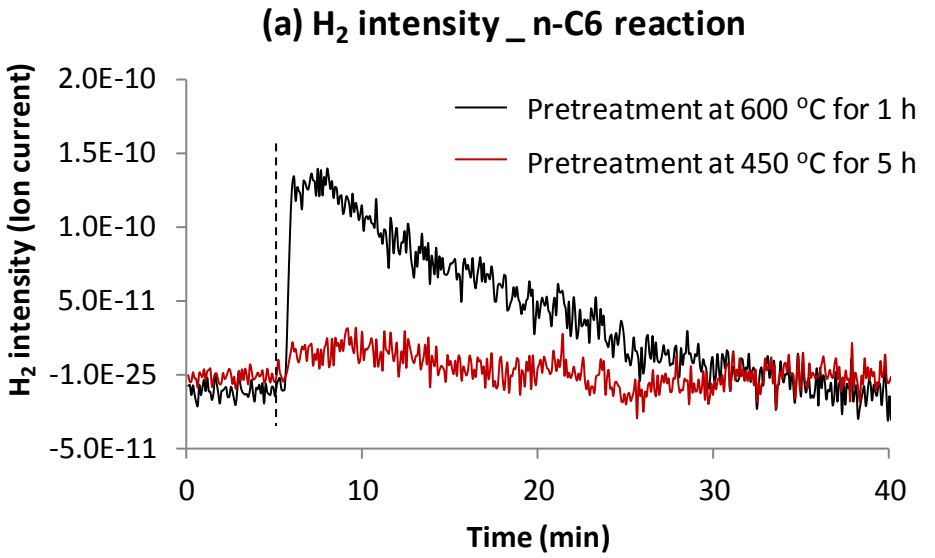

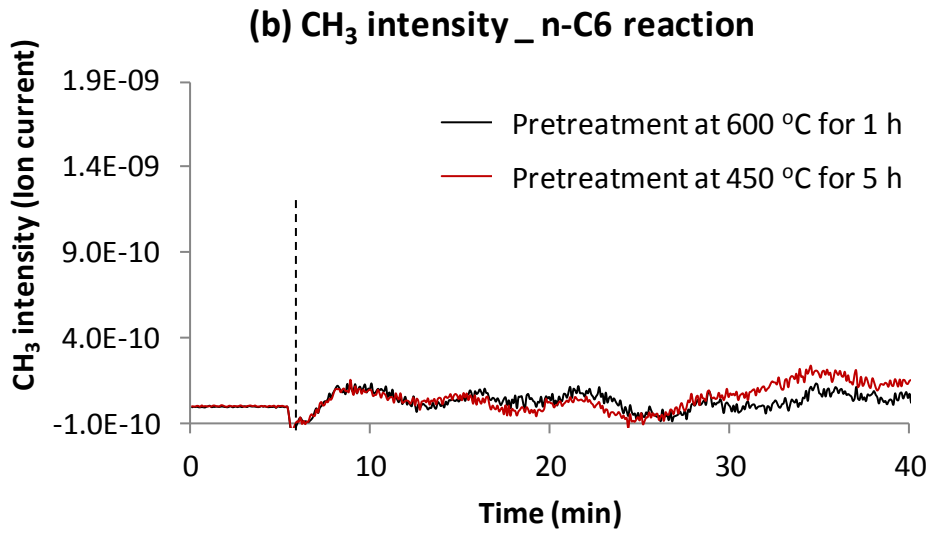

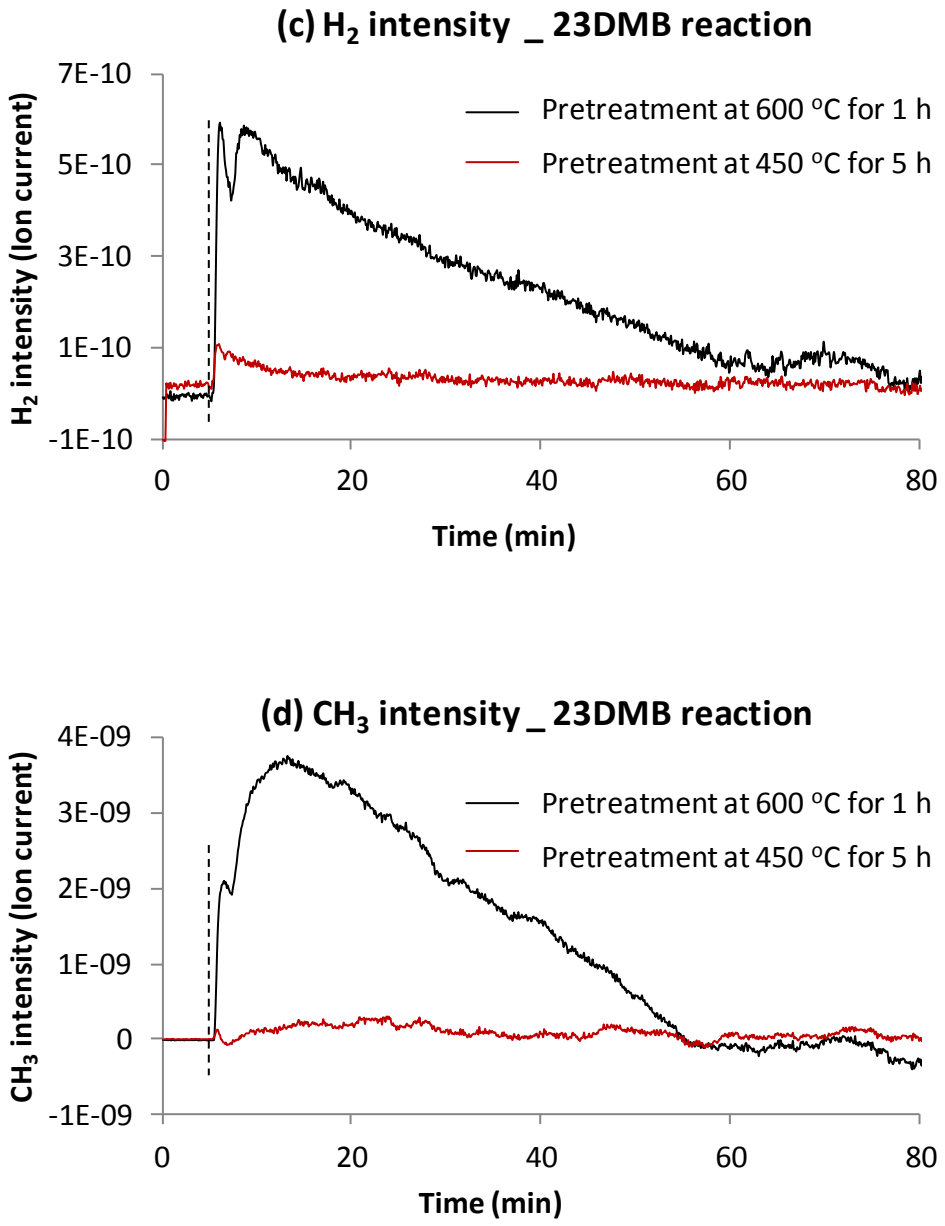

Figure 21. Change of normalized H_2 (m/z = 2) and CH_3 (m/z = 15) intensities with time on stream in a continuous flow reaction of n-C6 at 500 °C (a,b) and 23DMB at 450 °C (c,d) over the CBV780 zeolite pretreated at different conditions. The dashed line indicates the time of switching from pure He to reactant flow.

A summary of the changes in product selectivity observed upon increasing catalyst pretreatment severity (i.e., temperature and time) is presented in Table 3. In

general, for all of the hexane isomers the HTT not only enhances catalyst activity but also favors the dehydrogenation pathway. The molecular structure of the reactant has an effect on the extent of changes caused by HTT. In the cracking of n-C6, HTT enhanced only the dehydrogenation products. However, with the branched hydrocarbons the HTT caused an increase in the production of methane, indicating an enhancement in the protolytic cracking.

Table 3. Effect of increasing catalyst pretreatment severity to product selectivity

	n-hexane	**3-methyl pentane**	**2,3-dimethyl butane**
Paraffins	Decreases in C2 & C3	Increases in C1 & C4 Slight decrease in C3 Decrease in C6	Increase in C1 Slight increase in C4 Slight decrease in C3 Significant decrease in C6
Olefins	Increases in C2= & C4= Decrease in C3=	Increases in C2= & C4= Decreases in C3= Maxima in C5= & C6=	Increases in C2= & C4= Decreases in C3= Maxima in C5= & C6=
Aromatics	Slight increase	Very low selectivity No change	Very low selectivity No change
Hydrogen	Increase	N/A	Increase
O/P in cracked products (C1-C5)	Increase	Decrease	decrease
O/P in total products	Increase (similar in cracked product since no isomerization occur)	Slight decrease (C6 selectivity drops less significantly than in 2,3DMB reaction)	Slight increase (mainly due to significant decrease in C6 isomer selectivity)

2.3.4 Regeneration of the synergistic active sites created by HTT

To study whether the activity of the synergistic active sites created by HTT can be regenerated by desorption of strongly adsorbed species, after the HTT catalyst lost its initial (enhanced) activity during the first set of 10 n-C6 pulses, the catalyst was flushed in a high flow rate (200 mL/m) of pure He at 500 °C for 3 h. As shown in Figure 22, the next n-C6 pulse injected after the regeneration resulted in essentially the same high activity as the first pulse in the series. With subsequent pulses, the activity decreased at practically the same rate as that observed on the fresh HTT catalyst. Also, as shown in Figure 23, the initial product selectivity was recovered after the regeneration.

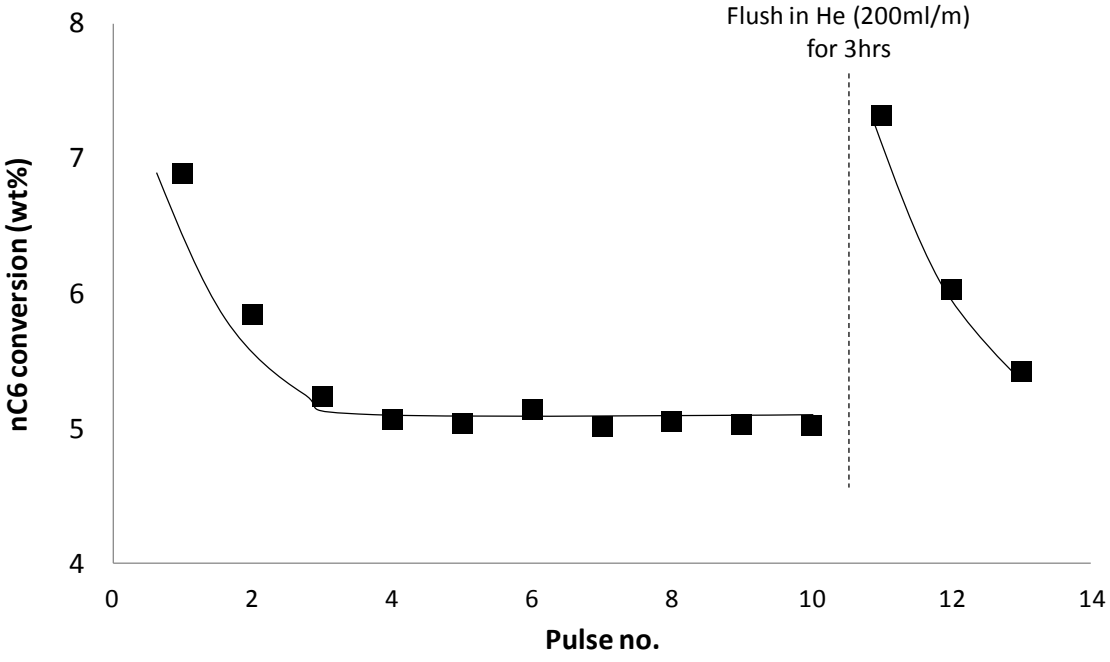

Figure 22. Conversion change with pulse number in n-C6 reaction at 500 °C over CBV780 before and after catalyst regeneration by thermal treatment. The catalyst was pretreated in He flow (200 sccm) at 500 °C for 20 hours

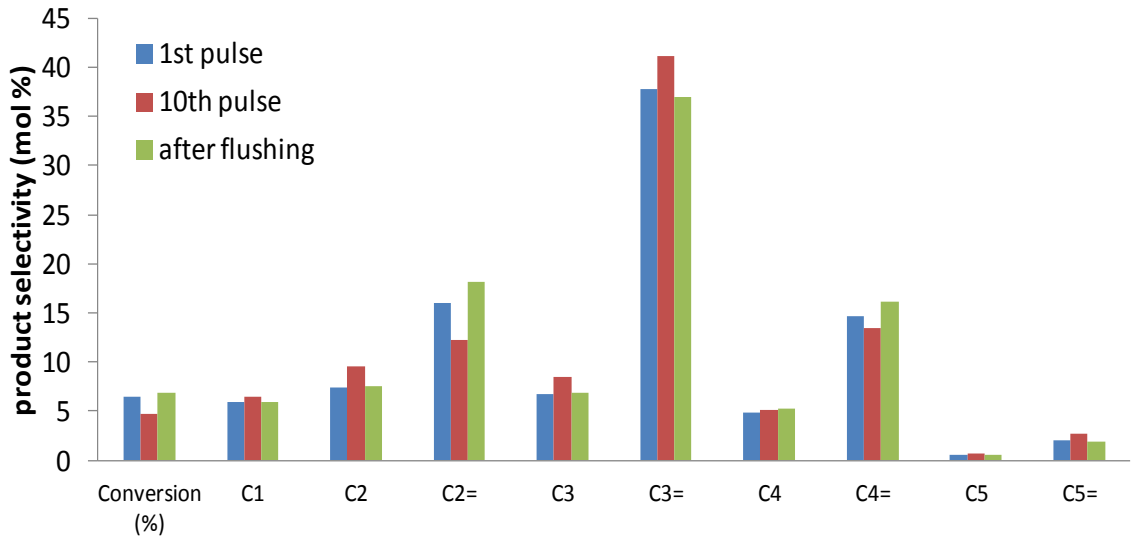

Figure 23. Product selectivity in the 1st and 10th pulses and after flushing in Helium flow (200 sccm) in n-C6 reaction at 500 °C over CBV780

2.3.5 Conversion of olefins after different pretreatment conditions

In marked contrast to the behavior observed with paraffins, the thermal pretreatment of the zeolite did not show any activity enhancement in the reactions of olefins. Figures 24 a and b show the evolution of conversion with pulse number in the reactions of C3= and 2M2P, respectively, when pretreated under different conditions. Data for the reaction of 2M2P over the catalyst without any thermal pretreatment are also included. No increase in conversion of the olefins was observed after HTT. The conversion of 2M2P even decreased slightly with the catalyst pretreated at 600 °C compared to the one pretreated at 500 °C or even without pretreatment.

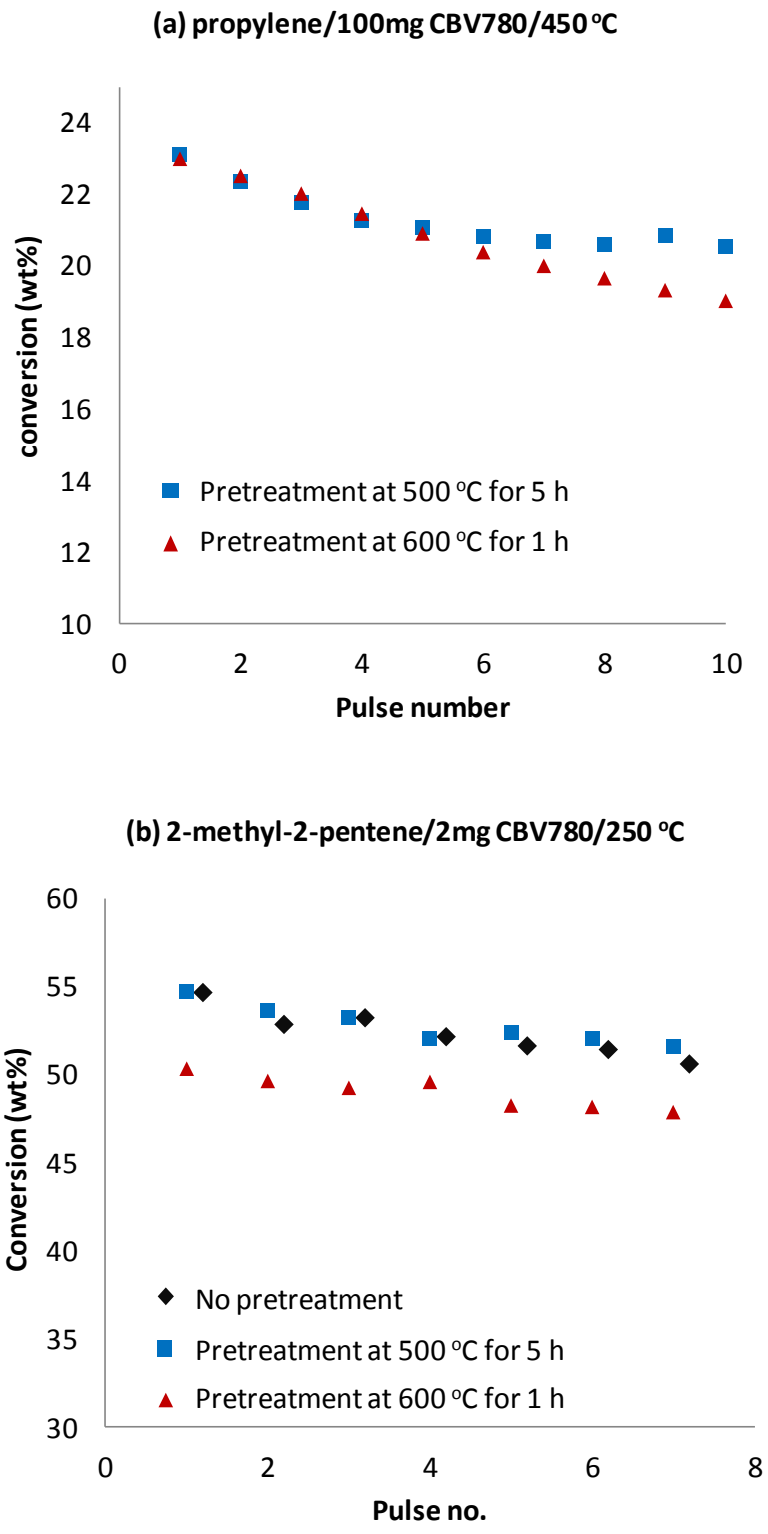

Figure 24. Evolution of conversion with pulse number for (a) propylene (C3=) at 450 °C; and (b) 2-methyl-2-pentene (2M2P) at 250 °C, over CBV780 zeolite pretreated at different conditions

As these results show, the new sites generated by the HTT that show unique activity for the reaction of paraffins do not display any enhancement for the reaction of olefins. Also, a decrease in conversion with pulse number, probably due to the formation of oligomers and coke [103, 104] was observed for the reaction of olefins. It must be emphasized that with the paraffin feeds the synergistic sites created by HTT rapidly deactivated, but the conventional BAS kept their activity after subsequent pulses. In contrast, with the olefin feeds a uniform deactivation was observed, regardless of the pretreatment temperature. Also, the product distribution for the reactions with olefins (not shown) did not change with the pretreatment severity.

2.4 Discussions

2.4.1 New active sites generated by high-temperature pretreatment of the zeolite

We have clearly shown that a high-temperature pretreatment significantly enhances the activity of HY catalysts for the cracking of hexane isomers. However, this enhancement is only apparent on the freshly treated HTT catalyst, and it diminishes as additional hydrocarbon pulses are sent over the catalyst. Interestingly, after a few pulses a stable conversion level is reached, which is the same level as that obtained on the catalyst pretreated at lower temperatures. Furthermore, the enhanced activity is accompanied by a significant change in product distribution. Along with conversion, the changes in product selectivity were observed only on the initial pulses, and the differences diminished with subsequent pulses, reaching essentially the same product distribution as that obtained without the HTT. An important result shown in Figures 19 and 20 is that the variation of product distribution with conversion (enhanced by HTT)

is the opposite of that obtained by simply adding more active sites. This difference indicates that HTT generates new active sites with different properties from those of the normal BAS. In line with these results, high initial alkane conversions have previously been observed on freshly treated zeolites [105-107]. Also, these enhanced activities were observed to quickly decrease after a short time on stream, reaching a stable conversion. The high-temperature pretreatment used on those catalysts before reaction, that is, 580 °C in a stream of air [106, 107], might be responsible for the observed enhanced initial activity, as shown here.

To describe the nature of these synergistic sites, we must emphasize the correlation between the dehydroxylation of the zeolite observed by TG-MS analysis and the enhancement in activity. In fact, the generation by dehydroxylation of LAS, which interact synergistically with BAS, has been widely proposed in the literature to explain the enhanced activity upon HTT [93-97]. The nature of the synergistic sites thus created depends on the type of LAS involved. For example, Gonzales et al. [96] have shown that trigonally coordinated Si atoms directly connected to the acidic OH group can cause the highest enhancement in BAS strength. In contrast, Li et al. [97] have proposed that the $Al(OH)_3$ and $Al(OH)^{2+}$ species adjacent to the acidic OH group in the supercage reduced the proton affinity of the BAS more than the others. Dehydroxylation of BAS and further framework dealumination, as shown in below scheme, can result in formation of LAS [99, 108]. The resulting non-framework alumina species can occur in different forms, such as oxoaluminum cations (AlO^+, $Al(OH)_2^+$, and $AlOH^{2+}$), neutral species (AlOOH and $Al(OH)_3$), or an alumina cluster having boehmite-type topology inside the supercage of the HY zeolite [109].

Moreover, dehydroxylation of silanols to form trigonally coordinated Si has also been proposed as a source of LAS [99].

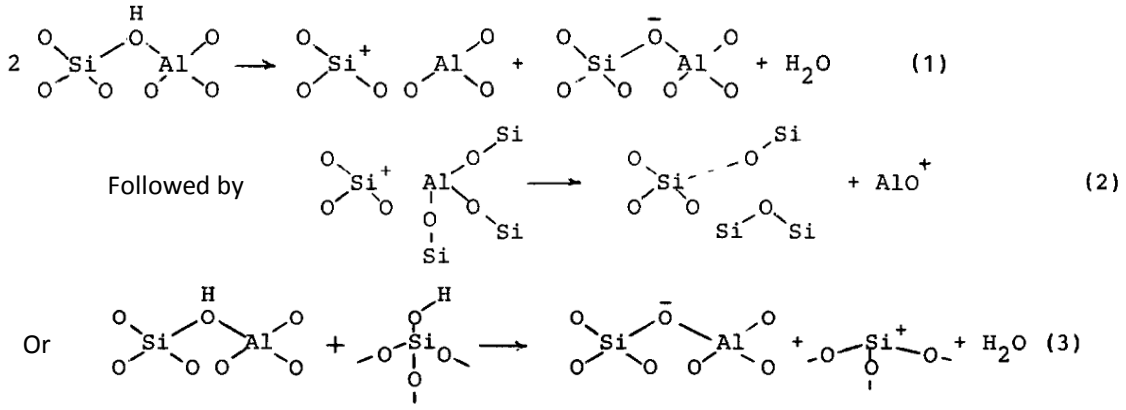

Scheme – Dehydroxylation of BAS and silanol groups in zeolite. Reprinted from [99].

Our IPA–TPD measurements (Figure 11a) strongly suggest that the observed dehydroxylation upon HTT does not involve the BAS because the density of these sites is practically unaffected by the HTT. On the other hand, the reduction in sites that adsorb IPA weakly (Figure 11b) might indicate that dehydroxylation is associated with nonframework alumina or silanol species, which are responsible for nondissociative IPA adsorption/desorption. As a result, we may conclude that the synergistic sites responsible for the observed enhancements in paraffin cracking may be a combination of these dehydroxylated species with adjacent BAS, as proposed in previous studies [96, 97].

Another interesting result reported here is that the activity enhancement upon generation of these synergistic sites was not observed in the reaction of olefins (Figure 24). This result illustrates the uniqueness of the synergistic sites in catalyzing the protolytic reaction pathways of paraffins, rather than the carbenium ion path.

Protonation of an olefin is a fast reaction [70] with a much lower energy barrier than the protonation of a paraffin [110]. Hence, while protonation of paraffins is the rate-determining step in paraffin cracking [107], this is not the case for the reaction of olefins. That is, increasing the protonation ability of a BAS by synergism with a LAS would enhance the rate of conversion of paraffins but not of olefins.

We must note that the conversion on the HTT catalysts drops rather quickly (with only a few pulses). However, the size of each pulse is rather small compared to the amount of catalyst (i.e., reactant/BAS molar ratio ~ 0.07). Thus, one can infer that the number of synergistic sites responsible for the high activity should account for only a small fraction of the total acid sites, and they quickly deactivate. Therefore, it is remarkable that this small fraction of sites increases the conversion of n-C6 by a factor of 2 and its branched isomers by a factor of 5. It is also interesting to note that although the synergistic sites deactivate quickly, they are easily regenerated by simply reheating the catalyst at high temperature. As shown in Figure 22, after all synergistic sites were deactivated and the stable activity could be ascribed to the normal BAS, reheating the catalyst under a high He flow rate recovered the enhanced activity and product selectivity of the fresh HTT catalyst (Figure 23). The enhanced activity might also be due to stronger adsorption of synergistic site as suggested by van Bokhoven et al. [91] and Shannon et al. [109]. However, strong adsorption of hydrocarbon species might also cause fast deactivation of these sites. And retreat the catalyst at high temperature and He flow rate might facilitate desorption of these hydrocarbon species, and regenerate the synergistic sites.

Pretreatment time also affects the extent of activity enhancement but not as significant as pretreatment temperature. For example, the longer pretreatment time at 500 ^{o}C, the higher activity of the fresh catalyst. And 20 h pretreatment seems to be enough to fully activate the synergistic sites at 500 °C (Figure 14). But pretreatment of the catalyst at 600 ^{o}C for only 1 h enhances the activity of the fresh catalyst even more than pretreatment at 500 ^{o}C for 20 h.

2.4.2 Possible reaction pathways over synergistic sites

Conversion of paraffins over zeolite might occur through three main pathways [111-114]. They are (i) the protolytic cracking of a C–C bond in the pentacoordinated carbonium ion formed when the catalyst protonates the paraffin, (ii) protolytic dehydrogenation of the carbonium ion, and (iii) hydride transfer with a surface carbenium ion. The first two pathways are monomolecular reactions between paraffin with the pristine BAS bearing the H^{+}. Protonation of either the C–C bond or C–H bond results in different transition states for protolytic cracking or dehydrogenation reactions [110, 114, 115], respectively. The third pathway occurs via chain propagation after formation of a carbenium ion [72]. The three possible pathways for n-C6 conversion are illustrated in Figure 25.

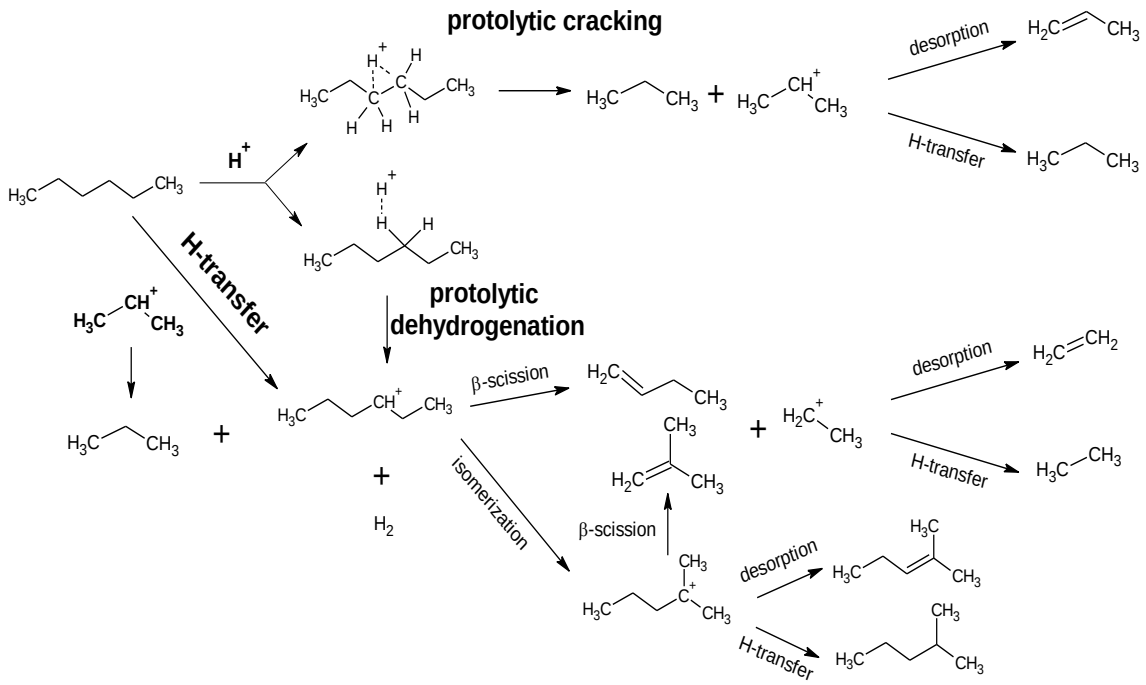

Figure 25. Reaction pathways of paraffin over zeolites

Density functional theory (DFT) calculations have revealed that the protolytic cracking of a linear paraffin occurs through the formation of an early transition state; that is, it resembles the starting state [115, 116]. By contrast, dehydrogenation involves the formation of a late transition state, resembling the final products; that is, the H_2 molecular fragment is almost formed and rather loose [115]. Instead, in the reaction of a branched paraffin such as isobutane [110, 114, 117, 118], both protolytic cracking and dehydrogenation occur through the formation of a late transition state, with CH_4 and H_2 being formed at comparable rates. The late transition state has higher entropy (i.e., it is a looser species) than the early one, but the reactions that go through a late transition state have to overcome a higher enthalpy barrier. As a result, reactions involving looser transition states should be more sensitive to entropic effects, such as geometric constraints of the surrounding environment [119, 120].

Gounder and Iglesia [119] have proposed that in mordenites (MOR), propane and n-butane react much more readily in the partially confined eight-membered ring (8-MR) voids than in the more completely confined 12-MR channels. With a shorter depth (0.37 nm), the 8-MR side pockets do not allow the alkane chain to fit completely. At the high temperatures needed for alkane activation, this partial confinement causes a reduced interaction with the framework, which results in higher entropy for the transition state compared to that on the 12-MR channels, which compensates for the weaker binding. As a result, the reaction rate increases on 8-MR sites compared to 12MR, particularly for dehydrogenation, which involves a late transition state. Interestingly, in the case of isobutane, the protolytic cracking path involves a later and looser transition state than the dehydrogenation path. As a result, the opposite trend to that of propane and n-butane was observed [120]. Even though the partial confinement in 8-MR pockets still enhances both dehydrogenation and protolytic cracking, the latter is more favored. That is, the enhanced entropic effects benefit reactions occurring through looser transition states and result in variation of preferred reaction pathways for different paraffinic molecules (i.e., dehydrogenation is preferred with linear paraffins, and protolytic demethylation is preferred with branched paraffins).

To make the connection with our results, we can point out that LAS and EFAL sites in HY may also cause similar effects as those observed by partial confinement in other zeolites. For example, Narbeshuber et al. [106] have reported that EFAL sites enhance dehydrogenation of propane and n-butane over HY zeolite, especially at short residence times [107]. In contrast, and in parallel with the results shown with the MOR catalysts, the isobutane reaction over the steamed H-USY catalyst (having more EFAL

sites) shows an enhancement in protolytic cracking compared to dehydrogenation [121]. Likewise, opposite changes in selectivity toward protolytic cracking and dehydrogenation reactions for propane compared to isobutane have been observed on high-temperature pretreated H-ZSM-5 (825 °C in N_2), which may exhibit enhanced EFAL formation. That is, in the propane reaction the selectivity to dehydrogenation increased upon HTT, but in the isobutane reaction the selectivity to protolytic cracking increased [89, 90].

One can incorporate these concepts to explain the results reported in this article. In fact, one can compare the effect of HTT on the product distribution of n-C6 and 23DMB reactions (see Table 3). The higher O/P ratios observed during the first pulses of n-C6 (Figure 18a) and significant H_2 production (Figure 21a) when the catalyst was pretreated at higher temperature are consistent with a more favored monomolecular dehydrogenation rather than with protolytic cracking, as seen above for the case of propane. In contrast, with the branched hexane (e.g. 23DMB), the changes in product distribution are more complicated because of an enhanced contribution of hydride transfer (bimolecular) reactions. However, the significant decrease in isomerization products (Figure 17a) and slight increase of O/Ps ratio in the total products (Table 3) indicates a decrease in bimolecular hydride transfer reactions and an increase in monomolecular protolytic cracking and dehydrogenation paths. Furthermore, increase in C1 selectivity (Figure 17a) and decrease in O/P ratio in the cracked products (Figure 18b) also showed that protolytic cracking to C1 products was enhanced more than dehydrogenation of 23DMB. These results are similar to what was observed with the contribution of EFAL [106, 107, 121] and the zeolite spatial confinement effect [119,

120] discussed above. Therefore, it is reasonable to speculate that the LAS in the synergistic sites generated by HTT might also include the entropic effects to the cracking or dehydrogenation transition states.

Van der Waals interaction of the Lewis species with the hydrocarbon chain (but not with the three-center/two-electron part) might affect the entropy of the transition state similarly to the reaction of n-butane over a zeolite cluster as described by Sharada et al. [115]. The hydrocarbon chain might arrange closely to the zeolite framework in the early transition state of n-C6 cracking, and it might direct away from the framework in the late transition state of the dehydrogenation reaction. Hence, stronger interaction between the Lewis species with the hydrocarbon chain of the cracking transition state might be expected, resulting in lower activation entropy for the cracking reaction. Finally, we must note that in the reaction of 23DMB, protolytic cracking to C1 and dehydrogenation might proceed through a late transition state, in a similar manner to the previously studied isobutane reaction [110, 114, 117, 118]. Therefore, the interaction between the hydrocarbon chain and the Lewis species would be weak in both reactions. In the monomolecular conversion of branched paraffin, a higher probability [122] as well as a higher activation entropy [123] for the terminal cracking to methane were also observed. Hence, the synergistic sites might enhance protolytic cracking more than dehydrogenation in the reaction of 23DMB.

2.5 Summary

The catalytic activity of the HY zeolite is enhanced upon high temperature pretreatment. This activity enhancement parallels dehydroxylation of the zeolite

observed by TG-MS analysis. The synergism between LAS created by dehydroxylation and the original BAS might form a new type of site (synergistic site) that displays enhanced activity for both, protolytic cracking and dehydrogenation reactions of paraffins. The activity enhancement caused by the synergistic sites is clearly evident for the monomolecular protolytic reaction, but it is not apparent in the conversion of olefins. With n-C6 feed, the enhancement for dehydrogenation is greater than for protolytic cracking, but the opposite trend was observed in the conversion of 23DMB. The opposing trends in product selectivity changes for the different hexane isomers are related to different effects of Van der Waals interactions between the Lewis species and the hydrocarbon chain, which might vary the activation entropy of the different reaction paths. The interaction between the Lewis species and the transition states is weaker for n-C6 dehydrogenation and 23DMB terminal cracking than for n-C6 cracking and 23DMB dehydrogenation. This weaker interaction results in higher entropy of the transition state and hence higher reaction rates for n-C6 dehydrogenation and 23DMB protolytic terminal cracking than for the other reactions. The synergistic sites were also deactivated very quickly by strong adsorption of hydrocarbon species, but could be regenerated by a subsequent high temperature treatment.

Chapter 3: Reaction of m-cresol over fresh HY and HZSM-5 zeolites using a micro-pulse reaction system

3.1 Introduction

Biomass pyrolysis, a thermochemical conversion technology to convert lignocellulosic biomass to biofuels, has been considered as a promising strategy for renewable fuel production. However, due to its high oxygenates content the pyrolysis oil has poor properties for using as fuels or blending with hydrocarbon fuels. Therefore, further upgrading of the pyrolysis oil or its fractions to remove oxygen and produce hydrocarbons have been an attractive topic in chemical engineering research [6, 8, 13, 124].

Among many catalytic upgrading strategies, zeolites have been used widely in many researches for producing biofuels from biomass thermal conversion via catalytic pyrolysis [125-127], or catalytic upgrading of the pyrolysis oil vapors [127, 128]. Comparing to hydrodeoxygenation processes [38], zeolite upgrading operates at much lower pressure (normally at atmospheric pressure) with minimum requirement of hydrogen which bring advantages to this strategy in terms of capital investment and operation cost [128, 129]. Furthermore, co-prossesing pyrolysis oil or partially upgraded bio-oil in the refinery's units is also a promising strategy to produce and blend bio-fuels with traditional hydrocarbon fuels. Using existing infrastructure of the refinery helps reducing investment cost for bio-fuel production. And current large refining capacity of these units is also favorable for boosting the production of bio-fuels in large scale. Among many process technologies in the refinery, fluid catalytic cracking (FCC), in which zeolite is a main catalytic active component, is a prospective

candidate for co-processing bio-fuels due to its large capacity and flexibility in processing different type of feedstocks [42, 61, 63, 64, 129].

Therefore, it is important to study the interaction of the oxygenated compounds presenting in pyrolysis oil with zeolites. In fact, zeolite upgrading of model oxygenated compounds [50, 51, 53, 130, 131] have been studied extensively. Among others, phenolic compounds have shown low activity in conversion to hydrocarbons. Major reactions of phenolic compounds are isomerization and transalkylation forming isomeric or alkylated phenolic products while very low selectivity to aromatic is observed. Condensation reaction results in water release and formation of heavy ethers which are coke precursors [50, 53, 131, 132]. Besides, molecular adsorption of these phenolic compounds on both Brønsted acid sites (BAS) and Lewis acid sites (LAS) of the zeolites also enhance carbonaceous deposition and catalyst deactivation [63, 75, 76]. In our previous study about m-cresol conversion over H-beta zeolite using a micro-pulse reaction system [133], the clean zeolite surface showed a very high efficiency in capturing the feed molecules. This effect could not be seen in the continuous flow reactor in which product analysis was done after the reaction started for a certain period and the catalyst was covered and saturated by the phenolic compounds. Therefore, it is important to design experiments that allow us to measure the activity of the fresh zeolite in the conversion of the phenolic compounds.

In this contribution, conversion of m-cresol, which is a representative of phenolic compounds, has been studied over HY and HZSM-5 zeolites using the micropulse reaction system. Quantitative analysis of the fractions of the feed that are

captured by the zeolite, desorbed, and reacted to products was carried out to understand the interaction of the phenolic compounds with the clean catalyst surface.

3.2 Experimental

3.2.1 Materials

The two zeolites used as catalysts in this study were provided by Zeolyst International. One of them was a dealuminated HY (CBV780) with Si/Al = 40 and the other was a NH_4ZSM-5 (CBV8014), with the same Si/Al = 40. In order to obtain the HZSM-5, the CBV8014 material was treated under 100 sccm flow of air with a linear heating ramp of 2^{o}C/min to 600 ^{o}C and holding at this temperature for 6 h. Before reaction, the catalysts were pelletized and sieved into 90 – 250 μm particles. m-Cresol (99%+, from SAFC), toluene and o-xylene (99%+ from Sigma Aldrich) were used as feed without further purification.

3.2.2 Catalyst characterizations

3.2.2.1 Acidity measurement

Temperature programmed desorption (TPD) of adsorbed isopropylamine (IPA) was used to quantify the density of Brønsted acid sites (BAS) [82]. In each TPD measurement, 50 mg of catalyst was used. The catalysts were pretreated under 20 sccm of He at 400 ^{o}C for 1 h. After pretreatment, the catalyst was cooled down to 100 ^{o}C and exposed to ten consecutive 2 μl-pulses of IPA. After flushing under He for 6 h at 100 ^{o}C to remove weakly adsorbed IPA, a 10 ^{o}C/min linear heating ramp was started up to 600 ^{o}C. The desorbed products were analyzed and quantified on a Cirrus MS. To

quantify the Brønsted acid site (BAS) density, the propylene signal (m/z=41) was calibrated with 100 μl propylene pulses.

3.2.2.2 N_2 adsorption

BET surface area of the catalysts was measured by N_2 adsorption in a Micromeritics ASAP 2010 unit. Before measurement, the catalyst was evacuated in vacuum at 300 ^oC for 24 h.

3.2.2.3 HRTEM

High resolution transmission electron microscopy (HRTEM) images were obtained on a JEOL 2010-F scanning transmission research electron microscope with field emission voltage of 200kV and magnification up to 8,000,000x.

3.2.3 Catalytic measurements

The conversion of m-cresol was evaluated in a micro-pulse reactor at atmospheric pressure of He carrier gas. In each experiment, 100 mg of catalyst was pretreated under 200 sccm He flow at 600 ^oC for 1 h. After pretreatment, the temperature was adjusted to required reaction temperature (400 – 600 ^oC) and the He flow rate was lowered to 20 sccm. When the reactor's temperature was stable, a 0.15 μmol pulse of vaporish m-cresol diluted in He (i.e., 1.1 mol% of m-cresol in He) was sent over the catalyst bed. The products were analyzed on-line using an HP5890 gas chromatograph (GC), equipped with an HP-1 column and a flame ionization detector (FID). Pulse experiments with more concentrated m-cresol in He (i.e., 11.3 mol% of m-cresol in He) and hence a larger m-cresol pulse (1.5 μmol), were carried out to study the catalyst deactivation.

Reactions of toluene (1.9 mol% of toluene in He, corresponding to 0.24 μmol toluene/pulse) and o-xylene (1.6 mol% of toluene in He, corresponding to 0.21 μmol toluene/pulse) were also carried out at 600 ^{o}C in order to investigate the possible secondary reactions of the aromatic products derived from the m-cresol conversion. In this case, the product analysis was carried out on the GC-FID using an HP-PLOT/Al_2O_3/"S" column.

During the 1-hour periods between each pulse, the catalyst was exposed to continuous flow of He. Products were identified and quantified by using mixtures of reference compounds of calibrated concentrations. All conversion values reported in this work have been corrected for the small contribution of non-catalytic thermal conversion at each corresponding temperature. To quantify the extent of thermal conversion, pulses of m-cresol, toluene, and o-xylene were injected over an inert bed (acid-washed glass beads, 100 μm in diameter) under the same reaction conditions as used with the catalysts. As expected, thermal conversion of m-cresol increased with reaction temperature, but was very small in all cases, reaching a maximum of 0.8 % at 600 ^{o}C. Thermal conversion of toluene and o-xylene was negligible (< 0.1%).

3.2.4 Temperature programmed oxidation (TPO) and decomposition (TPDe) of the carbonaceous deposits

On each sample, TPO runs were used to quantify the amount of carbonaceous deposits remaining on the catalyst after reaction. The same reactor tube containing the spent catalyst was connected to the TPO system, equipped with a Cirrus mass spectrometer (MS) to measure the evolution of CO_2 (m/z = 44) during the TPO ramp. To oxidize the carbonaceous deposits, a stream of 20 sccm of He/O_2 (5% volume O_2)

was used. Following reaction and after the furnace temperature was stable at 50 ^{o}C, the reactor was heated linearly with a 10 ^{o}C/min ramp up to 700 ^{o}C and held at this temperature until the CO_2 signal reached the baseline. For quantification, the CO_2 signal (m/z=44) was calibrated with 100 μl pulses of pure CO_2.

TPDe of the carbonaceous deposits on the spent catalyst was also carried out to study the activity of the phenolic pool formed after m-cresol reaction. A Microvision Plus MS, scanning over a 1 – 200 m/z range at a speed of 15 cycles/min, was connected to the reactor outlet to detect product evolution during pulses of m-cresol through the catalyst bed and TPDe of the spent catalyst after that. After 10 pulses of m-cresol (1.5 μmol m-cresol/pulse each) over 50 mg catalyst-bed at 400 ^{o}C (or 500 ^{o}C), the catalyst was flushed for 20 minutes to remove all weakly adsorbed species. Then, a 5 ^{o}C/min linear heating ramp was initiated; when reaching the target temperature (500 – 600 ^{o}C) it was held constant until all signals reached the baseline. In order to quantify the evolution rate of major products upon TPDe, pulses of toluene, benzene and methane with known amount was sent through an inert bed to the MS for calibration.

3.3 Results and discussions

3.3.1 Catalyst characterizations

The measured acidity and surface area of the two zeolites were presented in Table 4. Comparing to the acidity calculated by the Si/Al ratio, BAS density of HZSM-5 zeolite measured by IPA-TPD was similar to that of the theoretical value. However, the measured value for HY zeolite was much lower than theoretical value. This significant difference might be due to the inaccessibility of IPA molecules to BAS

located at the sodalite cages or contribution of EFAl species. The measured surface area are similar to the value reported by the catalyst supplier.

Table 4. Physical properties of the zeolites

Zeolites	Si/Al	BAS density (μmol/g)		Surface area (m^2/g)	
		Theoretical *	IPA-TPD	Zeolyst **	N_2 adsorption
CBV780	40	406	70	780	701 ± 19
CBV8014	40	406	372	425	362 ± 10

* Calculated based on Si/Al ratio

** http://www.zeolyst.com/our-products/ standard-zeolite-powders.aspx

The HRTEM images in Figure 26 show well ordered crystalline structures of both CBV780 and CBV8014 zeolites.

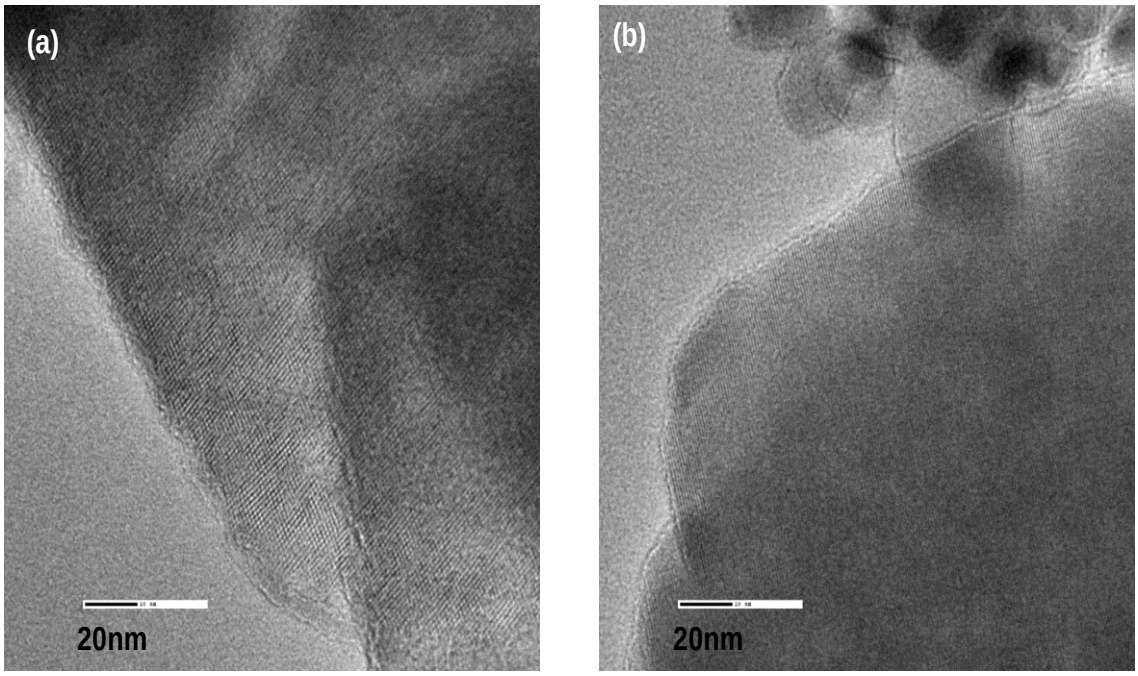

Figure 26. HRTEM images of (a) HY and (b) HZSM-5 zeolites

3.3.2 Effect of reaction temperature on product evolution and the formation of carbonaceous deposits

The conversion of diluted m-cresol (i.e., 1.1 mol% of m-cresol in He) over HY and HZSM-5 zeolites at varying temperatures (400 – 600 ^{o}C) was investigated in a micro-pulse reactor. Due to the high dilution and small size of the pulse, the amount of m-cresol injected in a pulse was much smaller than the amount of catalyst (i.e., catalyst/reactant mass ratio is ~ 6,000 per pulse). As a result, the deactivation of the catalyst in these experiments was negligible. In fact, the product yields were practically unchanged with the pulse number for all temperatures. Therefore, accumulated yields of the products and total output after 9 pulses of m-cresol are reported. After 9 consecutive pulses, the amount of carbonaceous deposits was quantified and compared to the observed total output to determine the carbon balance.

Figure 27 shows the accumulated yields of the products together with unconverted m-cresol that leaves the reactor (i.e., total output) after 9 pulses and the carbonaceous deposits remaining over the catalyst (HY and HZSM-5 zeolites) at different temperatures. It is important to note that, depending on the temperature, a significant fraction of the feed was trapped in the catalyst bed. This fraction is subsequently oxidized during the TPO measurement together with the coke. For instance, at 400 ^{o}C, no products or unconverted reactant come out of the catalyst bed, and all of the feed is trapped and counted as carbonaceous deposits. As the reaction temperature increased, the total output increased, including products together with a small fraction of unconverted m-cresol. By contrast, the yield of carbonaceous deposits decreased, although even at the highest temperature investigated (600 ^{o}C) about 60 wt%

of the feed remained trapped (adsorbed or forming coke) in the catalyst bed. When accounting for the carbon retained on the catalyst, the mass balance for the reactions was very good (i.e., over 90%). The strong adsorption of the oxygenated aromatics on the acid sites of the zeolites is responsible for the high extent of feed trapping. This phenomenon is responsible for the high degree of pore blockage and catalyst deactivation observed in continuous flow experiments using phenolics as feed components [75, 76, 133].

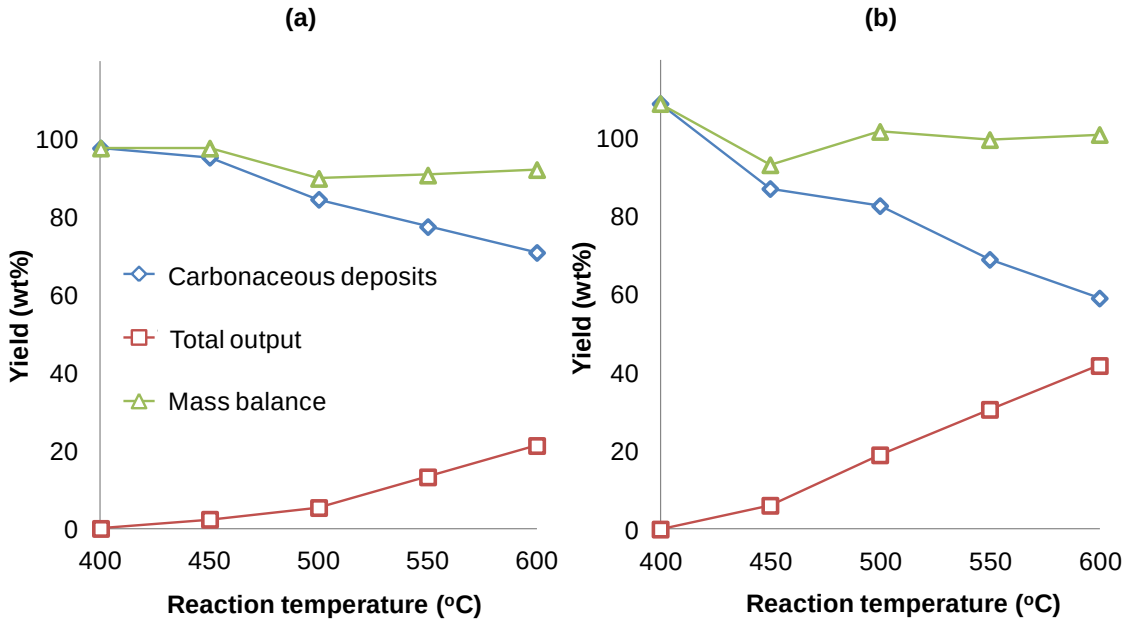

Figure 27. Accumulated yields of total output and carbonaceous deposit after 9 pulses of m-cresol over (a) HY and (b) HZSM-5 zeolites at different temperatures

As summarized in Figure 28, the m-cresol deoxygenation was very effective on these fresh catalysts since the main products were BTX aromatics (benzene, toluene, and xylenes). Unreacted m-cresol and other oxygenated aromatics only account for up to 20 wt% of the total output. Also, only traces of light hydrocarbons (mostly methane) were observed. As the reaction temperature increased, the product yield increased.

Interestingly, the unreacted m-cresol and O-containing phenolic products started to come off at temperatures above 450 ^{o}C. Hence, it is clear that, along with a higher extent of deoxygenation to aromatic products, a lower extent phenolic trapping contributes to the observed reduction in carbonaceous deposits as reaction temperature increases.

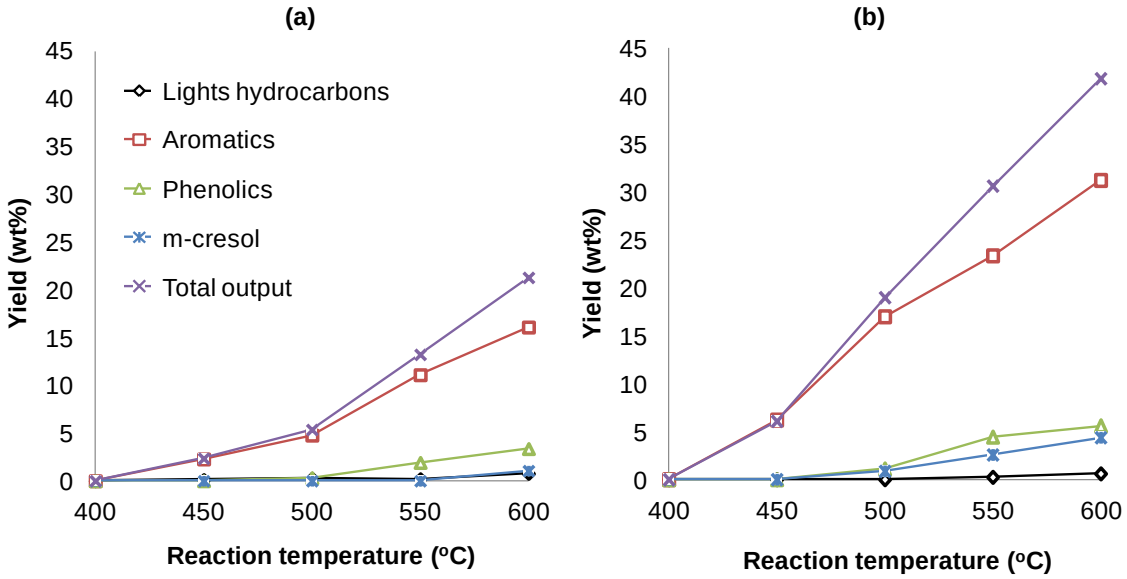

Figure 28. Accumulated yields of products and remaining m-cresol after 9 pulses of m-cresol over (a) HY and (b) HZSM-5 zeolites at different temperatures

In terms of product selectivity, it is observed that the fraction of phenolic products increases with reaction temperature. As shown in Figure 29, while at 450 ^{o}C only aromatics are seen in the reactor output, phenolics account for more than 20% in the total output at 600 ^{o}C. The distribution of products in the phenolic output includes cresol isomers, xylenols, and heavier phenolic species. Phenol was only observed as a minor product over HZSM-5 at 600 ^{o}C. It is well known that isomerization and transalkylation of cresols readily occurs over acidic zeolites at moderate reaction temperature [131, 134, 135]. However, due to strong adsorption, these phenolic compounds remain trapped inside the zeolite. It is important to emphasize that this

effective trapping is more clearly evident in the small-pulse experiments conducted in this study, in which the clean catalyst was in a He environment before being exposed to a small amount of reactant. Under these conditions, it can be observed that the catalyst can trap m-cresol and its phenolic products much more effectively than in a continuous-flow experiment, in which the catalyst adsorption sites become saturated under the flow of reactant. At higher reaction temperatures desorption of phenolics is possible, leading to an increase in yield and selectivity in the total output.

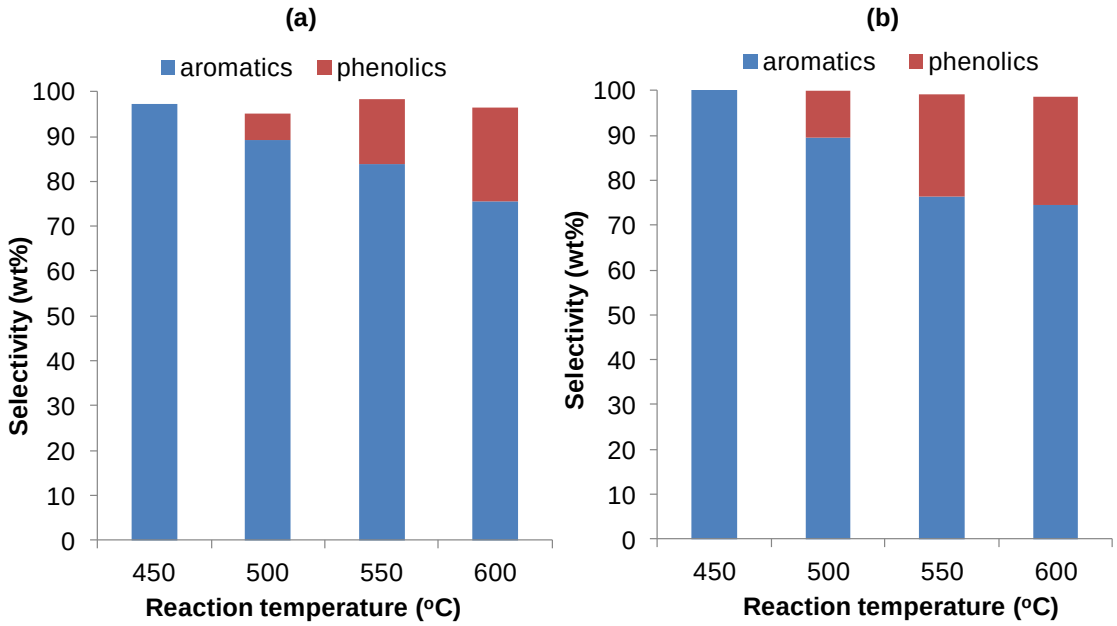

Figure 29. Selectivity to aromatics and phenolic products in the total output in m-cresol conversion over (a) HY and (b) HZSM-5 zeolites at different temperatures

Another important effect of reaction temperature is the changes in selectivity of the specific BTX aromatics (see Figure 30). At low reaction temperature, toluene was the major aromatic product; but, when the temperature increased, the selectivity to toluene decreased and benzene increased. Instead, the selectivity to the xylene isomers increased to a maximum at an intermediate temperature, i.e. 500 ^{o}C, and then decreased

as the reaction temperature increased. This variation in selectivity is a combination of several possible reactions, which requires some analysis. For instance, since toluene was the major product from the conversion of m-cresol at the lower temperature, one could infer that direct dehydroxylation of this phenolic compound might have occurred [63]. In fact, further reactions of toluene, such as the disproportionation to xylenes and benzene [136], and dealkylation to benzene [137] could explain the evolution of these products at higher temperatures (i.e., higher benzene/toluene ratio at high temperature as shown in Figure 31). However, as discussed further below, we believe that production of aromatic products from m-cresol does not occur via a direct deoxygenation pathway, but rather through the formation and cracking of a surface pool of oxygenated aromatic (i.e. phenolic pool).

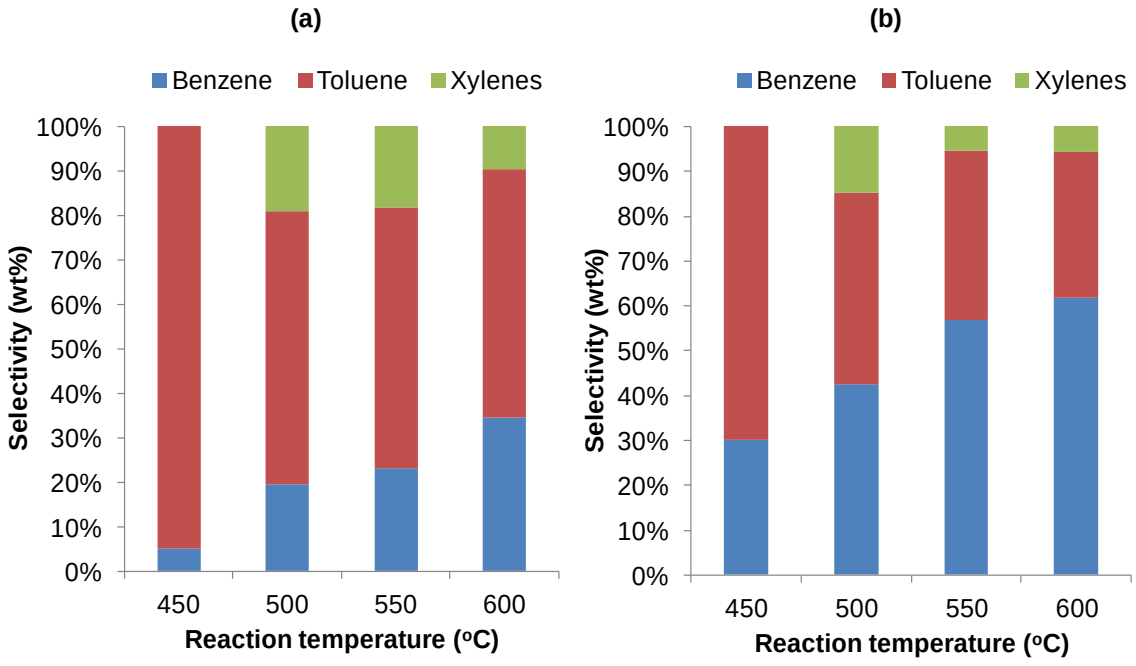

Figure 30. Selectivity of different aromatics in total aromatic products in m-cresol conversion over (a) HY and (b) HZSM-5 zeolites at different temperatures

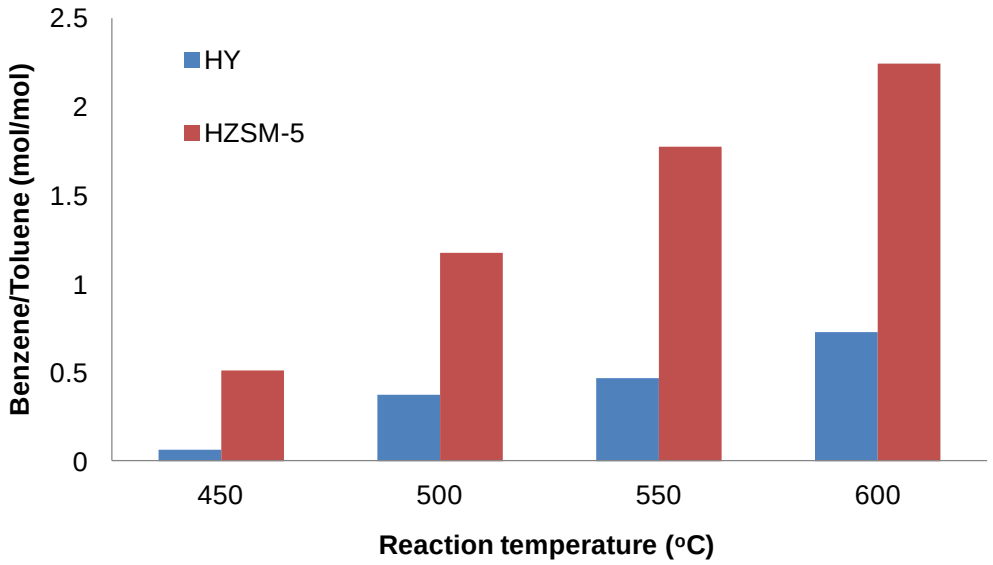

Figure 31. Molar ratio of benzene/toluene in m-cresol conversion over HY and HZSM-5 zeolites at different temperatures

3.3.3 Analysis of carbonaceous deposits on the spent catalyst

It is very interesting to note that the observed trend of formation of carbonaceous deposits with reaction temperature in the conversion of m-cresol over zeolites is directly opposite to that typically observed with hydrocarbons. For instance, Figure 32 compares the amounts of coke, as measured by TPO, as a function of reaction temperature from m-cresol and n-hexane over a HY zeolite. Two important aspects can be emphasized in this comparison. First, the usual trend of increasing carbonaceous deposits with increasing temperature observed in this study (Figure 32b) and literatures with paraffinic [138, 139] or aromatic hydrocarbons [140] is not observed with phenolics, but just the opposite. Second, it is remarkable that even though a much lower amount of m-cresol was sent over the catalyst compared to that of n-hexane (i.e. 1.35 μmol and 80 μmol in total, respectively), the coke amount was still much larger. The coke amounts were less than 1μmol of C in n-hexane conversion, accounting for

only less than 0.2% of C in the total the feed. Meanwhile, the coke amounts in m-cresol conversion were at least 6 times higher than that (i.e., from 6 – 9 μmol of C). More than 60% of the feed was trapped in the catalyst bed. A similar comparison was done over the HZSM-5 zeolite, with comparable results. These results give direct evidence to the strong adsorption and carbon deposition tendency of the phenolic compounds over the acidic zeolites, as previously implied [75, 76, 133].

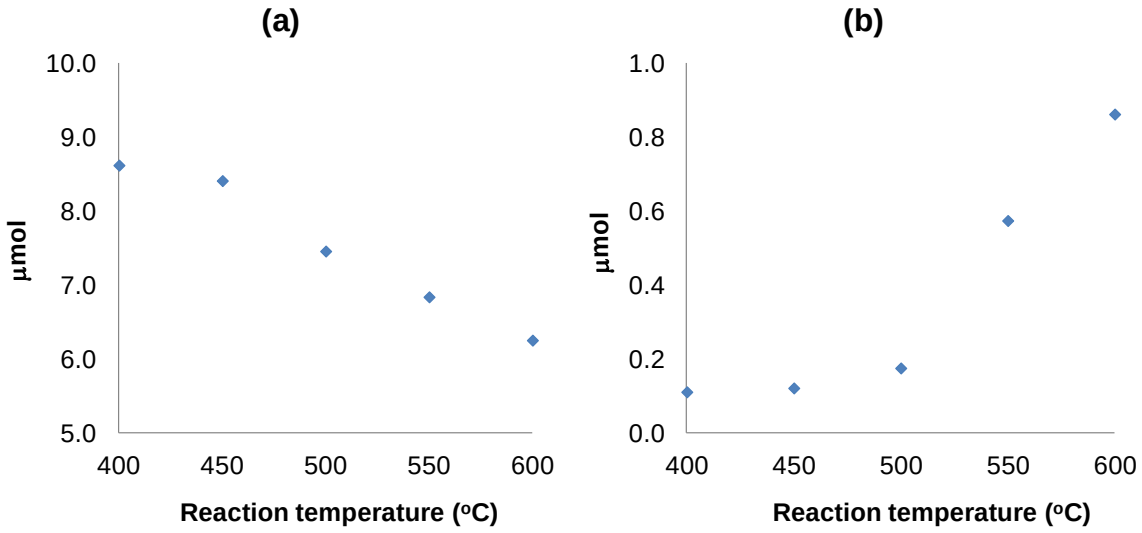

Figure 32. Amount of C in the spent catalyst after (a) 9 pulses of m-cresol (0.15 μmol/pulse) or (b) 20 pulses of n-hexane (4 μmol/pulse) over 100mg of HY zeolite at different temperatures

The shape of the TPO profiles can shed more light into the nature of the carbonaceous deposits. For instance, CO_2 (m/z = 44) evolution profiles of the spent HZSM-5 zeolite after 9 pulses of m-cresol are compared in Figure 33 for different temperatures. It is clear that, as the reaction temperature increases, the fraction of carbonaceous deposit that can be oxidized at lower temperatures (i.e. below 500 ^{o}C) drops significantly. At the same time, the CO_2 evolution peak shifts to higher temperature (i.e. from 550 to 620 ^{o}C). A very similar trend was observed for the spent

HY zeolite. This shift indicates the formation of more refractory coke deposits (i.e more graphitic). Similar trends in the reactivity of carbonaceous deposits toward oxygen with increasing reaction temperatures have been previously observed during the conversion of furan over HZSM-5 zeolite [141]. Also, as reaction temperature increased, the low-temperature-coke decreased, which can be due to a lower amount of trapped reactants and products during reaction, as demonstrated in the pulse experiments. Therefore, it is clear that the total amount of coke decreases as the reaction temperature increases; however, the fraction of graphitic coke increases while the fraction of oxygenated coke gradually vanishes.

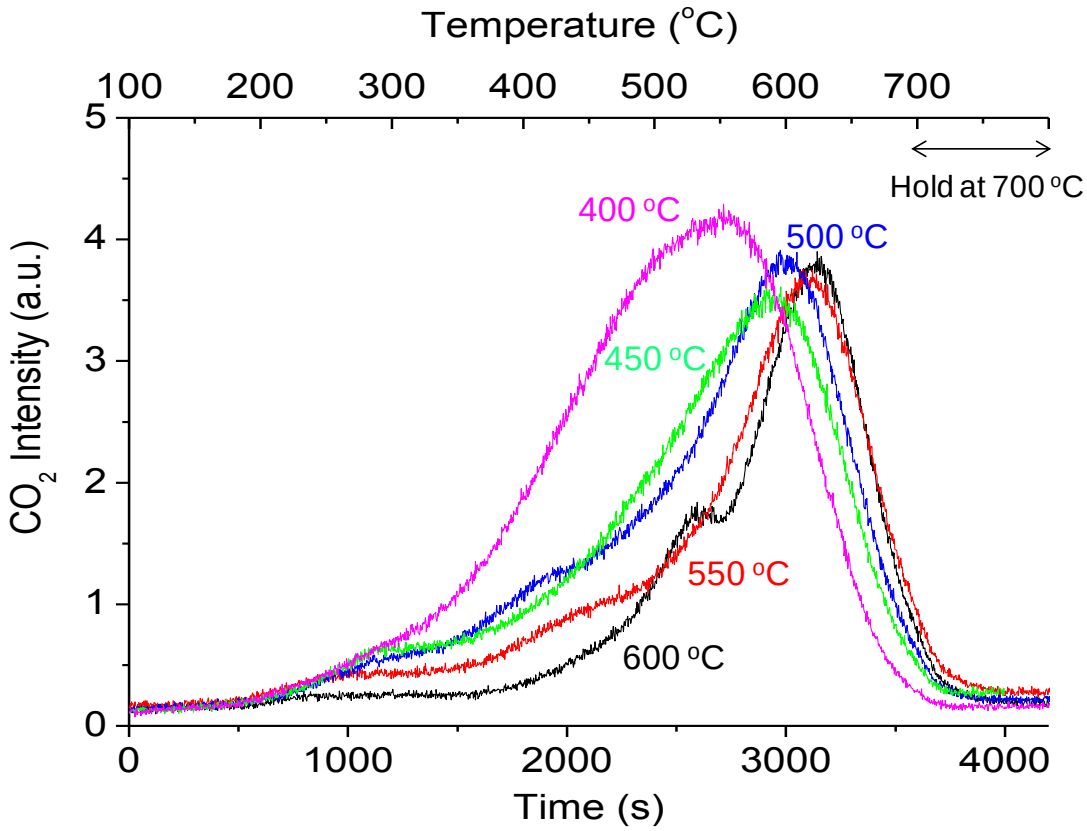

Figure 33. Evolution of CO_2 (m/z = 44) during TPO of the spent catalyst after 9 pulses of m-cresol over HZSM-5 zeolite at different reaction temperatures

This interesting trend is opposite to that typically observed in the catalytic cracking of hydrocarbon, in which coke formation increases with reaction temperature. In that case, coke forms from a series of bimolecular reactions such as oligomerization of olefins, H-transfer, cyclization, and alkylation which generate polyaromatic products that strongly adsorb on the acid sites, causing deactivation of the active site and pore blockage [142]. Furthermore, in methanol conversion to hydrocarbon (MTH) over zeolites, which proceeds through the hydrocarbon pool mechanism [143-145], coke formation also increases with the reaction temperature leading to higher rate of deactivation [146]. It is widely accepted that, the hydrocarbon pool, including aromatic and olefinic species builds up on the catalyst surface by methylation reaction [144, 145]. Cracking of the olefinic pool and dealkylation of the aromatic pool produce hydrocarbons, while hydride transfer and cyclization form polyaromatic species that lead to coke. When the reaction temperature increases, hydride transfer and cyclization reactions are enhanced, which facilitate the coke formation. Meanwhile, in the conversion of oxygenated aromatic compounds, such as phenolic and furanic compounds, formation of the oligomeric species mainly proceed via condensation reaction. For example, an evidence of this condensation is the appearance of diphenylether species in the products, deriving from the etherification of phenols [131]. These products were also proposed as important intermediate for aromatic production via cracking reaction. Oligomeric compounds were also formed via Diels – Alder condensation of furan over HZSM-5 zeolite [141]. Benzofuran and dibenzofuran were identified as important intermediate for this reaction. Further condensation with furan and alkylation with allylic products from furan decarbonylation can produce larger

oligomeric oxygenated species. Extraction and analysis of the carbonaceous deposits also confirmed considerable amount of O in the spent catalyst. Hence, the pool formed by reaction of phenolic or furanic compounds contains oxygenated aromatic hydrocarbons, i.e a phenolic pool produced by condensation reactions.

Subsequent cracking of this pool into fragments might be the main pathway for the production of the aromatics obtained as products, as previously proposed [133, 141]. Aromatic production via hydrocarbon pool mechanism has also been proposed by Carlson et al. [147] in recent studies of glucose conversion over HZSM-5. Conversion of a mixture of ^{13}C-labeled and unlabeled glucose showed a high extent of C scrambling in the aromatic products, but no scrambling in the oxygenated products. The authors suggested that direct dehydration and bond cleavage of glucose are responsible for the observed oxygenated products, but these oxygenates also condense to form a surface pool, which subsequently cracks with evolution of aromatic compounds. As observed in our pulse experiments of m-cresol conversion over zeolites, with increasing reaction temperature, enhanced cracking of the phenolic pool occurs, forming more aromatic and trapping less phenolic compounds. Hydride transfer and cyclization reactions are also enhanced at higher temperatures, leading to more refractory (i.e. more graphitic) coke.

From the results of the pulse experiments and TPO analysis of the spent catalyst, it is reasonable to infer that the phenolic pool that forms at low reaction temperature might be still active for further reaction at higher temperature and release fragments to the gas phase, while becoming a more refractory coke. In order to confirm the activity of the phenolic pool produced at low reaction temperature, TPDe of the spent catalyst was carried out. The reactor outlet was directly connected to a Microvision Plus MS,

scanning over a 1 – 200 m/z range, to detect product evolution during pulses of m-cresol through the catalyst bed and subsequent TPD of the surface species on the spent catalyst. Due to the low sensitivity of the MS, in order to make the product evolution detectable, a more concentrated m-cresol pulse (11.3 mol% of m-cresol in He, 1.5 μmol m-cresol/pulse) was used. As shown in Figure 34, upon the injection of m-cresol pulses at 400 ^{o}C over 50 and 100 mg of HZSM-5 zeolite the evolution of water (m/z = 18), cresols (m/z = 107), and aromatics (m/z = 91) was monitored by MS. Even though the amount of m-cresols increased 10 times relative to the previous experiments (part 3a), all of them remained trapped on the 100 mg catalyst bed (Figure 34a). No evolution of hydrocarbons or any phenolic products were observed during 10 pulses of cresol. When the catalyst amount was reduced to 50 mg (Figure 34b), most of the cresol pulse was still trapped during the initial 3-4 injections, but started appearing in the subsequent pulses. It is clear that the strong adsorption and perhaps pore blockage by cresol reaches a saturation after about 100 μmol/g cat.

It is revealing to examine the evolution of water after each pulse. No water evolution occurs during the initial cresol pulses; however, water starts appearing after the 3rd pulse over the 100 mg bed (Figure 34a) and after the 2nd pulse over the 50mg bed (Figure 34b). It is interesting to note that water starts evolving much earlier than the unconverted cresol. In fact, water seems to be a product of the interaction of cresol with the catalyst and fully consistent with the concept of a phenolic pool formed by condensation of m-cresol, as previously discussed. In fact, during the initial pulses over a clean catalyst surface, no water produced. Then, the water production increased to a maximum intensity and slightly decreased in subsequent pulses. It is known that

phenolic compounds are trapped in acidic zeolites by adsorption on either BAS or LAS [75, 76]. They can also react with each other through condensation reactions, producing diphenyl ether species and water [131]. Accordingly, the observed results indicate that during the first m-cresol pulses on a clean catalyst surface, m-cresol adsorbs non-dissociatively, but during later pulses, m-cresol might react with the surface phenolic species via condensation reactions that release water. The resulting diphenyl ether species remain trapped inside zeolite pores; so, when subsequent m-cresol pulses are sent, further condensation reactions occur, eventually leading to catalyst deactivation. This deactivation results in the observed decrease in the extent of condensation reactions and water evolution, as shown in Figure 34b. When the amount of catalyst was doubled (Figure 34a), more sites were available for m-cresol to adsorb non-dissociatively and distribute on the catalyst surface. Hence, condensation reaction of m-cresol in the pulse with surface phenolic species only occurred on later pulses. Deactivation was also observed later, due to a larger amount of sample.

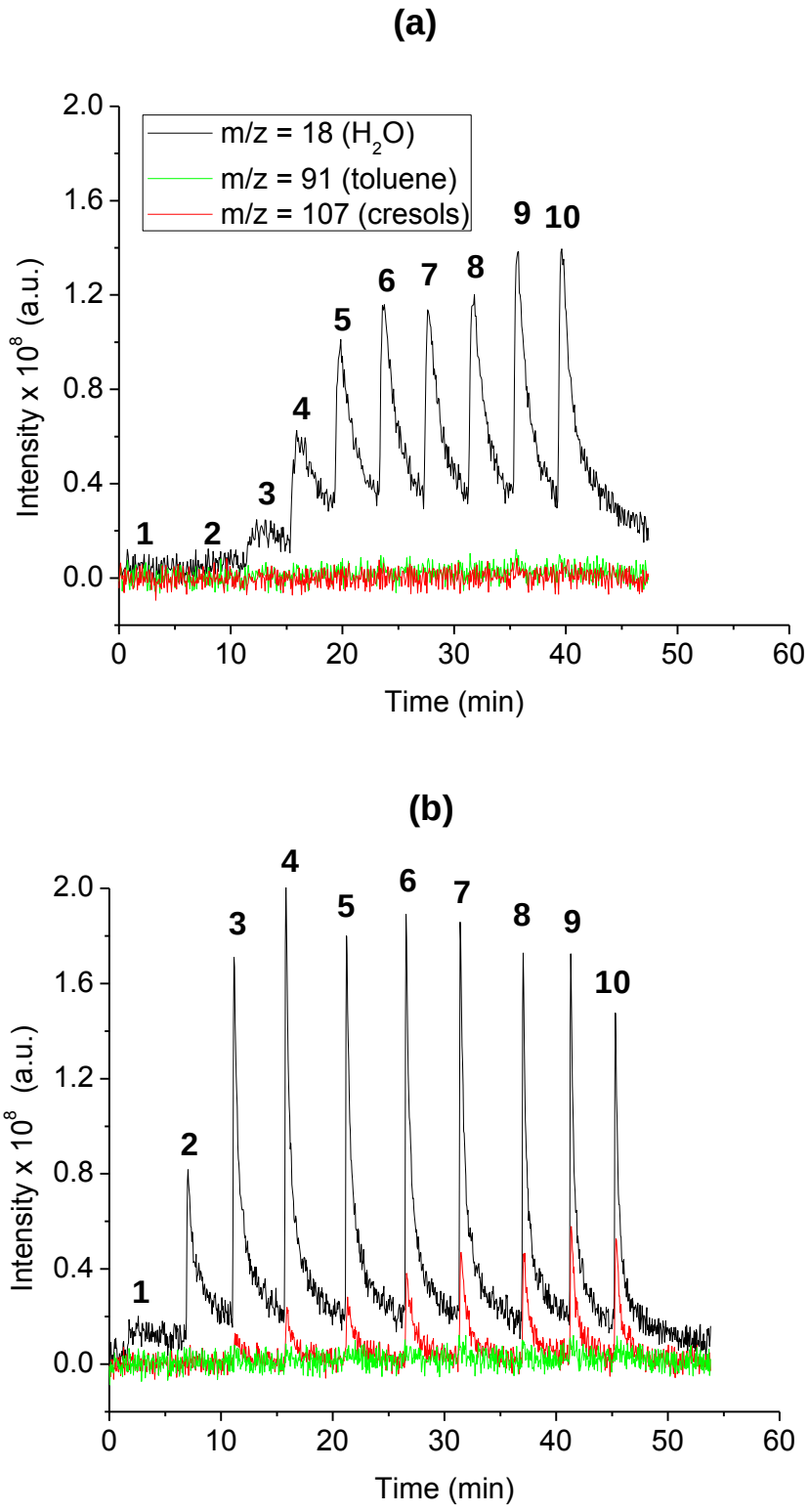

Figure 34. Evolution of H_2O (m/z = 18), cresols (m/z = 107) and toluene (m/z = 91) during pulses of m-cresol over (a) 100 mg and (b) 50 mg of HZSM-5 zeolite at 400 ^oC

To investigate the reactivity of the surface pool, the species trapped on the spent catalyst where heated in a linear temperature ramp while the product evolution was monitored by online MS. As illustrated in Figures 35a-c for the HY zeolite and Figures 36a-c for the HZSM-5 zeolite, after 10 pulses of m-cresol at 400 ^{o}C, the TPDe showed considerable amounts of hydrocarbons evolved from both spent catalysts. The evolved products include benzene (m/z = 78), toluene (m/z = 91) and methane (m/z = 16), indicating that the carbonaceous deposits formed at the low reaction temperature (400 ^{o}C) was still active for reaction at higher temperature. Remarkably, no phenolic compounds were detected as decomposition products. These results contrast with those observed in the pulse experiments, in which the selectivity to phenolic products increased with reaction temperature. That is, during the pulse experiments, the observed phenolic products do not derive from decomposition of the carbonaceous deposits, but rather from the direct reactions of m-cresol. At higher reaction temperatures, adsorption of phenolic compounds is reduced, i.e. less of them were trapped by the zeolite, and hence, more of them were released. A similar phenomenon has been recently observed during the conversion of glucose on HZSM-5; in that case, it was proposed that oxygenated products formed directly from the dehydration of glucose, while aromatics were produced from cracking of the hydrocarbon pool [147]. TPDe of the phenolic pool formed from the reaction at 500 ^{o}C were also shown in Figure 35d and 36d. After reaction at 500 ^{o}C, the reactor's temperature was stabilized at 400 ^{o}C before applying temperature ramp, so that the TPDe profile can be comparable to that of the pool formed from the reaction at 400 ^{o}C (Figure 35c and 36c). The initial evolution of hydrocarbons at temperature lower than 500 ^{o}C disappeared in

the TPDe of the phenolic pool formed at 500 ^{o}C compared to that at 400 ^{o}C. The results indicated that the pool formed at 500 ^{o}C were still active for the reaction, but only at higher temperature.

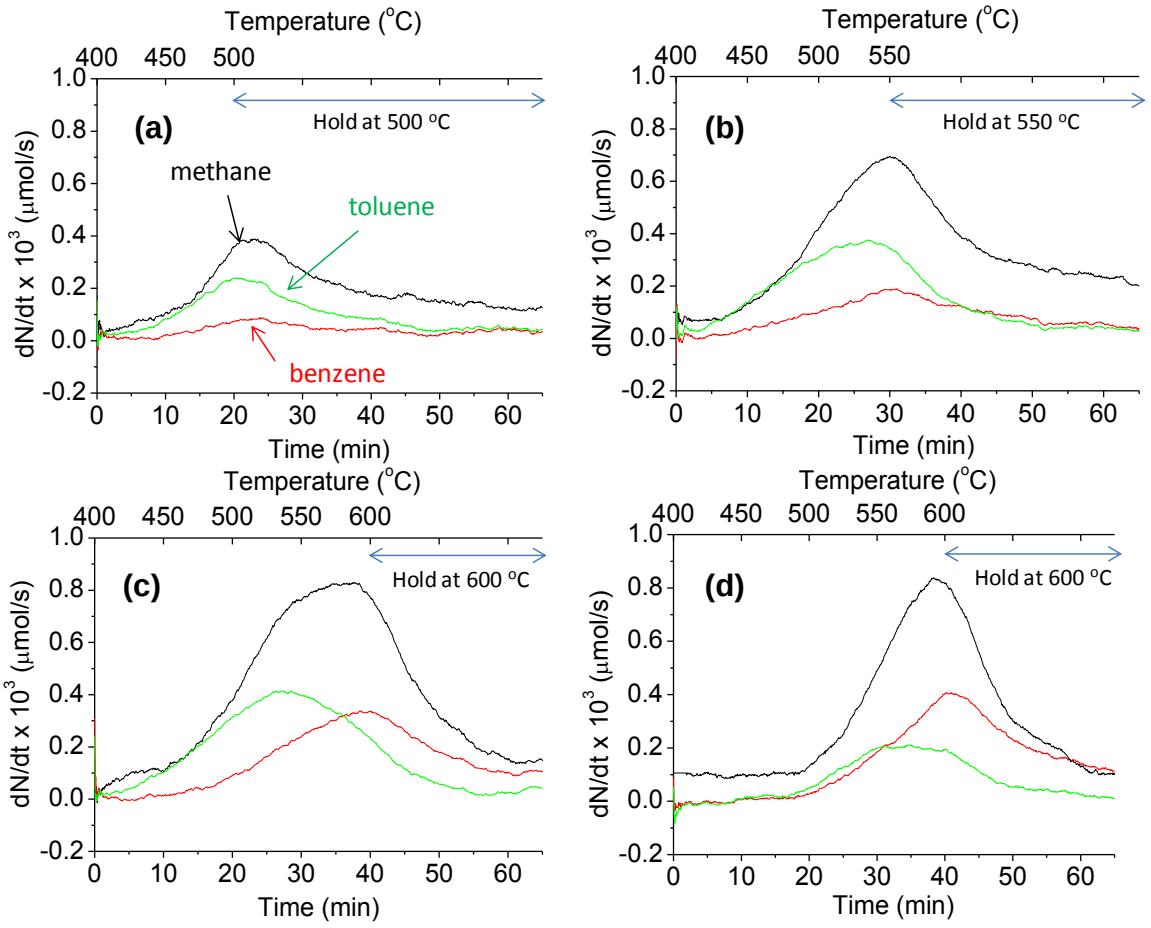

Figure 35. Temperature programmed decomposition of the phenolic pool formed by m-cresol reaction at 400 ^{o}C (a-c) and 500 ^{o}C (d) over 50 mg of HY zeolite. A linear ramp of 5 ^{o}C/min from 400 ^{o}C followed by isothermal hold period at (a) 500 ^{o}C, (b) 550 ^{o}C, (c) and (d) 600 ^{o}C

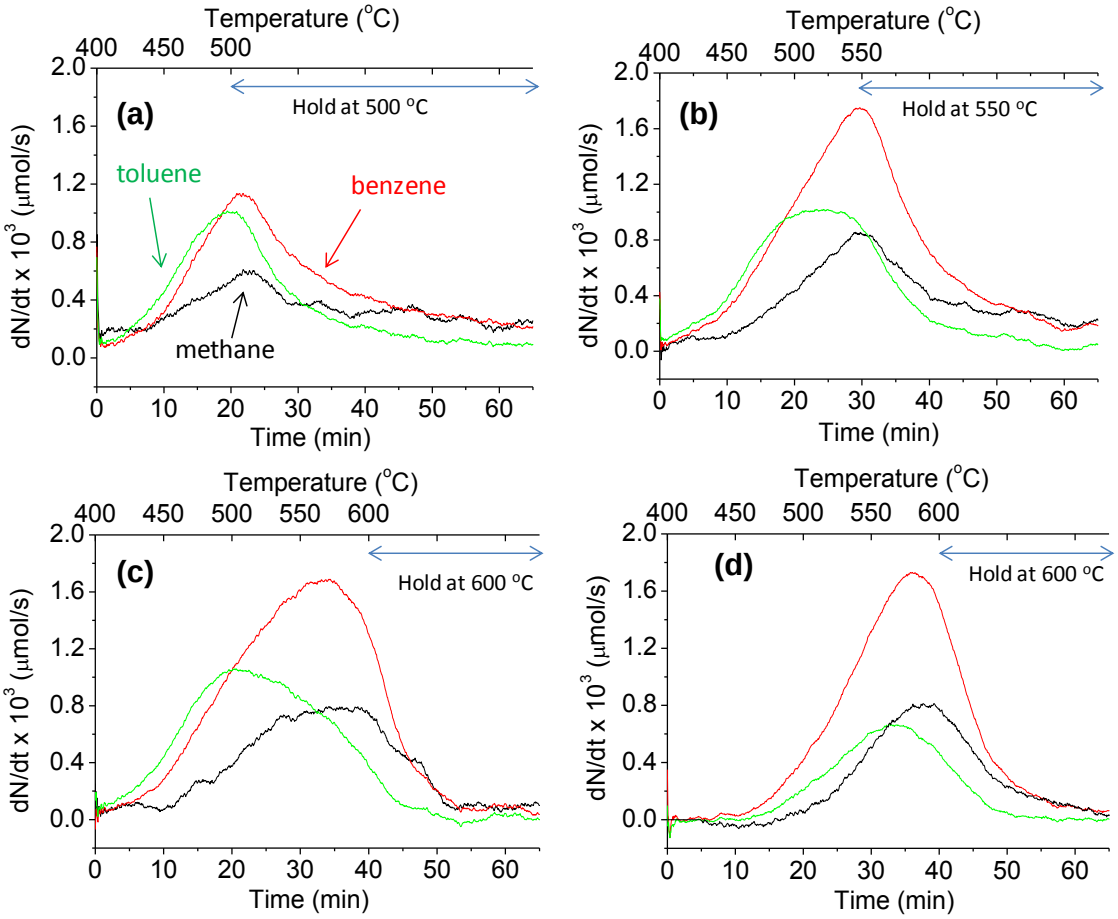

Figure 36. Temperature programmed decomposition of the phenolic pool formed by m-cresol reaction at 400 °C (a-c) and 500 °C (d) over 50 mg of HZSM-5 zeolite. A linear ramp of 5 °C/min from 400 °C followed by isothermal hold period at (a) 500 °C, (b) 550 °C, (c) and (d) 600 °C

Figure 35a-c and 36a-c showed the production rate of the detected hydrocarbons upon different TPDe ramps of the spent catalyst at the reaction temperature of 400 °C. And the produced amount of these compounds was reported in the Table 5. As the temperature increased up to 600 °C in the TPDe experiment (Figure 35c and 36c), toluene was produced at the beginning and then benzene and methane started to come off at about 50 °C later than that. And when toluene production rate maximized at around 500 – 520 °C, the peaks for benzene and methane production rate were at higher temperature (575 – 590 °C). Hence, the ratio of benzene to toluene produced upon

TPDe also increased with the reaction temperature (Table 5). These results were consistent with the benzene to toluene ratio observed in the pulse experiment (Figure 31).

Table 5. Product formation (μmol) from temperature programmed decomposition of the phenolic pool formed by m-cresol reaction at 400 ^{o}C over 50 mg of HY and HZSM-5 zeolites

Catalyst	Isothermal hold (^{o}C)	Methane	Benzene	Toluene	$\frac{\text{Benzene}}{\text{Toluene}}$	Note
HY	500	0.3	0.04	0.2	0.200	Fig. 35a
	550	0.6	0.15	0.4	0.375	Fig. 35b
	600	1.0	0.35	0.55	0.636	Fig. 35c
HZSM-5	500	0.3	1.2	1.0	1.200	Fig. 36a
	550	0.7	2.0	1.3	1.538	Fig. 36b
	600	1.0	2.4	1.4	1.714	Fig. 36c
	600 (x2) *	2.5	5.0	2.8	1.786	

* The catalyst amount was doubled (100 mg)

One can infer that increase in benzene selectivity in the pulse experiment, and benzene and methane production rate with reaction temperature might come from further dealkylation of toluene, which was formed earlier at low temperature. However, direct toluene dealkylation forming benzene and methane normally was carried out in the H_2 atmosphere thermally [148] or with metal oxide catalysts [149, 150]. Meanwhile, transformation of toluene over zeolites mainly proceeds via bimolecular

disproportionation reaction [151, 152] forming benzene and xylenes. In the pulse experiment, small amount of xylenes were observed might indicate the presence of toluene disproportionation. However, the selectivity of benzene was always much higher than that of xylenes. And there was no xylenes produced in the TPDe experiment. These results indicated that further disproportionation reaction of toluene was insignificant. Besides, the study of Al Khattaf [140] about toluene transformation over USY zeolite also showed that selectivity to benzene did not depend on reaction temperature, which is different from our results with m-cresol conversion. Light hydrocarbons that produced from toluene reaction were mostly C3 and C4 hydrocarbons, while very little methane was observed.

To verify further reactions of aromatics produced from the phenolic pool, we carried out pulse experiment of toluene or o-xylene over the two zeolites (i.e. HY and HZSM-5) at 600 ^{o}C and the results were shown in Tables 6 and 7, respectively. And even at that high temperature, methane was only observed as trace amount. The main reactions for toluene and o-xylene at 600 ^{o}C were disproportionation and isomerization, which were consistent with the literatures [136, 140, 151-154]. Dealkylation of methylated benzenes to methane was negligible. Conversion of m-cresol over Beta zeolites also showed that demethylation of m-cresol to phenol was also insignificant [133]. Hence, the enhanced production of benzene and methane at high temperature should mainly come from reaction of the phenolic pool rather than dealkylation reaction.

Table 6. Conversion and product yields from toluene thermal cracking or catalytic cracking reactions over 50 mg of HY or HZSM-5 zeolites at 600 ^{o}C. Data at the 1st pulse

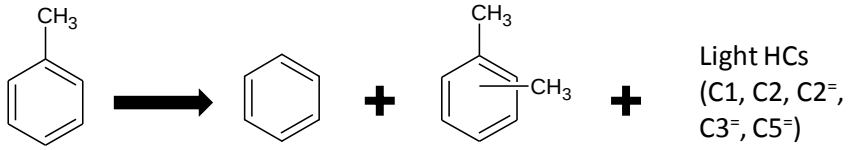

Catalysts	Conversion	Product yields (wt%)		
		Benzene	Xylenes	Light hydrocarbons
No catalyst	0.3	0	0.06	0.26
HY	11.5	5.2	6	0.25
HZSM-5	28.5	12.2	16	0.24

Table 7. Conversion and product yields from o-xylene reaction over 10 mg of HY or HZSM-5 zeolites at 600 ^{o}C. Data at the 1st pulse

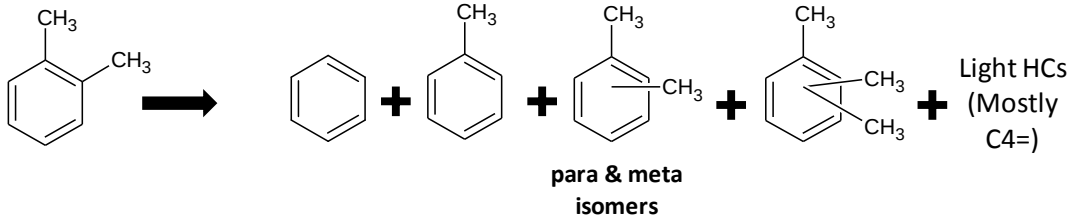

Catalysts	Conversion	Product yields (wt%)				
		Benzene	Toluene	p&m-Xylenes	Trimethyl benzenes	Light hydrocarbons
HY	63	0.1	5	52	5.7	0.2
HZSM-5	72.3	0.9	2.8	59.8	8.5	0.2

The TPDe experiments were carried out with different isothermal holds as shown in Figure 35a-c and 36a-c. When the final temperature was held at 500 ^{o}C (Figure 35a and 36a), the production rate of benzene, toluene and methane peaked at the same temperature, i.e. 500 ^{o}C. Then, the production rate dropped following first order decay. As the final temperature increased up to 550 ^{o}C (Figure 35b and 36b), benzene production rate reached maximum at 550 ^{o}C and dropped following first order decay during isothermal period. Toluene production rate reached the peak at about 520 ^{o}C and

dropped slowly when the temperature kept increasing. Until the temperature reached the isothermal period, production rate of toluene dropped following first order decay. And when the final temperature was hold at 600 ^{o}C (Figure 35c and 36c), the production rate of benzene increased to the peak at about 575 – 590 ^{o}C, then slowly drop when the temperature kept increasing. And the drops followed first order decay in the isothermal period. The production rate of toluene also showed similar trend with that of the TPDe to 550 ^{o}C, i.e. production rate peaked at 520 ^{o}C, slowly dropped with increasing reaction temperature and followed first order decay drop in the isothermal period. Production rates of hydrocarbons increased with the temperature due to the increase of reaction rate constant and availability of the phenolic pool that can react at that temperature. During the isothermal period, the rate constant does not change, while the pool was continuously consumed. Hence, production rates of hydrocarbons decrease following first order decay. Availability of the phenolic pool for production of benzene and toluene might reach maximum at different temperatures before 600 ^{o}C. After those maxima, even though the deposit was continuously consumed, but the rate constant still increased with temperature. Hence the production rate dropped slowly, but not as fast as first order decay in the isothermal period. The TPDe profiles at different isothermal period also indicate that benzene and toluene might be formed mainly from the reaction of the phenolic pool. However, the pools that were available to form these aromatics might be varied, represented by maximum production rates at different temperatures.

TPDe of phenolic pool formed at 400 ^{o}C after m-cresol pulses over different amount of catalyst (i.e. 50 mg and 100 mg) was also carried out. And the total amounts

of hydrocarbons produced were compared in the Table 5. When the catalyst amount was doubled, as a result of more trapping (Figure 34), more hydrocarbons were produced from the phenolic pool upon TPDe. However, the TPDe profile and ratio of benzene/toluene were the same for 2 cases. This result might indicate that the compositions of the phenolic pool were similar and the only difference was the amount of the pool formed.

3.3.4 Effect of zeolite's structure on conversion of m-cresol

Even though the reaction of m-cresol over HY and HZSM-5 zeolites showed similar trends with the reaction temperature, there were considerable differences in the conversion of m-cresol over HY compared to that with HZSM-5 due to the differences in their pore structure. The results in Figure 27 show that m-cresol was trapped and formed carbonaceous deposits more in HY than that in HZSM-5 zeolites. As a result, more products were released in HZSM-5 zeolite than in HY zeolite. The selectivities to aromatic and phenolic products were similar for the two zeolites as shown in Figure 29. However, in the aromatic products, conversion of m-cresol over HZSM-5 zeolite had higher benzene selectivity while lower toluene and xylenes selectivity than that over HY zeolite (Figure 30). The remarkable differences in aromatic yields and selectivities were not only observed in the pulse experiment, but also in the TPDe of the phenolic pool, as shown in Table 5. With the same amount of m-cresol adsorbed on 50 mg of the catalysts, TPDe of the spent HZSM-5 yielded over four times more aromatics than TPDe of the spent HY zeolite. Furthermore, ratio of benzene/toluene was also higher from TPDe of the phenolic pool on HZSM-5 zeolite than on HY zeolite, which was consistent with the results from pulse experiments (Figure 31). The similarities in the

aromatic production trend in the pulse experiment and TPD of the phenolic pool over HY and HZSM-5 zeolite consolidate the hypothesis of aromatic production from the phenolic pool.

In previous pulse experiments (part 3.3.2), deactivation was not observed because the amount of m-cresol in one pulse was very small comparing to the amount of catalyst (i.e., catalyst/reactant ratio in 1 pulse is ~ 6000 wt/wt). Therefore, in order to compare stability of the zeolites and study the change of product yield upon catalyst deactivation, the concentration of m-cresol pulse, and hence the amount of m-cresol in one pulse was increased 10 times (11.3 mol% of m-cresol in He, 1.5 μmol m-cresol/pulse), and only 50 mg of catalyst was used. Figure 37 shows evolution of product yields and unreacted m-cresol with pulse number in the reaction of m-cresol over HY and HZSM-5 zeolites at 500 ^{o}C. It is evident that deactivation is much more pronounced in the reaction over HY than HZSM-5 zeolite. HZSM-5 catalyst was stable up to 10 pulses of m-cresol, i.e. product yields almost did not change with pulse number. While in m-cresol conversion over HY zeolite, total output increased with pulse number due to more evolution of phenolic compounds and unreacted m-cresol. This trend indicates that less phenolic compound was trapped in the catalyst bed. Besides, yield of aromatic products slightly decrease was also an evidence for catalyst deactivation. Due to deactivation, selectivity to aromatic products decreased considerably in the reaction over HY zeolite. In the 1st pulse, aromatics were major products in the output. However, phenolic products became dominant in the 10th pulse. Fast deactivation in the reaction over HY zeolite was possibly due to significant trapping of the material at the initial pulses causing pore blockage to the catalyst. In the

reaction over HZSM-5 zeolite, even though the material was also trapped considerably, but catalyst deactivation was not apparent. Aromatics were always the major products in the reaction over HZSM-5 zeolite, and the selectivity did not change up to 10 pulses.

HZSM-5 zeolite contains 2 type of medium pore channels, i.e 10-ring straight and sinusoidal channels, interconnected that allows the molecule diffuse in 3-dimensions. HY zeolite also has 3-dimensional structure with a large void surrounded by 12-ring windows [80]. Coke formation from hydrocarbon conversion over zeolites depends strongly on the zeolite's pore structure [142, 155, 156]. The zeolite with relatively large void/aperture size ratio, such as Y zeolite, has higher trapping ability than the one that has similar size of cavity and channel such as ZSM-5 zeolite. Steric constraints in ZSM-5 restrict the formation of carbonaceous deposits, which proceeds via bimolecular reactions and produce smaller coke molecules compared to that in Y zeolite. While the cokes in Y zeolite are large polyaromatic hydrocarbons, the cokes in ZSM-5 usually have 1 or 2 aromatic rings with alkyl chain. Coke formation in conversion of oxygenated compounds also depends on the zeolite structure [147]. Large pore zeolite, such as Y, has shown to have high coke deposition, while intermediate pore zeolite, such as ZSM-5, has less coke formation and produces highest aromatic yields from catalytic fast pyrolysis of glucose. Hence, in the reaction of m-cresol over zeolites, high trapping ability of HY zeolite increase the carbonaceous deposits compared to that of HZSM-5 zeolite. Besides, the phenolic pool formed on HZSM-5 zeolite might have smaller size than that on HY zeolite due to the steric constraint. As a result, more separate pools were formed on HZSM-5 zeolite than on HY zeolite when the same amount of m-cresol was trapped leading to higher amount of

aromatic hydrocarbons produced during cracking of the phenolic pool on HZSM-5 zeolite than that on HY zeolite. Larger phenolic pool in HY zeolite might also cause severe pore blockage that deactivates the catalyst quickly. Hence, with increasing pulse number, the phenolic compounds trapped by the HY zeolite reduced, leading to increasing in phenolic product selectivity.

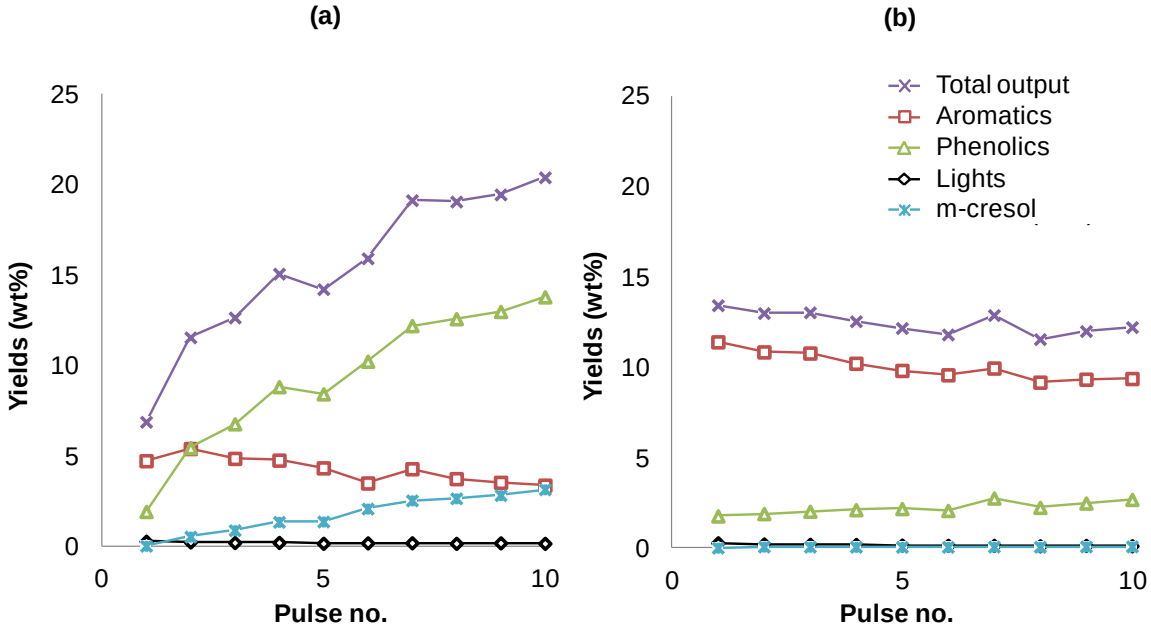

Figure 37. Evolution of product yields and unreacted m-cresol with pulse number in the reaction of m-cresol over (a) HY and (b) HZSM-5 zeolites at 500 ^{o}C

3.3.5 Aromatic production from the phenolic pool

Conversion of cresols over zeolites has been studied extensively in the continuous flow experiment system [131, 133-135, 157]. Main products were other phenolics from isomerization and transalkylation reactions of cresol while very little aromatic were observed. Due to their low selectivity, mechanism of aromatic production was not well discussed. Even though coke formation was high, but trapping of the feed was not as significant as observed in this study.

As shown in the deactivation study of HY zeolite (Figure 37), selectivity to aromatic and phenolic products changed significantly due to catalyst deactivation. With the fresh catalyst, significant trapping of the material was observed, and major products in the output were aromatics. Increasing catalyst deactivation due to pore blockage increased phenolic product release and reduced selectivity to aromatics. Besides, catalyst deactivation occurs very fast, when little amount of m-cresol was sent through the catalyst bed. Meanwhile, in the continuous flow experiment, even though product analysis might be done few minutes after the reaction started, this time on stream is still long enough for severe catalyst deactivation occur. And the activity of the fresh catalyst and initial catalyst deactivation behavior might not be observed. These phenomena, however, can be observed in the pulse experiment in this study. Reaction of m-cresol over the fresh catalyst showed significant material trapping and aromatics were major products in the output. Besides isomerization and transalkylation of m-cresol, condensation reactions of m-cresol and phenolic products might also occur as evidenced by significant water formation. As a result, oligomeric phenolic species were formed and adsorbed on the catalyst surface (i.e. phenolic pool). Zeolite structure has strong influence on the formation of this phenolic pool. Due to its large void volume and aperture channel, HY zeolite traps the phenolic compounds more effectively than HZSM-5 zeolite, and forms larger phenolic pool. And with the same amount of m-cresol trapped, less separate pools were formed in HY zeolite than in HZSM-5 zeolite. Further cracking of the pool forms aromatic product, mainly benzene and toluene, and methane. Overall reaction pathway for m-cresol conversion over zeolite is proposed as in Figure 38.

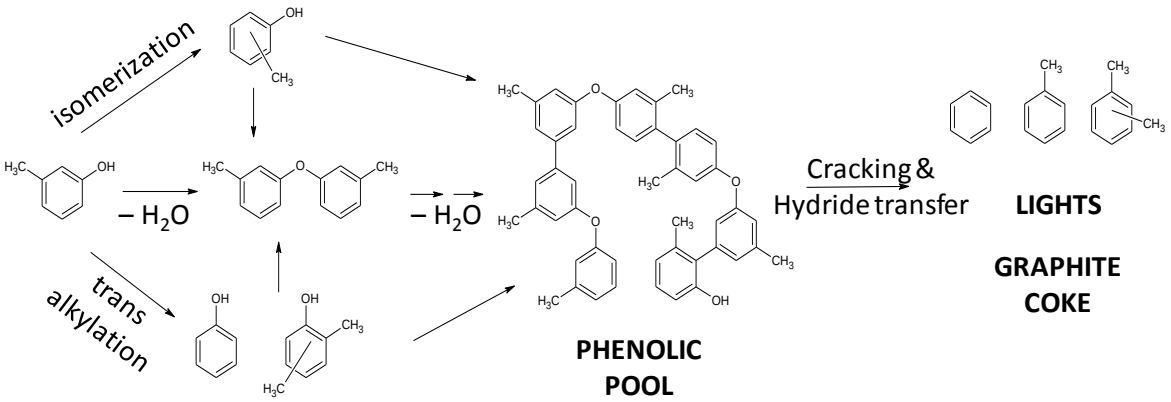

Figure 38. Proposed reaction pathway for m-cresol conversion over zeolites

3.4 Summary

Conversions of m-cresol over zeolites have been studied using micro-pulse reaction system to investigate the activity of the fresh catalysts. Significant trapping of the materials was observed. Major products in the output were aromatic while phenolic products were minor because most of them were trapped in the catalyst via condensation reaction forming phenolic pools. The pools are oxygenated polyaromatic hydrocarbons, and still active for reaction upon high temperature to produce aromatics and light hydrocarbons, mostly methane. With increased reaction temperature, along with enhanced cracking to aromatics, the phenolic products were also captured less which caused less carbonaceous deposition. Porous structure has strong influence on material trapping ability, aromatic production and deactivation of the zeolites. HZSM-5 is a better catalyst than HY in term of aromatic production and catalyst stability.

Chapter 4: Co-feeding of m-cresol to catalytic cracking of hexane isomers over HY zeolite at different reactant's partial pressures

4.1 Introduction

Liquid fuels production from renewable biomass sources has become an attractive alternative for fossil fuels. Among the various approaches for production of biomass-derived liquids investigated during the last few decades, fast pyrolysis and catalytic pyrolysis appear as potential options [158]. The products from these pyrolysis processes (i.e. bio-oils or pyrolysis oil) comprise different amounts of acids, esters, alcohols, furan derivatives, aldehydes (including benzaldehyde with methyl and/or hydroxyl groups), and phenolics (phenol with methyl, methoxy and/or propenyl groups) [6, 22, 159, 160]. Their high oxygen and water contents cause chemical instability, immiscibility with hydrocarbon fuels, high viscosity, high acidity, and low heating value [161]. Consequently, the oils directly obtained from fast pyrolysis (or even catalytic pyrolysis) processes cannot be directly used as transportation fuels without a prior upgrade.

Among other bio-oils upgrading strategies, co-processing with intermediate streams in the refinery units, for example in the Fluid Catalytic Cracking (FCC) unit [39, 42, 59, 61-64] or the hydro-treating or hydro-desulfurization (HDT or HDS) units [61, 62, 64-66], was considered as a potential strategy for processing pyrolysis oil in the industrial standpoint. Usage of the existing infrastructure of the refinery helps reduce the investment cost for bio-fuel production significantly. Besides, with the current large processing capacity of the refining industry, large amounts of pyrolysis oil can be processed, so that rapid change in usage of bio-fuels as transportation can be

achieved in the short term. This processing pathway was considered more competitive than fuels obtained from biomass gasification and biodiesels from vegetable oils [59, 61]. The FCC process represents a promising upgrading alternative since it is one of the largest refinery processes. It has flexibility for handling varying feedstocks, and does not require hydrogen, a valuable commodity.

The co-processing of hydrotreated pyrolysis oil with Long residue and vacuum gasoil (VGO) was studied by Mercader et al. [39, 42] and Foggasy et.al [59], respectively. They found that co-processing gives much lower yields of dry gas and coke as compared to direct processing of pyrolysis oil, and even lower than those calculated from the dilution ratio. Analysis of gasoline fraction showed that there were more branched paraffin and short benzene derivatives produced at the expense of linear paraffin comparing to the reaction of the pure feed. Formation of CO and CO_2 in the gas product, as well as the reduction of oxygen content in the products, showed that deoxygenation was achieved. Less H_2 production in pyrolysis oil co-feeding comparing to reaction of gas oil showed that possibly more hydrogen transfer reaction occurs between hydrocarbons and oxygenates to remove oxygen in the feed.

Effects of adding oxygenates to the cracking reaction of hydrocarbons was also studied with model compounds by Graca et al. [75-78]. In their studies, either phenol or guaiacol was co-fed with n-heptane or methylcyclohexane for cracking reactions over HY and HZSM-5 zeolites. Strong adsorption of phenolic species on the catalysts caused severe deactivation to the cracking reaction of methylcyclohexane and n-heptane. The product selectivity changed slightly, but mostly due to the increased coke formation by phenols rather than the interaction of phenols with hydrocarbon feeds. However, when

the phenolic compounds were co-fed with the gas oil fraction, they observed some aromatic products from dehydration and alkylation of both phenol and guaiacol in the gasoline fraction products. Hence, there might have been some hydrocarbon molecules in the gasoil feed that could transfer hydrogen with the phenolics to deoxygenate these molecules [63, 78]. In our previous study, enhanced hydride transfer from the hydrocarbon (i.e. tetralin) was demonstrated to reduce coke formation and catalyst deactivation in anisole conversion [162].

Bio-oil derived from lignocellulosic biomass comprises a large number of different phenolic compounds (guaiacol, vanillin, eugenol, etc.), which contain various oxygen functionalities (carbonyl, OH, methoxy). They are known to be much more refractory than other oxygenates in bio-oil [50, 51, 53, 56]. Moreover, they tend to accelerate catalyst deactivation due to enhanced coke formation and strong adsorption on acid sites [75, 76]. Therefore, study activity of these phenolic compounds and their deactivation effect to hydrocarbon catalytic cracking reaction are crucial for evaluating the co-processing strategy. In this contribution, effects of co-feeding m-cresol to catalytic cracking reactions of n-hexane and 2,3-dimethyl butane, which represent for paraffinic hydrocarbons with different hydride transfer ability, over HY zeolite was studied in the aspects of deactivation and influence to different reaction pathways of paraffins. Contribution of paraffin reaction pathways was varied by changing the reaction parameters (i.e. reactant's concentration) as well as co-feeding with m-cresol. On the other hand, interaction of the hydrocarbon with phenolic species via hydride transfer was also discussed.

4.2 Experimental

4.2.1 Materials

Hexane isomers used in this study include n-hexane (n-C6, 99% pure) from Sigma Aldrich and 2,3-dimethylbutane (23DMB, 99%+) from Tokyo Chemicals Inc. m-Cresol (99%+) from SAFC and 1-hexene (99%+) from Sigma Aldrich were used for the co-feeding experiment. These hydrocarbons and m-cresol were used for the reaction without further purification. Dealuminated HY zeolite with Si/Al = 40 (CBV780) from Zeolyst International was used as catalyst. The catalyst was pelletized to 90 – 250 μm particles for the reaction. The Brønsted acid site (BAS) density of the catalyst was quantified as 0.07 mmol/g using temperature programmed desorption of isopropyl amine (IPA-TPD) technique as shown in previous part (3.3.1).

4.2.2 Catalytic measurements

Conversion of hexane isomers in He carrier gas over the zeolite was evaluated on a micropulse reactor. For the reactions of n-C6 at different feed's concentrations, 100 mg of catalyst was pretreated under 200 sccm Helium (He) flow at 600 °C for 1 h. After pretreatment, the He flow rate was lowered to 20 sccm and reactor's temperature was adjusted to 500 ^{o}C for reaction. When the reactor's temperature was stable, a pulse of the reactant diluted in He was sent over the catalyst bed. Reactions were carried out with different concentrations of n-C6 in a pulse, i.e. 3.7, 10 and 30 mol% of n-C6 in He. Because the volume of the pulse was kept constant (500 μl), when n-C6 concentration was varied, the amount of n-C6 in a pulse also changed (0.5, 1.4 and 4.1 μmol, respectively). During the 1 h period between each pulse, the catalyst was exposed to continuous flow of He. The products were analyzed on-line by using an HP5890 gas

chromatograph (GC), equipped with an HP-PLOT/Al_2O_3/"S" column and a flame ionization detector (FID) directly connected to the reactor's outlet. Experimental procedure for 23DMB reaction was also similar, except that the catalyst was pretreated at 500 ^oC for 5 hours and the reaction was carried out at 450 ^oC. In the reaction of mixed feed, mass ratio of hexanes/m-cresol or hexanes/1-hexene was kept constant at 95/5, no matter what concentration of paraffin in He is. Therefore, when concentration of paraffin increased, the concentration and amount of olefins or m-cresol in a pulse also increased. Conversion of pure m-cresol at the same concentration and condition with that in the mixed feed was also carried out to compare aromatic production and coke formation with the mixed feed.

To quantify the extent of non-catalytic thermal conversion, pulse of each of the reactant was injected over an inert bed (acid-washed glass beads, 100 μm in diameter) under the same reaction conditions as used with the catalysts. In all cases, the contribution of thermal conversion was lower than 0.2% and was subtracted from the total conversion in each of the conversion values reported below. Each experiment was carried out in duplicate. The differences were always less than 10% and in most cases less than 5%. Therefore, each of the reported values is the average of the two measurements. Products were identified and quantified by using mixtures of reference compounds of calibrated concentrations.

4.2.3 Temperature programmed oxidation (TPO) of the spent catalyst

TPO experiment was used to quantify coke amount on the catalyst after the reaction. The same reactor tube containing spent catalyst was installed in the TPO system, connected with a Cirrus mass spectrometry (MS) to measure evolution of CO_2

(m/z = 44) during the TPO process. 20 sccm of O_2/He (5% volume O_2) was used to oxidize the carbonaceous deposits. After the furnace's temperature was stable at 100 ^oC, a 10 ^oC/min linear heating ramp was started up to 700 ^oC and hold at this temperature until CO_2 signal reach the baseline. To quantify the amount of carbon in m-cresol turned into coke, the CO_2 signal (m/z=44) was calibrated with 100 μl CO_2 pulses.

4.3 Results and discussions

4.3.1 Reactions of hexane isomers at different reactant's concentrations

Evolution of n-C6 and 23DMB conversions with pulse number over HY zeolite at different feed's concentrations in He was shown in Figure 39. Reactions of 23DMB were carried out at lower temperature (i.e. 450 ^oC) due to its higher activity than n-C6. In the reactions of n-C6 or 23DMB, conversion at initial pulses was much higher than the constant conversion region after the 5^{th} pulse. This activity enhancement in the fresh catalyst was explained previously by the contribution of synergistic sites produced upon high temperature pretreatment (chapter 2). These new sites deactivated fast due to strong adsorption of hydrocarbon species. Hence, with increasing pulse number, the conversion dropped considerably until all of these sites were covered. And the reaction from the 5^{th} pulse only occurred on the normal BAS. Deactivation of the BAS was negligible since the amount of reactant in a pulse was rather small comparing to the number of BAS. As shown in Figure 39, increased concentration in a pulse almost did not change the conversion of these paraffins over normal BAS or with contribution of the synergistic sites. Catalytic cracking and dehydrogenation of paraffins over BAS are

first–order dependent on feed's concentration (or partial pressure) [85, 107, 139]. Hence, when the hydrocarbon concentration increased, the reaction rate should increase as well. On the other hand, the amount of hydrocarbon in a pulse also increases with the concentration, leading to reduction of catalyst/reactant ratio. Therefore, the conversion of the feed (X) in the first–order reaction does not depend on the reactant concentration, but rather on the residence time of a pulse (τ) as following expression:

$$X = 1 - e^{-k\tau}$$

In these pulse experiments, the carrier gas flow rate, and hence the residence time of a pulse, was kept constant. Therefore, the conversion should be similar when the reactant's concentration was varied as shown in Figure 39. The conversion of these paraffins over synergistic sites deserved more discussion. As discussed in the Chapter 2, contribution of these synergistic sites enhances protolytic cracking and dehydrogenation paths, which are first–order reactions. Hence, variation of paraffin's concentration in the feed stream also should not change the conversions over these synergistic sites, if deactivation was not taken into account. As mentioned earlier, strong adsorption of hydrocarbon species might cause fast deactivation of these synergistic sites, resulting in considerable drop in conversion at later pulses. The higher hydrocarbon's concentration was in the feed, the higher amount the reactant was sent in a pulse. Hence, the hydrocarbons that adsorbed and deactivated the synergistic sites were supposed to increase, leading to faster deactivation of these sites when reactant's concentration increased. However, the results in Figure 39 showed that deactivation behavior was similar for all feed's concentrations. This interesting behavior can be explained by the varied contribution of hydride transfer in overall reaction with

paraffin's concentration, which affected the product selectivity and coke formation as will be discussed later.

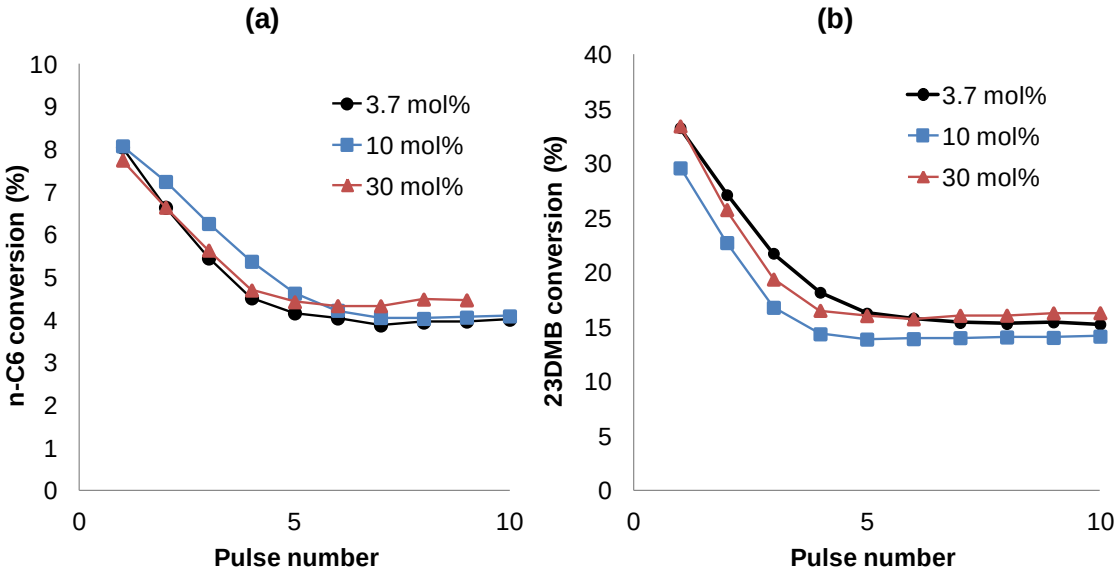

Figure 39. Evolution of conversion with pulse number in the reactions of hexane isomers over HY zeolite: (a) n-C6 at 500 ^{o}C and (b) 23-DMB at 450 ^{o}C

Main pathways for paraffin conversion over zeolites have been studied extensively in the literature [69, 71, 72, 84, 85, 111-113, 123, 139, 163-165]. They are (i) the protolytic cracking of a C–C bond in the pentacoordinated carbonium ion formed when the catalyst protonates the paraffin, (ii) protolytic dehydrogenation of the carbonium ion, and (iii) hydride transfer with a surface carbenium ion. The first two pathways are monomolecular reactions between paraffin with the pristine BAS bearing the H^{+}, while the third pathway occurs after the formation of a carbenium ion. Besides hydride transfer with the paraffinic feed, i.e. route (iii), other reactions following the formation of carbenium ion include isomerization, β-scission and desorption to regenerate the BAS. And in paraffin conversion over zeolites, monomolecular and bimolecular pathways always co-exist and compete with each other in the chain

mechanism, and their contributions vary depending on reaction conditions [85, 139, 166]. In order to compare the contribution of monomolecular protolytic cracking and bimolecular hydride transfer (or β-scission) reaction pathways, the ratio of olefins to paraffins in the products have been used commonly [72, 167]. The ratio of different products, such as (C1 + C2)/iso-butane (i.e. cracking mechanism ratio) [168], was also used to identify relative contribution of protolytic cracking and β-scission cracking routes in the reaction of n-hexane and 3-methylpentane. Besides, Wojciechowski et al. used kinetic chain length [139, 166], which was defined as the ratio of overall rate to rate of initiation, to quantify the significance of chain propagation mechanism via hydride transfer or disproportionation between the paraffinic feed and surface carbenium ion. No matter what criteria have been used, contribution of each pathway depends on similar parameters of the reaction system [72, 85, 113, 139, 169]. That is, monomolecular reaction is more favored at high reaction temperature, low paraffin concentration and low conversion, where olefinic product's concentration is low. In opposite, bimolecular hydride transfer reaction is more favored at high reaction temperature with high paraffin and olefinic product's concentration. Besides, structure of the paraffins also has a strong effect on the hydride transfer ability of the paraffin. Branched paraffin having tertiary carbons is a better hydride donor than a linear paraffin because the tertiary carbenium ion is more stable than the secondary one, resulting in longer life-time of the former carbenium ion on the catalyst surface and higher possibility for hydride transfer reaction to occur [164]. Catalyst structure is also an important parameter affecting contribution of each pathway. Due to its larger transition

state, bimolecular hydride transfer is suppressed in the small pore zeolites such as HZSM-5 [166, 167].

In this study, cracking of n-C6 yielded mainly C2–C5 olefins (C2= to C5=) and C1–C5 paraffins (C1 to C5), while small amounts of hexenes (C6=) and light aromatics (i.e., benzene, toluene, ethylbenzene and xylenes) were also produced. Isomerization products (C6 isomers) were not observed in the reaction of n-C6. However, in the conversion of 23DMB, which is a better hydride donor [111-113, 164], isomerization became an important contribution and production of C6 isomers was among the dominant pathways. As shown in Figure 25 for possible reaction pathways of n-C6 conversion over a BAS, protolytic dehydrogenation followed by β-scission or desorption yields olefinic products, while protolytic cracking and hydride transfer produce paraffins. Hence, the ratio between these two types of product (O/P) can be used to compare relatively the contribution of different reaction pathways of the feed:

$$\frac{\text{Protolytic dehydrogenation}}{\text{Protolytic cracking + hydride transfer}} = \frac{\text{Olefins}}{\text{Paraffins}}$$

Even though conversion of paraffins was not affected by reactant's concentration (Figure 39), product selectivity changed considerably. These changes in product selectivity indicate the variations in contribution of different reaction pathways with reactant's concentration. And the O/P ratio was used to evaluate this variation (Figure 40). Product selectivity from the reaction of a poor hydride donor (i.e. n-C6) at high temperature (i.e. 500 ^{o}C) shows significant contribution from protolytic cracking and protolytic dehydrogenation pathways while the reaction of better hydride donor such as 23DMB at lower temperature (i.e. 450 ^{o}C) has considerable contribution from hydride transfer reaction. Indeed, higher O/P ratio in the products of n-C6 than 23DMB

(Figure 40) and high selectivity to isomerization products in 23DMB conversion confirm the difference in hydride transfer ability of these compounds. As shown in Figure 40, the O/P ratio decreased when reactant's concentration increased. This trend occurred for the reactions of both n-C6 and 23DMB over the normal BAS (at the 8^{th} pulse) or when there were contributions from the synergistic sites (at the 1^{st} pulse).

More detailed changes in product selectivity with concentration for the reaction over normal BAS (i.e. conversion at the 8^{th} pulse) were presented in Figures 41 and 42. In n-C6 conversions, reduction in C3-C5 olefins and increase in C3-C5 paraffins selectivity accounted for the decrease of the O/P ratio. Similar trend was observed in the conversion of 23DMB. Furthermore, significant increase in selectivity to C6 isomers with reactant concentration was also observed. These changes indicate more contribution from hydride transfer reaction pathway with increasing reactant's concentration, because protolytic cracking should produce more small paraffins (C1 and C2) rather than larger ones [72].

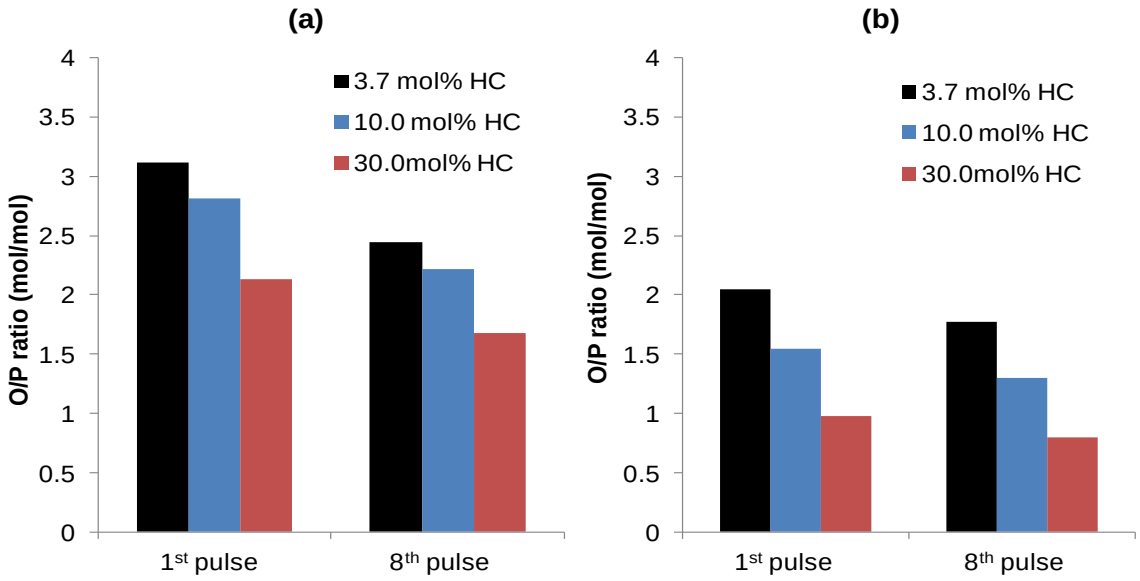

Figure 40. O/P ratio in the cracked products (C1 – C6) in the conversion of (a) n-C6 at 500 ^{o}C and (b) 23-DMB at 450 ^{o}C over HY zeolite with different hydrocarbon's (HC) concentration

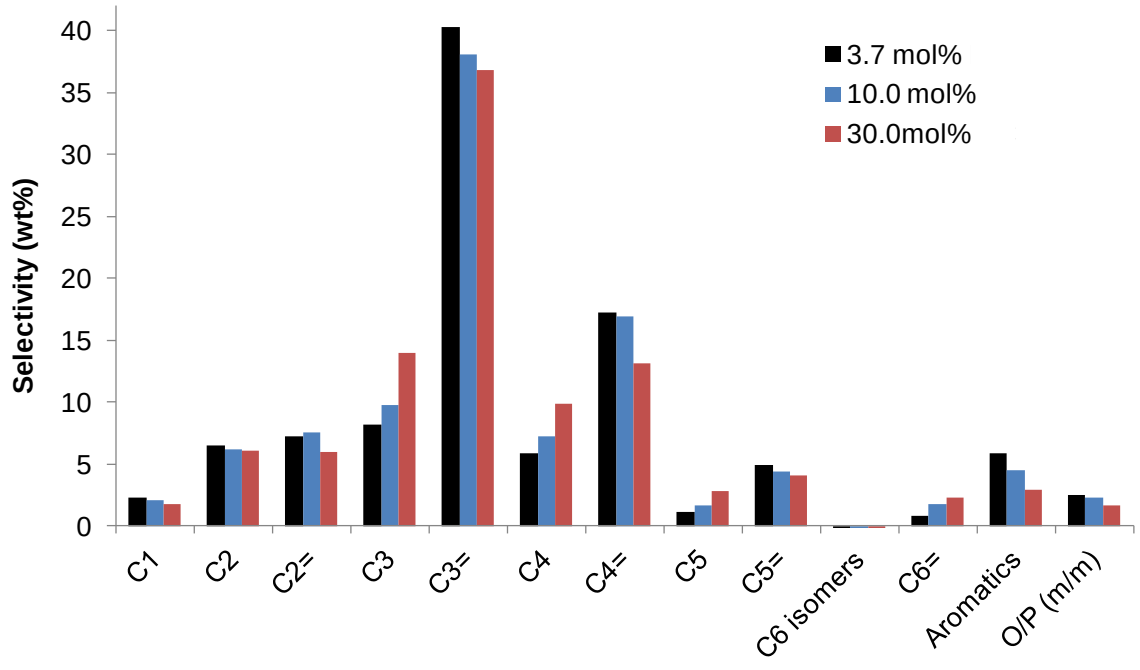

Figure 41. Product selectivity at the 8th pulse in the reactions of n-C6 over HY zeolite at 500 ^{o}C with different feed's concentration

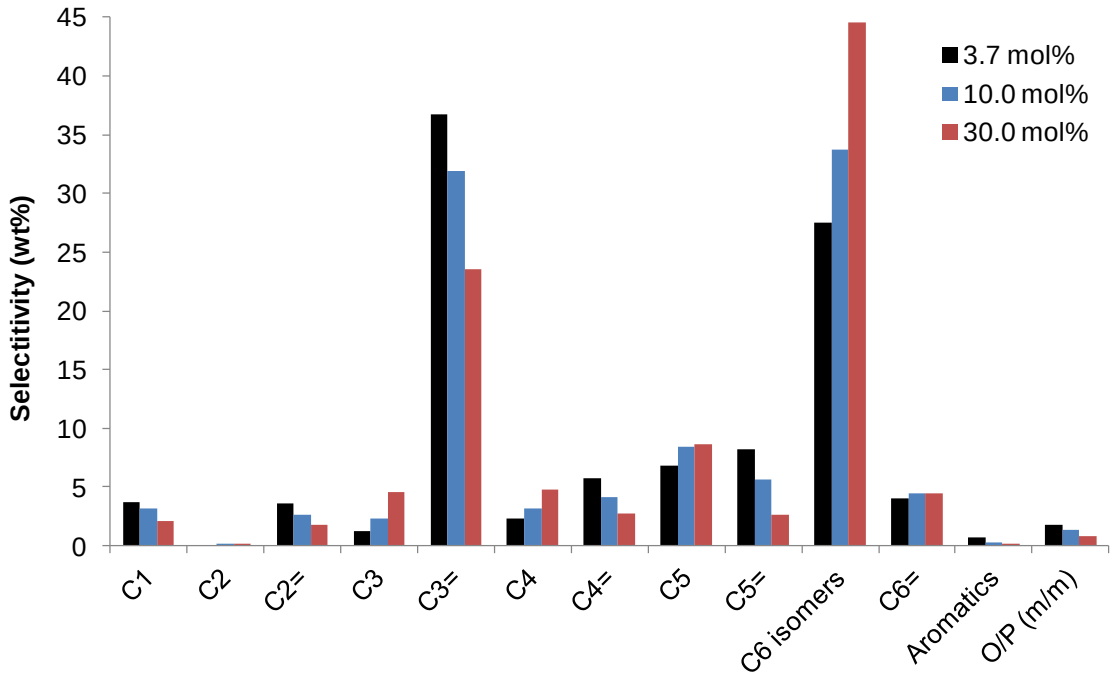

Figure 42. Product selectivity at the 8th pulse in the reactions of 23DMB over HY zeolite at 450 ^{o}C with different feed's concentration

In addition, the selectivity to aromatic products also decreased with the reactant's concentration as shown in Figures 41 and 42. Aromatics are produced through a series of bimolecular reactions such as oligomerization of olefins, dehydrogenation and cyclization reactions [142, 170]. Dehydrogenation occurs via hydride transfer followed by proton transfer (or desorption) to olefinic products. This is different from protolytic dehydrogenation described previously, which occurs via protonation of paraffin by BAS following by dehydrogenation and carbenium ion formation. Continuous dehydrogenation forms polyolefins, which then cyclizes to naphthenic products. Further dehydrogenation of napthenic products forms aromatics. The aromatic products can also go through series of alkylation, hydride transfer and cylization reactions and eventually forms polyaromatic hydrocarbons (i.e. coke) that absorb strongly on the catalyst surface [142, 170]. Even though contribution of hydride

transfer reaction increased with paraffin's concentration, it occurred mostly between paraffinic feed and the surface carbenium ion forming paraffinic products. The possibility of a carbenium ion going through proton transfer to form olefins and further dehydrogenation to form polyolefins, in fact, decreased owing to hydride transfer from the paraffinic feed. Hence, the aromatic selectivity in paraffin conversion decreased with more contribution from hydride transfer reaction. Lower selectivity to aromatic products in the reaction of a better hydride donor and at lower temperature (i.e. 23DMB at 450 ^{o}C in Figure 42 comparing to n-C6 at 500 ^{o}C in Figure 41) also confirms the effect of hydride transfer on aromatic production. Since aromatics are coke precursors, selectivity to these products decrease might also affect selectivity to coke. Coke formation of the spent catalyst after 10 pulses was measured by TPO and presented in Table 8. It is interesting to note that, even though the amount of reactant increased 8 times when the concentration of hexanes in He was increased from 3.7 to 30 mol%, the coke amount after 10 pulses of the reactants were essentially the same. These results mean that coke selectivity decreased significantly with the paraffin's concentration. And for the reaction of 23DMB, which is a better hydride donor and at lower temperature, coke formation was less than that in the reaction of n-C6. The role of hydride transfer in coke reduction and catalyst decay prevention was also presented in the cracking of n-hexane and 2-methylpentane [139] or n-pentane and isobutane [164] in which coke formation in a better hydride donor (i.e. iso-paraffin) was less than the poor hydride donor (n-paraffin).

Table 8. Coke amount (μmol C) in the spent catalyst after 10 pulses of hydrocarbons

Reactant's concentration (mol%)	Reactant's amount in 1 pulse (μmol)	Coke amount (μmol C) after 10 pulses	
		n-C6 reaction at 500 ^{o}C	23DMB reaction at 450 ^{o}C
3.7	0.5	0.9	0.7
30	4.1	0.9	0.7

As shown in Figure 25 , presence of carbenium ion has an important role in the contribution of monomolecular and bimolecular reactions. The carbenium ion occupies the BAS, hence, inhibits the conversion of the feed via protolytic cracking while promote the chain propagation reaction via hydride transfer [113]. Abbot et al. [113] and Zhao et al. [139] studied effect of co-feeding small amount of olefins in the catalytic cracking of paraffin. And they found that addition of small amount of olefins in the feed enhanced conversion of branched paraffin (i.e, 2-methylpentane or 2,3-dimethylbutane) while did not change or slightly reduced conversion of linear paraffin (i.e. n-hexane). Addition of olefins helped generating the carbenium ion, which then promote the hydride transfer step in chain propagation reaction. And the enhancement was clear in the reaction of a good hydride donor, such as branched hexanes, since the contribution of hydride transfer in overall reaction was high. Similar experiment was also carried out in this study to confirm the variation in contribution of hydride transfer reaction. Conversion of paraffins in the reaction of the mixture of 1-hexene (5 wt%) in n-C6 or 23DMB was compared with that in the pure paraffinic feed (Figure 43). At low

hydrocarbon concentration, paraffin conversion in the pure feed and mixed feed were almost identical. And when hydrocarbon concentration increased, while paraffin conversion in the pure feed almost did not change, the conversion in the mixed feed increased, especially the one at high concentration (i.e. 30 mol%). The same trend was observed when n-C6 and 23DMB used as the feed. As previously discussed, contribution of different reaction pathways depends on paraffin concentration. At high paraffin concentration (i.e. 30 mol%), hydride transfer is considerable for both paraffinic reactants, and co-feeding olefins should enhance their conversion. However, it is interesting that co-feeding 1-hexene did not enhance 23DMB conversion at low concentration (i.e. 3.7 mol%), even though 23DMB is a better hydride donor than n-C6. High O/P ratio in the reaction of 23DMB (ca. 2) might indicate that at this low concentration, hydride transfer still did not have important contribution in overall reaction scheme. Major reaction paths might be protolytic dehydrogenation of the tertiary carbon and demethylation to methane (as discussed in Chapter 2). Hence, co-feeding of 1-hexene did not have clear effect on the conversion of 23DMB. These results indicate that, besides the paraffinic structure, concentration is also an important parameter effecting contribution of hydride transfer reaction.

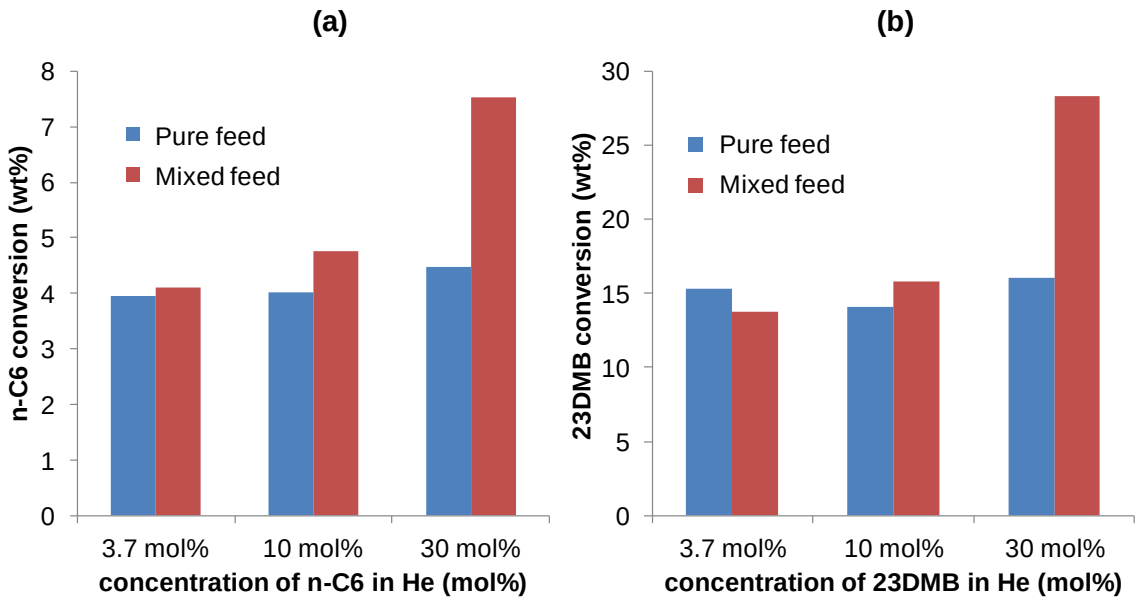

Figure 43. Conversion at the 8th pulse of the paraffins in the pure feed and their mixture with 1-hexene over HY zeolite with different feed's concentration: (a) pure n-C6 and mixed feed at 500 °C and (b) pure 23DMB and mixed feed at 450 °C

4.3.2 Co-feeding m-cresol to reaction of hexane isomers at different reactant's concentrations

Effect of co-feeding m-cresol to the conversion of hexane isomers at different reactant's concentration was shown in Figure 44 and 45 for n-C6 and 23DMB reactions, respectively. For the reaction of n-C6 at low paraffin's concentration (i.e. 3.7 mol%) co-feeding of m-cresol caused significant deactivation, especially to the synergistic sites. Conversion at initial pulses, where activity was enhanced by the synergistic sites, dropped dramatically when m-cresol was co-fed (Figure 44a). However, deactivation of the normal BAS (after the 5th pulse) was less severe. And the difference in conversion over normal BAS between the pure feed and mixed feed did not varied with pulse number.

Strong adsorption and coke formation of m-cresol (and phenolic compounds in general) on zeolite have been major reasons for accelerated catalyst deactivation [63, 77, 78, 133, 162]. Small addition of phenol caused considerable deactivation in the cracking reaction of methylcyclohexane [63] and n-heptane [77]. Graca et al. proposed that molecular adsorption of phenol on both BAS and LAS at early time on stream, which resulting in coke formation enhancement and micropore volume reduction, caused fast deactivation to the conversion of these hydrocarbons. Other study of Graca et al. [78] also showed strong deactivation effect when co-feeding another phenolic compound, i.e. guaiacol, in the catalytic cracking reaction of n-heptane over HY and HZSM-5 zeolites. In previous results about the conversion of m-cresol over zeolites (Chapter 3) using the pulse reaction system, significant trapping of the feed was also observed which resulted in fast catalyst deactivation. For the catalyst in our study, even though the synergistic site has much higher activity than BAS, but the number of these sites only accounts for a small fraction of the total acid sites (as discussed in Chapter 2). And they deactivated rapidly even in the reaction of pure paraffins by strong adsorption of hydrocarbon species. In addition to that, strong adsorption and coke formation of m-cresol on these sites might cause deactivation more detrimental. However, even though BAS also trapped the phenolic compounds strongly, amount of m-cresol in a pulse was so small comparing to the number of BAS that accumulation of m-cresol during pulses did not cause continuous decrease in the conversion over BAS. Nevertheless, the constant difference in conversion of n-C6 between the pure feed and the mixed feed after the 5^{th} pulse might indicate that deactivation by m-cresol still occurred and it was due to competitive adsorption of m-cresol.

Interestingly, when the feed's concentration increased, the deactivation effect of m-cresol to both the synergistic site and BAS was diminished. That is, the conversion drops when co-feeding m-cresol reduced as reactant's concentration increased. And at high n-C6 concentration, i.e. 30 mol%, m-cresol did not have deactivation effect to n-C6 conversion (Figure 44c). It is also important to note that, since the mass ratio of m-cresol in the mixed feed was kept constant (i.e. 5 wt%), when feed's concentration increased, m-cresol concentration in the pulse also increased. That is, larger amount of m-cresol was sent in a pulse at higher reactant's concentration. Therefore, more coke formation, which might result in more deactivation, should be expected. However, the opposite results indicated that changing paraffin's concentration influenced deactivation effect of m-cresol remarkably. As discussed previously, when paraffin's concentration increased, the contribution of hydride transfer reaction from the paraffinic feed became more important. And the enhancement of hydride transfer from the paraffin might ease the deactivation effect of m-cresol. The results from reaction of 23DMB and its mixture with m-cresol can further confirm this hypothesis (Figure 45). At low 23DMB concentration (Figure 45a), co-feeding m-cresol still cause considerable deactivation to 23DMB conversion. However, comparing to the reaction of n-C6 at the same concentration, the deactivation effect was less, especially on the synergistic site. Because 23DMB is a better hydride donor than n-C6, and its reaction was at lower temperature, contribution of hydride transfer in overall reaction was higher than that in n-C6 reaction. Hence, less deactivation of m-cresol to 23DMB conversion might also be related to enhancement of hydride transfer from the feed. Similar to n-C6 reaction, when 23DMB concentration increased, the deactivation effect by m-cresol was

diminished. Deactivation was even disappeared at lower concentration than reaction of n-C6 (i.e. at 10 mol% of 23DMB, Figure 45b).

Effect of hydride transfer ability of hydrocarbon to deactivation in anisole conversion was also reported in our previous study [162]. Due to its strong adsorption and coke formation tendency, anisole conversion dropped remarkably with reaction time on stream as catalyst was deactivated. When anisole was co-fed with a good hydride donor such as tetralin [171], catalyst activity enhanced significantly, and catalyst deactivation could not be observed during the same time on stream period with pure anisole reaction. Co-feeding anisole with benzene, which is not a hydride donating molecule, did not change catalyst activity and stability comparing to the reaction of pure anisole. Interestingly, small addition of tetralin to the mixture of anisole and benzene showed significant activity enhancement in anisole conversion, even though it was lower than the reaction of anisole and tetralin mixture. And co-feeding anisole with a poor hydride donor such as n-decane [171] only increased the activity slightly comparing to pure anisole conversion. The reason for slight conversion increase was possibly due to dilution effect of n-decane that preventing condensation of anisole into coke, because the paraffin concentration in this case was small (i.e. 2-3 mol% in He). TPO analysis of the spent catalysts also showed that coke amount in the reaction of anisole and tetralin mixture was lower comparing to the reaction of pure anisole, even though more material was sent through the catalyst bed in the case of the mixed feed. The roles of hydride transfer from tetralin were to promote desorption of the surface species and minimize hydride transfer from the coke precursor that helped reducing coke formation in anisole conversion. In this study, similar effect of hydride transfer to

the deactivation by m-cresol was also expected when paraffin's concentration was increased or a better hydride donor was used. Perhaps, one might think that dilution effect of the paraffins might play an important role in reducing catalyst deactivation. However, the mass ratio between hydrocarbon/m-cresol was always kept constant at 95/5 in all cases. And the fact that a better hydride donor such as 23DMB had less deactivation than a poor one (i.e. n-C6) supported the roles of hydride transfer in reducing deactivation effect by m-cresol.

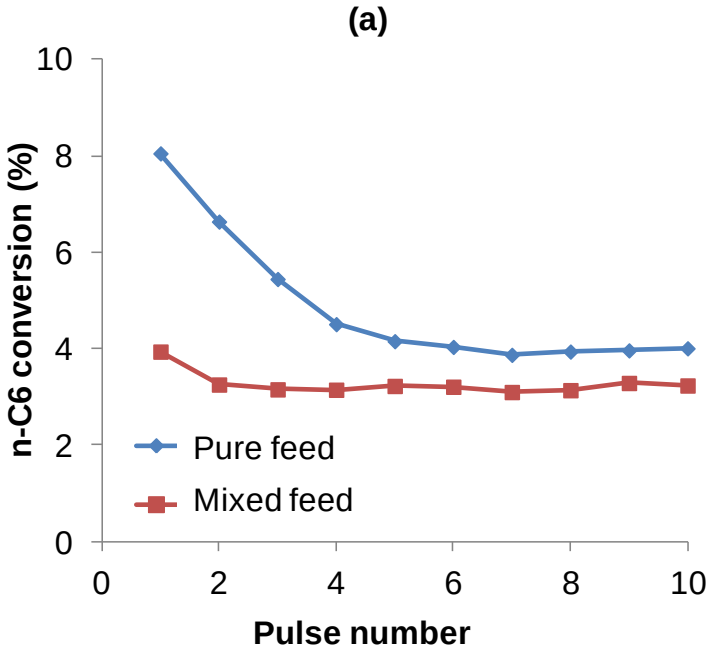

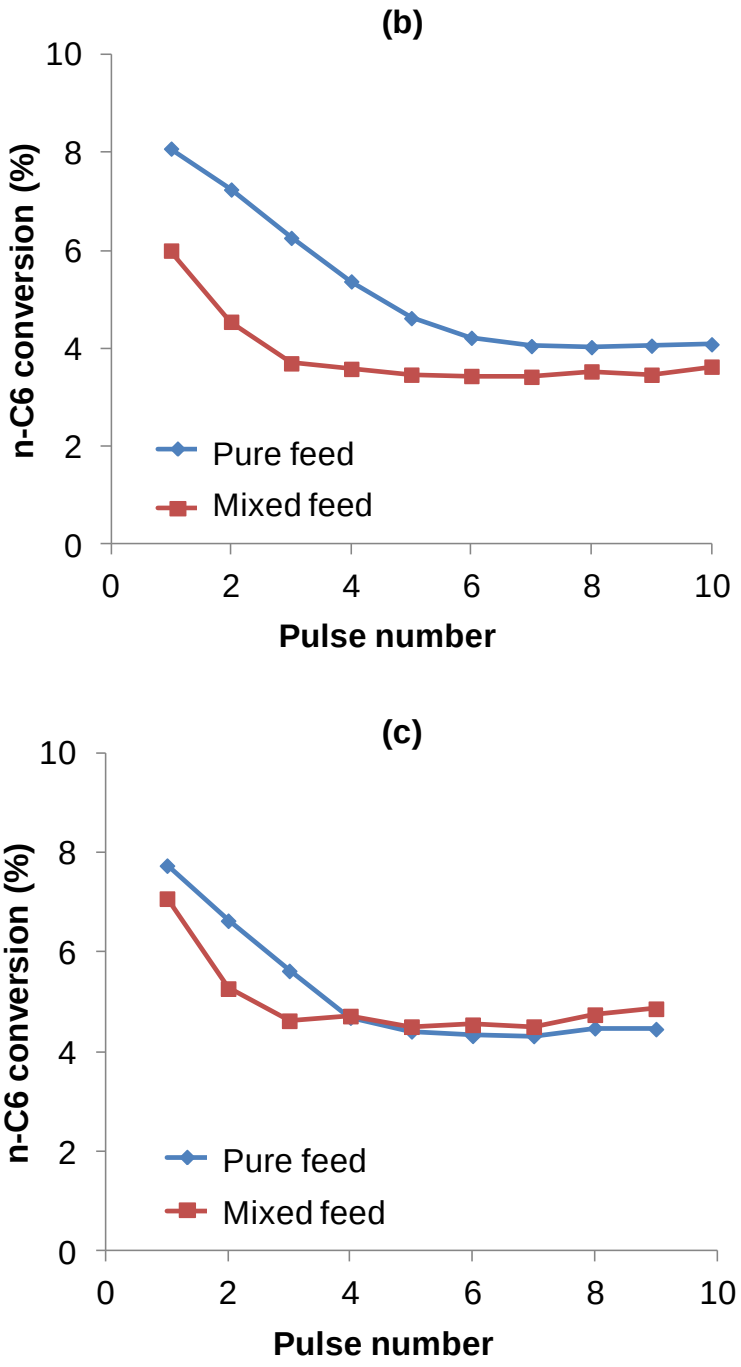

Figure 44. Evolution of n-C6 conversion with pulse number in the reactions of pure n-C6 and its mixture with m-cresol over HY zeolite at 500 ^{o}C with different n-C6 concentration in He: (a) 3.7 mol%, (b) 10 mol% and (c) 30 mol%

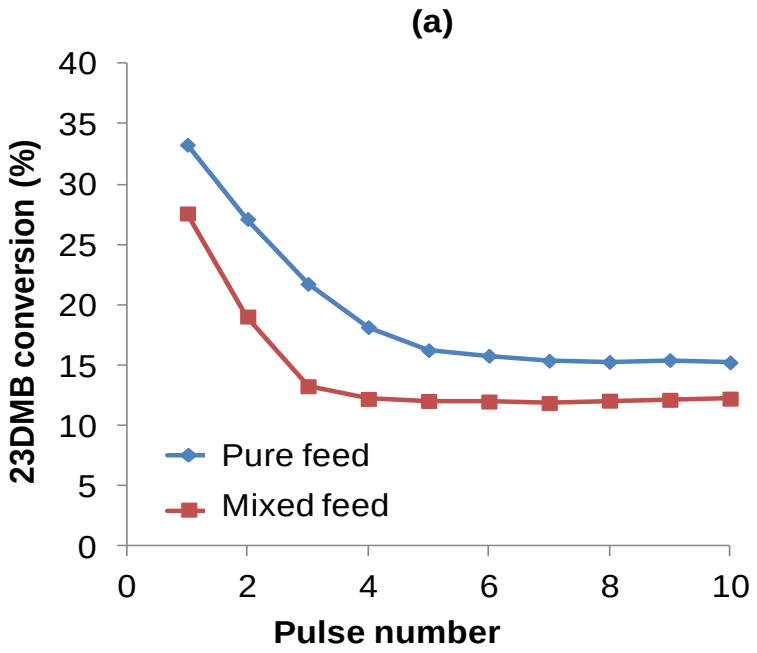
(a)
23DMB conversion (%)
40
35
30
25
20
15
10
5
0
0
2
4
6
8
10
Pulse number
Pure feed
Mixed feed

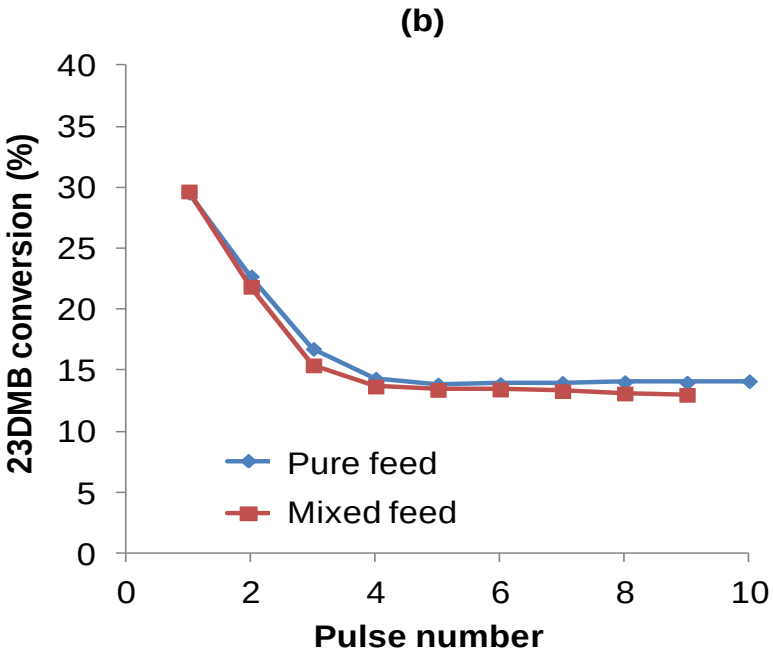
(b)
23DMB conversion (%)
40
35
30
25
20
15
10
5
0
0
2
4
6
8
10
Pulse number
Pure feed
Mixed feed

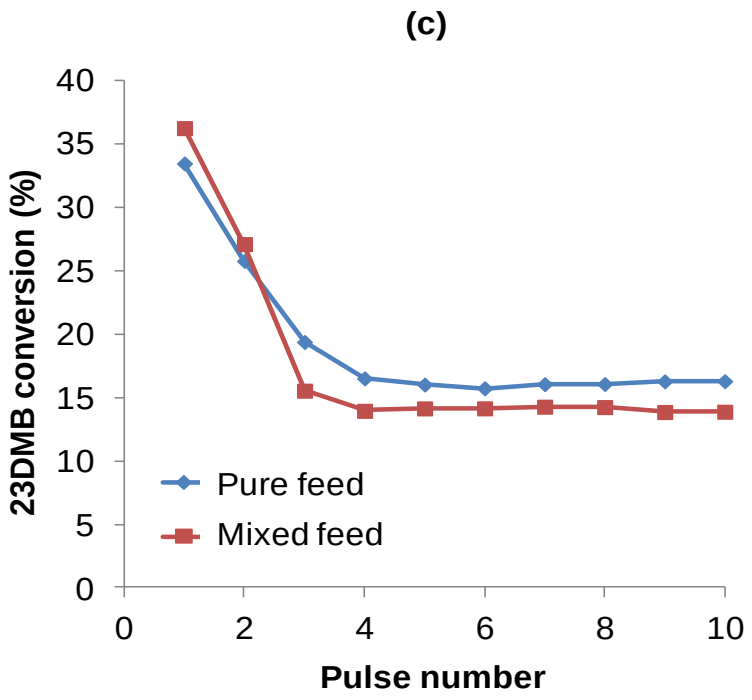

Figure 45. Evolution of 23DMB conversion with pulse number in the reactions of pure 23DMB and its mixture with m-cresol over HY zeolite at 450 ^{o}C with different 23DMB concentration in He: (a) 3.7 mol%, (b) 10 mol% and (c) 30 mol%

In order to confirm the role of hydride transfer, coke analysis of the spent catalysts was also carried out after 10 pulses of the pure m-cresol and its mixture with hexanes at different feed's concentrations. Amount of m-cresol in the pure feed was the same with that of m-cresol in the mixed feed (i.e. corresponding to 5wt% of m-cresol in hexanes), and the concentration of the feed was adjusted according to paraffin's concentration. The results were presented in Figure 46. At low feed's concentration (Figure 46a), all of m-cresol was trapped in the catalyst bed, either in the mixed feed or pure feed. And due to additional coke formation from hydrocarbon reaction, coke amount in the mixed feed was higher than that in the pure feed. Due to higher contribution of hydride transfer at the low reaction temperature (i.e. 450 ^{o}C) and with a better hydride donating molecule (i.e. 23DMB), coke formation in the mixture of m-

cresol with 23DMB was lower than that with n-C6. The interesting result was observed for the experiments at high feed's concentration, corresponding to 30 mol% of paraffin in He (Figure 46b). In m-cresol reaction, almost all of m-cresol was trapped in the catalyst bed (i.e. over 92%). Because of the larger amount of feed in a pulse, not all materials were trapped into coke, and the coke amount was higher than that in the low feed's concentration case. Coke amount from m-cresol conversion at lower reaction temperature was higher due to more trapping by the zeolite (as shown in Chapter 3). Interestingly, when m-cresol was co-fed with paraffins, the coke amount was lower comparing to the pure m-cresol reactions, even though much more amount of material was sent in a pulse. At high concentration of paraffin in the feed, contribution of hydride transfer in overall reaction is important which results in lower coke selectivity in paraffin conversion as shown previously (Table 8). Hence, coke formation from paraffin reaction was insignificant in this case. Furthermore, lower coke amount in the mixed feed comparing to pure m-cresol conversion also confirm the role of hydride transfer in reducing coke formation from conversion of a phenolic compound as previously reported [162]. This result is also consistent with the decrease in deactivation effect of m-cresol to paraffin cracking reaction when the feed's concentration increased as reported in this study (Figures 44 and 45).

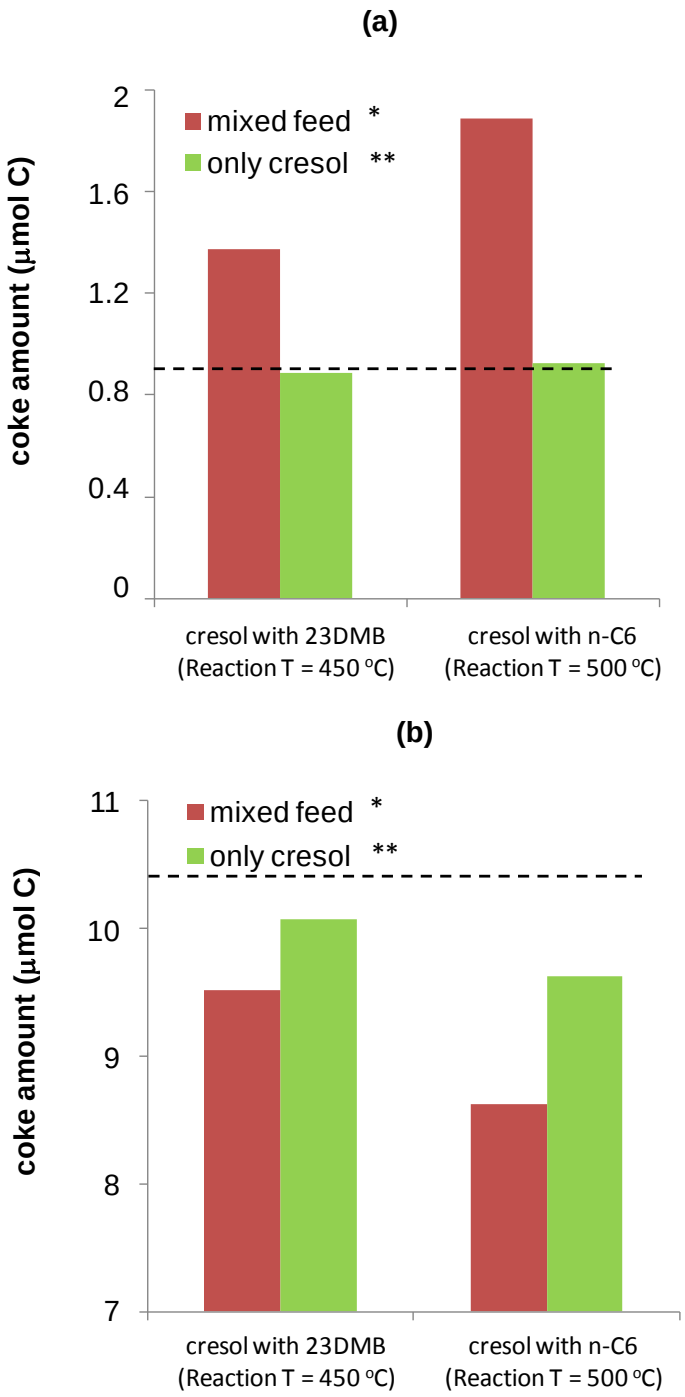

Figure 46. Coke amount after 10 pulses of m-cresol or its mixtures with hydrocarbons over 100mg of HY zeolite at different feed's concentration in He, corresponding to: (a) 3.7 mol% hydrocarbon and (b) 30 mol% hydrocarbon

* mixed feed: hydrocarbon/m-cresol (95/5 wt/wt)

** only cresol: m-cresol with the same amount in the mixed feed

Dashed lines: total amount of C in 10 m-cresol pulses

Co-feeding of m-cresol also affected the selectivity to different pathways in the reaction of paraffins. In order to compare changes in contribution of different reaction paths, O/P ratio in the reaction of the mixed feed was compared with that in the pure paraffinic feed. And the differences (i.e. $O/P_{mixed\ feed} - O/P_{pure\ feed}$) were plotted for the reactions of n-C6 and 23DMB over the normal BAS (i.e. at 8^{th} pulse) as shown in Figure 47. For the reaction at the 8^{th} pulse, co-feeding m-cresol reduced the O/P ratio in the products for all cases. At low reactant's concentration, co-feeding m-cresol caused considerable deactivation to the reaction over BAS by competitive adsorption with the paraffinic feed. This deactivation not only affected the conversion, but also the selectivity to different reaction pathways of paraffin.

More detailed differences in product selectivity were presented in Figures 48 and 49 for the reactions of n-C6 and 23DMB over the BAS, respectively. At low concentration of n-C6, co-feeding m-cresol increased selectivity to light paraffins (C1 to C3), while decreased selectivity to light olefins (C2= to C4=). This change in product selectivity, leading to decrease of the O/P ratio, might indicate that deactivation suppressed protolytic dehydrogenation pathway comparing to protolytic cracking path. Meanwhile, for the reaction of 23DMB, co-feeding of m-cresol increased selectivity to isomerization products (C6 isomers) while selectivity to other products decreased. As a result of that, O/P ratio also decreased. It was clear from the result that deactivation by m-cresol suppressed further protolytic cracking and protolytic dehydrogenation of the C6 isomers. Thus, co-feeding m-cresol in general decreased the O/P ratio in the products due to deactivation of the protolytic cracking and protolytic dehydrogenation paths of the paraffin. The reduction of O/P ratio was more pronounced for the reaction

of n-C6, since deactivation by m-cresol was more severe in n-C6 reaction than that in 23DMB. And it should be noticed that contribution of hydride transfer at low reactant's concentration was negligible.

However, when the reactant concentration increased, the differences in O/P ratio reduced. As shown previously in Figures 44 and 45, increase of reactant's concentration decreases catalyst deactivation because enhanced contribution from hydride transfer might reduce the coke formation in catalytic cracking of either hydrocarbon or phenolic compounds (Figure 46). Hence differences in the O/P ratio might also be lessened along with the conversion differences. Perhaps, one might think that change in conversion was the only reason for the change of O/P ratio in the products when co-feeding m-cresol. However, more careful analysis of the change in product selectivity (Figures 48 and 49) might also show other effects of m-cresol to paraffin reaction other than deactivation of active sites. If the change in product selectivity was only caused by active site deactivation, which decreases overall paraffin conversion, activity preservation when increasing reactant's concentration should lessen the disparity in product selectivity. And there should be no difference in product selectivity, and hence the O/P ratio, at high reactant's concentration (n-C6 reaction at 30 mol% and 23DMB reactions at more than 10 mol%), where paraffin's conversions in the mixed feed and pure paraffinic feed were identical. However, when reactant's concentration increased, even though deactivation effect was diminished, changes in product selectivity were also evident for the drops in protolytic cracking (in 23DMB reaction) and protolytic dehydrogenation (in n-C6 reaction) pathways. For instance, selectivity to C6 isomers in the mixed feed was always higher than that in the pure

23DMB conversion, no matter what reactant's concentration was. And selectivity difference to C2= was always negative while those to C1 and C2 were always positive for n-C6 reaction. Furthermore, selectivity differences of some products were even larger with increasing reactant's concentration, such as C3= and C4 in n-C6 reactions, and C4, C4= and C5 in 23DMB reactions. In overall, the olefinic products had less negative or more positive difference, while selectivity differences of C4 and C5 were more negative. These trends in product selectivity corresponded to the less negative of the O/P ratio with increasing paraffin's concentration.

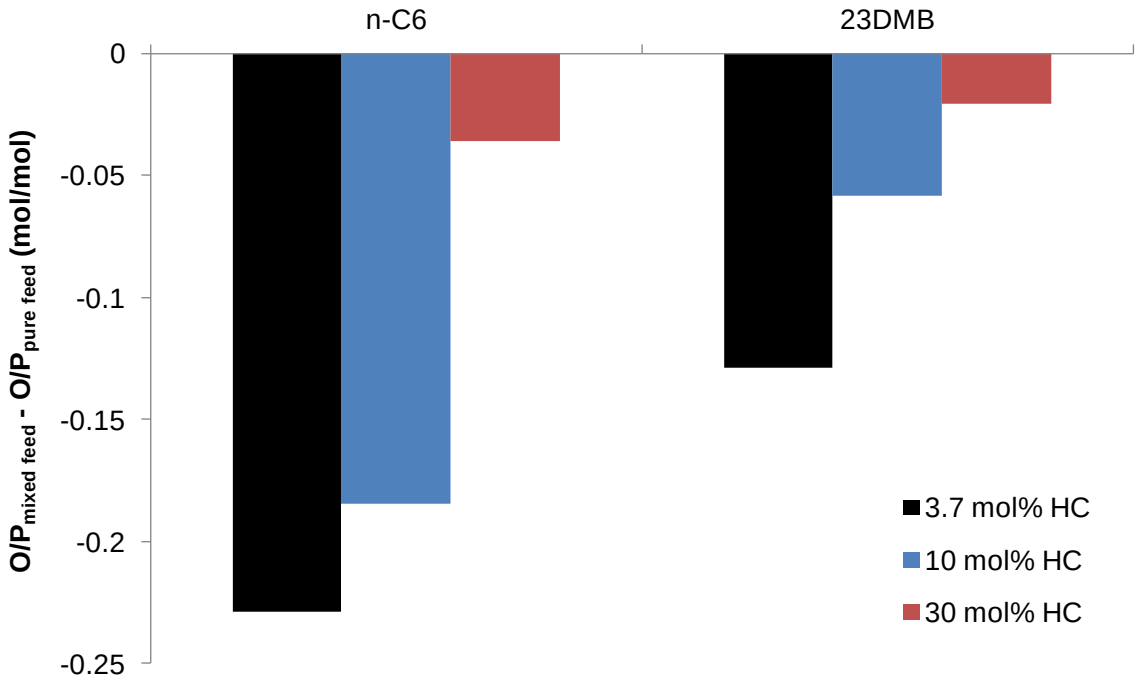

Figure 47. Differences in the O/P ratio in the cracked products (C1 – C6) between the mixed feed and the pure feed in the reaction of n-C6 and its mixture with m-cresol at 500 ^{o}C (n-C6); and 23-DMB and its mixture with m-cresol at 450 ^{o}C (23DMB) over HY zeolite with different hydrocarbon's (HC) concentration. Data at the 8th pulse

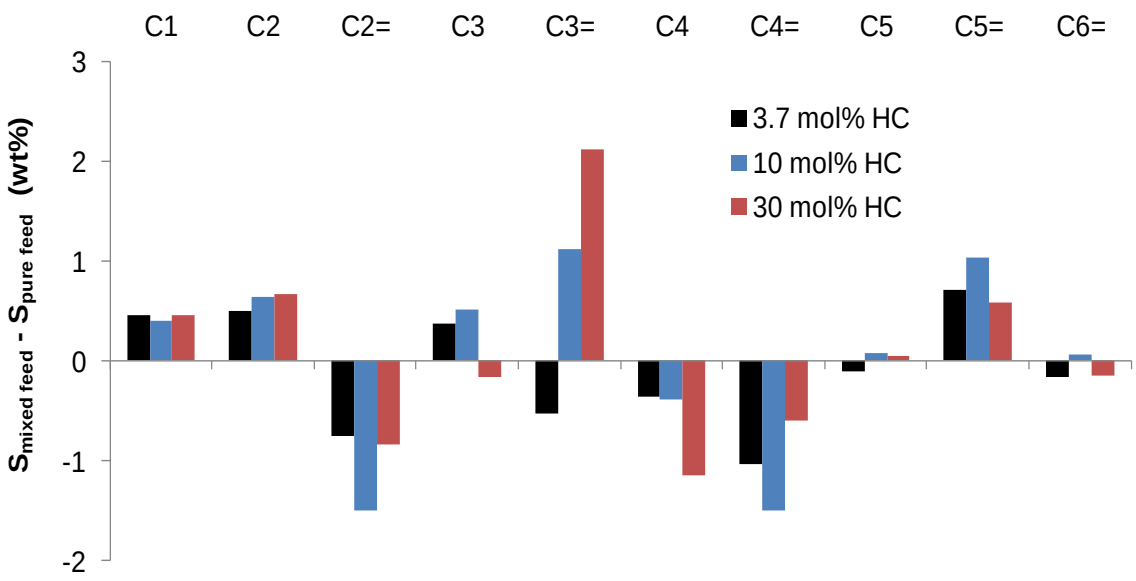

Figure 48. Differences in the product selectivity at the 8th pulse between the reaction of n-C6 and its mixture with m-cresol over HY zeolite at 500 °C with different hydrocarbon's (HC) concentration. Concentration of m-cresol in the mixed feed: 5 wt%.

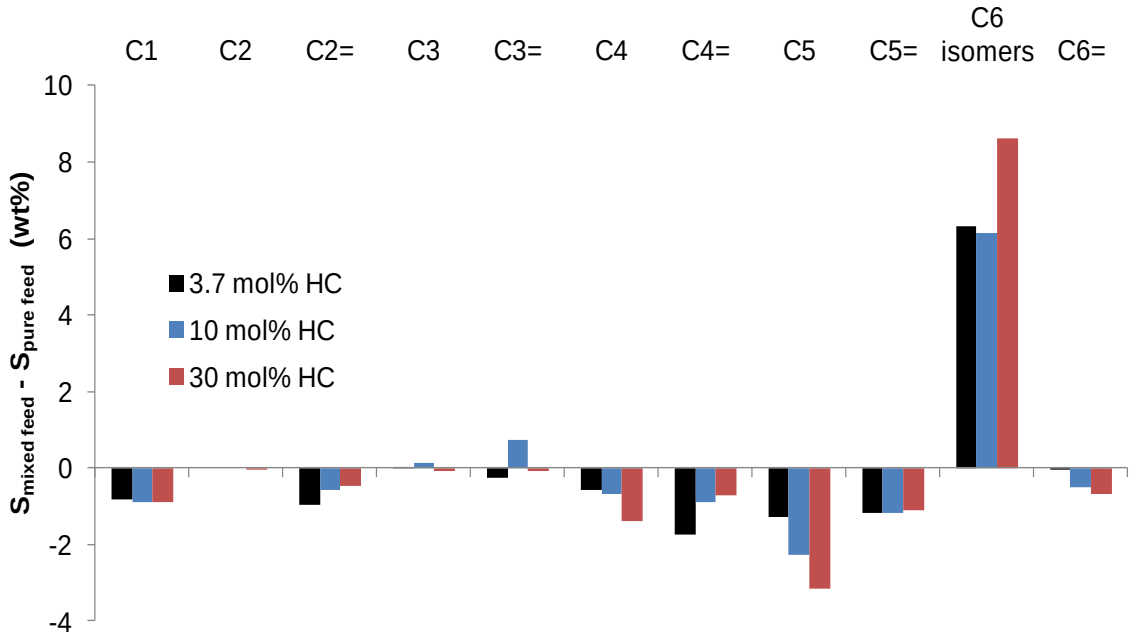

Figure 49. Differences in the product selectivity at the 8th pulse between the reaction of 23DMB and its mixture with m-cresol over HY zeolite at 450 °C with different hydrocarbon's (HC) concentration. Concentration of m-cresol in the mixed feed: 5 wt%.

As mentioned before, increase paraffin's concentration in the feed enhanced contribution of hydride transfer in overall reaction leading to higher selectivity to paraffinic products (part 4.3.1). And the fact that co-feeding m-cresol with paraffins at high reactant's concentration reduced the selectivity to paraffinic products (C4 and C5) more than that at low reactant's concentration might indicate that the phenolic pool formed by m-cresol (as described in Chapter 3) interfered hydride transfer reaction between the paraffinic feed and surface carbenium species. The interference of the phenolic pool to hydrocarbon reaction through hydride transfer can be visualized in Figure 50. In the chain propagation mechanism, the reaction of surface carbenium ions proceeds via either desorption or β-scission to produce olefinic products or hydride transfer from the feed to produce paraffins. The phenolic pool might act as a hydride acceptor, which would compete with the hydride transfer step between hydrocarbons. This interference would lead to reduction of hydride transfer reaction between hydrocarbons, and hence decrease in the selectivity to paraffinic products and increase in O/P ratios. Nevertheless, conversion of the feed would not drop because the carbenium ion of parent paraffin was still formed and continued to react via β-scission cracking, which would produce more olefins such as C3= and C4=.

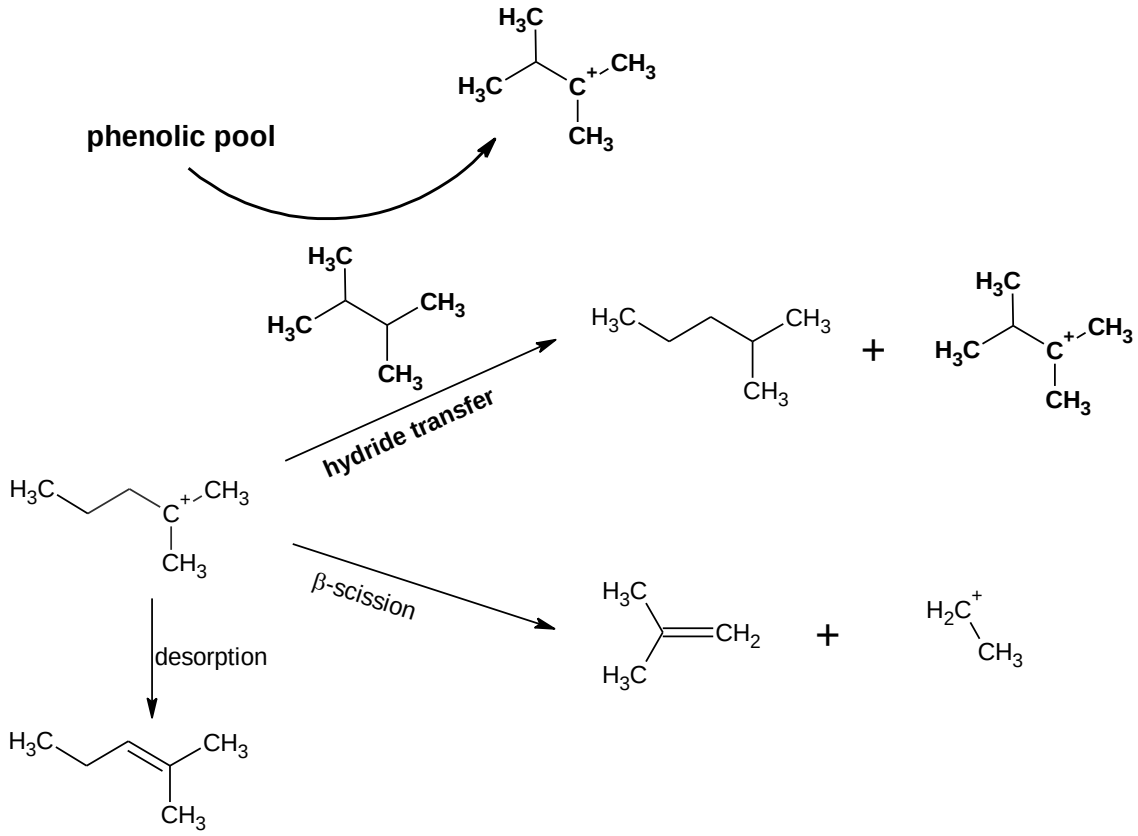

Figure 50. Proposed scheme for the interference of the phenolic pool to hydride transfer reaction between hydrocarbons

In overall, there are two possible effects of m-cresol that might change the contribution of different reaction pathways, which makes the variation of O/P ratio in the products more complicated. Deactivation by competitive adsorption of m-cresol decreases the contribution of protolytic cracking and protolytic dehydrogenation paths, leading to reduction of the O/P ratio. Intervention of the phenolic pool as a hydride acceptor suppresses hydride transfer between hydrocarbons while increases selectivity to β-scission cracking leading to increase in the O/P ratio. Overall change of the O/P in the products should be the combination of these two effects, which compensated each other. At low reactant's concentration, where contribution from hydride transfer was insignificant, the former effect was dominant, leading to considerable drop in the O/P

ratio. When reactant's concentration increased, the role of hydride transfer reaction became more important. And the effect of co-feeding m-cresol to hydride transfer step was more pronounced, resulting in less difference in the O/P ratio.

4.3.3 Effect of hydride transfer from paraffins on m-cresol conversion

Hydride transfer from the paraffin to the phenolic pool did not only vary the contribution of paraffin's reaction pathways, but also affected m-cresol conversion. While in the conversion of cresols over zeolites in the continuous flow experiment system [131, 133-135, 157], the main products were other phenolics from isomerization and transalkylation reactions of cresol. Aromatic production was very little, and the material trapping was insignificant. Conversion of m-cresol in the pulse system, however, showed strong adsorption of the material by the catalysts (Chapter 3). And major products in the output were aromatics (mainly benzene, toluene and xylenes) while there were very little or no phenolic products come off even at 500 ^{o}C. Aromatic production from m-cresol conversion over zeolites was proposed to proceed via the formation of the oligomeric phenolic species (i.e. phenolic pool), which was formed by condensation reaction of the phenolic compounds and adsorbed strongly on the catalyst surface. At high reaction temperature, rearrangement via cracking and hydride transfer of the phenolic pool produced aromatics and more graphitic coke.

Hydride transfer from tetralin was shown to enhance desorption of the phenolic compounds and minimize hydride transfer from the coke precursor leading to reduction of coke formation and catalyst deactivation [162]. It is possible that hydride transfer from paraffin might have similar effect to aromatic conversion from m-cresol conversion. In order to confirm the evolution of phenolic products in m-cresol

conversion, product analysis by HP-1 column was carried out. In the reaction of m-cresol and its mixture with hydrocarbon at low reactant's concentration, there was not any phenolic product detected. It was consistent with the observation from the TPO analysis (Figure 46a) that all m-cresol was trapped in the catalyst bed forming coke, even when it was co-fed with hydrocarbon. Meanwhile, in the reaction of the mixture of m-cresol and hydrocarbon at high reactant concentration (i.e. 30 mol% of hydrocarbon in He), small amount of phenolic products were observed, including cresol isomers, xylenols and other heavier phenolic products. These products were not observed in the reaction of pure m-cresol or pure hydrocarbon at the same condition (i.e reactant's concentrations). The amount of phenolic products came off was estimated by comparing the GC-FID area of those products with that of m-cresol in the feed. And the results were about 1.5% to 2% for the reactions of m-cresol in the mixed feeds. Even though the amount of phenolic was small, but it also indicated that desorption of phenolic compounds was enhanced by hydride transfer from hydrocarbon.

Aromatic production from the reaction of pure hydrocarbons, m-cresol and their mixtures at the 8^{th} pulse was also compared in the Table 9. As expected, no aromatic was produced in the conversion of m-cresol at low reactant's concentration (i.e. corresponding to 3.7 mol% hydrocarbon) since all of the material was trapped. And aromatic production from the reaction of m-cresol/hydrocarbon mixtures was slightly lower than that in the reaction of pure hydrocarbons. This slight difference might be due to deactivation of m-cresol to hydrocarbon conversion. In the conversion of m-cresol at high reactant's concentration (i.e. corresponding to 30 mol% hydrocarbon), small amount of aromatic was produced. Even though the aromatic production in the

mixed feed was higher than that in the conversion of pure m-cresol, one must consider that there was also contribution of aromatic production from hydrocarbons. Hence the aromatic productions from the reaction of pure hydrocarbons and m-cresol were combined in order to compare with the reaction of the mixed feed. And the results showed that aromatics were produced less in the reaction of the mixed feed than in the reaction of the pure components combined. It should be noticed that there was no deactivation to hydrocarbon conversion when m-cresol was co-fed at this high reactant's concentration. Hence, the drops in aromatic production should be due to m-cresol conversion. As shown in Chapter 3, aromatics are major products observed in m-cresol conversion over zeolites using the pulse reaction system. They are produced via cracking of the phenolic pool which was formed by condensation of the phenolic compounds. As discussed earlier, enhanced hydride transfer at high paraffin's concentration promoted desorption of the phenolic compounds. In consequence, formation of the phenolic pool would be suppressed, leading to reduction in aromatic production. Furthermore, decrease in coke formation as shown in Figure 46 was also a result of the suppression to phenolic pool growth due to enhanced hydride transfer from the paraffin.

Table 9. Aromatic production at the 8th pulse (μmol/1,000) for the reaction of pure and mixed feeds over HY zeolite at different feed's concentration in He, corresponding to 3.7 mol% and 30 mol% hydrocarbon

Feeds	3.7 mol% hydrocarbon				30 mol% hydrocarbon			
	Hydro-carbon	*m-cresol*	*Combined from pure feeds*	*Mixed feed **	*Hydro-carbon*	*m-cresol*	*Combined from pure feeds*	*Mixed feed **
nC6 T_r = 500 °C	1.15	0	1.15	1.05	5.91	16.52	22.43	19.87
23DMB T_r = 450 °C	0.52	0	0.52	0.50	0.72	8.19	8.91	7.71

* mixed feed: hydrocarbon/m-cresol (95/5 wt/wt)

4.4 Summary

In this section, the conversion of hexane isomers at different reactant's concentration was studied. And the effect of co-feeding small amount of m-cresol to conversion of these paraffins was also evaluated. Contribution of different reaction pathways in paraffin conversion showed strong dependence on the reactant's concentration and structure. Increasing reactant's concentration resulted in more contribution of hydride transfer in the overall reaction. And branched paraffin had better hydride transfer ability than linear paraffin. Furthermore, enhanced hydride transfer from the paraffin reduces life-time of the carbenium ion on the surfaces, leading to decrease in aromatic and coke formation. Co-feeding small amount of olefins can be used to evaluate the significance in contribution of hydride transfer reaction. When hydride transfer was considerable, co-feeding olefins enhanced paraffin conversion.

Co-feeding small amount of m-cresol at low reactant's concentration caused severed deactivation to the synergistic sites, while slightly deactivated the reaction over normal BAS due to competitive adsorption. Interestingly, when reactant's

concentration increased, deactivation effect of m-cresol diminished. Enhanced hydride transfer from the paraffin at higher reactant's concentration was used to explain for the less deactivation. Co-feeding m-cresol also affected contribution of different reaction pathways of paraffins. Competitive adsorption deactivated protolytic cracking and protolytic dehydrogenation paths. While the phenolic pool formed by condensation of phenolic compounds acted as hydride acceptors that compete with hydride transfer between hydrocarbons. In reverse, hydride transfer from hydrocarbons also promoted desorption of the phenolic compounds, suppressed the formation of the phenolic pool which then resulted in less aromatic and coke formation. Overall interaction between m-cresol conversion and the transformation paths of the surface carbenium ion via hydride transfer was shown in the below figure.

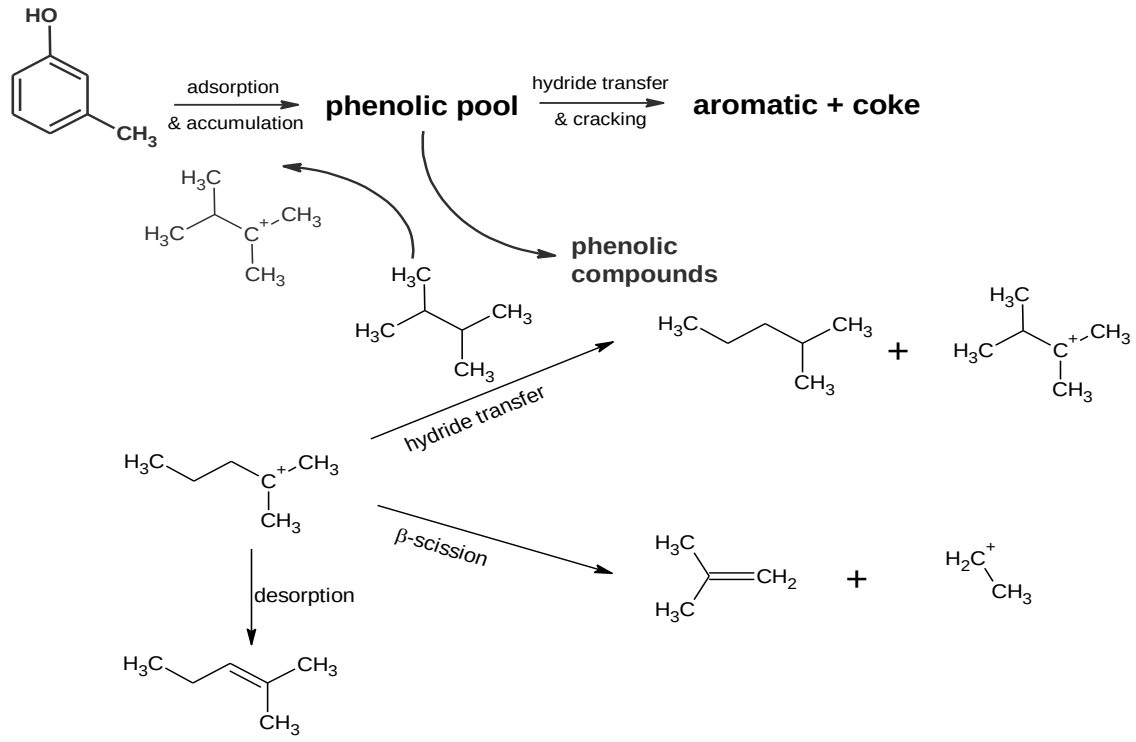

Figure 51. Interaction of the m-cresol and paraffin conversion pathways via hydride transfer

Chapter 5: Catalytic conversion of anisole over HY and HZSM-5 zeolites in the presence of different hydrocarbon mixtures

This material was a joint effort with Dr. Teerawit Prasomsri that was originally published on Applied Catalysis B: Enviromental 106 (2011) 204 – 211

5.1 Introduction

The unprecedented interest in renewable energy expressed in recent years by both government and industry has greatly accelerated research in this field [11]. As a result of these efforts, a significant increase in the role of renewable sources is expected for the near future [172]. In this regard, transportation is a crucial sector in which biomass-derived liquid fuels may have an important impact [173]. Among the various approaches for production of biomass-derived liquids investigated during the last few decades, fast pyrolysis and catalytic pyrolysis appear as potential options [158]. The products from these pyrolysis processes (so-called bio-oils) comprise different amounts of acids, esters, alcohols, furfural, aldehydes (including benzaldehyde with methyl and/or hydroxyl groups), and phenolics (phenol with methyl, methoxy and/or propenyl groups) [6, 22, 159, 160]. Consequently, the oils directly obtained from fast pyrolysis (or even catalytic pyrolysis) processes cannot be directly used as transportation fuels without a prior upgrade. Their high oxygen and water contents cause chemical instability, immiscibility with hydrocarbon fuels, high viscosity, high acidity, and low heating value [161].

A major challenge in processing bio-oils in commercial scale is the massive production volume that will need to be handled. Therefore, it will be desirable to utilize existing refining infrastructure. For example, fluid catalytic cracking (FCC) represents

a possible upgrading alternative since it is one of the largest refinery processes, it has flexibility for handling varying feedstocks, and does not require hydrogen, a valuable commodity. The primary function of the FCC process is to convert gas-oil streams containing high-boiling-point and high-molecular-weight hydrocarbons to more valuable products, such as high-octane gasoline and olefin-rich light gases, e.g. propylene. Co-processing bio-oils with conventional crude oil cuts in FCC units has been discussed in the literature [63, 65, 75, 76].

Oxygenated aromatics deriving from lignin represent a significant fraction of bio-oil and are known to be much more refractory than other oxygenates in bio-oil [50, 51, 53, 56]. Moreover, they tend to accelerate catalyst deactivation due to enhanced coke formation and strong adsorption on acid sites [75, 76]. Bio-oil derived from lignocellulosic biomass comprises a large number of different phenolic compounds (guaiacol, vanillin, eugenol, etc.), which contain various oxygen functionalities (carbonyl, OH, methoxy). In this study, anisole was selected as a representative model compound because it is the one with only one methoxyl functional group. Rather than using real bio-oil mixtures, which would greatly complicate the analysis and interpretation of the results, we have studied the conversion of this methoxyl compound, which is a characteristic functionality in bio-oil. The objective of this contribution is to quantify the deactivating tendency of compounds containing methoxy groups on acidic zeolites and to explore the combined effects of these compounds with hydrocarbons representative of FCC feeds. We conducted most of our studies on HY zeolites, which are typical active components in FCC catalysts [174]. Therefore, the selected reaction conditions in this work are similar to those of FCC processes, but are not necessarily

identical. This study does not attempt to simulate the FCC process, but rather investigate the chemistry of relevant molecules on relevant catalysts. A better understanding of the phenomena involved in the conversion of aromatics containing methoxy functionality and their mixtures with hydrocarbons over HY zeolites may certainly be of importance in FCC commercial units in which biomass-derived stream may be incorporated. For comparison, the behavior observed on an HZSM-5 zeolite was also investigated. The influence of feed composition on the activity, product selectivity, and catalyst stability was investigated for various hydrocarbons in a continuous flow reactor. In addition, experiments were performed using a pulse reactor to elucidate the reaction pathway for the specific mixture of anisole and tetralin, which is an effective H-donor.

5.2 Experimental

5.2.1 Catalytic measurements

The catalytic measurements were conducted on a 1/4 in. stainless steel tubular reactor. Commercial zeolites HY (Si/Al = 15 and 40) from Zeolyst International and HZSM-5 (Si/Al = 45) from Süd-Chemie were used as catalysts. Anisole, a model compound with methoxy functionality, typically present in bio-oil phenolics, was used as the main feed. Various hydrocarbons including propylene (C3=), benzene (Bz), n-decane (n-C10) and tetralin (Tet), were used as co-feeds. In each run, the catalyst sample (50 mg, 40–60 mesh) was placed at the center of the reactor and held in place with plugs of clean glass wool. The top and bottom parts of the packed bed were filled with 3 mm-diameter glass beads. The thermocouple was affixed to the outside wall of

the reactor, at the height corresponding to the center of the catalyst bed. The operating conditions were as follows: atmospheric pressure, 400 ^{o}C, He carrier gas (40 mL/min), space–time (W/F) 0.42 h, with respect to the mass flow rate of anisole in both pure and mixed feeds. Prior to each run, the feed was sent through a by-pass until the concentration stabilized. At this point, the feed stream was switched to enter the reactor. The feed was introduced from a syringe pump at a liquid flow rate 0.12 – 0.24 mL/h and vaporized before entering the reactor. All pipelines were kept heated at 300 ^{o}C to avoid condensation of reactants. With to the procedure mentioned above, we have been able to close the carbon mass balance for every run. By comparing the total mass of the by-pass and that of the reactor outlet, based on the response from the GC-FID signals, a correspondence within 5% was obtained in every run. The products were analyzed on-line using an HP5890 GC, equipped with an HP-5 column and a flame ionization detector (FID). In parallel, the effluent was trapped in methanol, and analyzed by GC–MS (Shimadzu QP2010s) with the same HP-5 column, using reference standard compounds for identification. The GC–MS was used only for qualitative identification of the different product. All quantitative analysis was done on the basis of the GC-FID. The space–time (W/F), expressed in hours, is defined as the ratio between the mass of the catalyst and the mass flow rate of the feed.

It must be noted that the thermal conversion (i.e. blank run with an inert Hisil silica at the same reaction temperature) was negligible for all mixed feeds investigated.

5.2.2 Pulse experiment

The same reactor system was modified to operate in the pulse mode. In this case, two six-port valves were placed in a heating box, connected to the reactor inlet,

outlet and sample loop to switch the flow and inject the pulse of reactant. The reactor includes two parallel 1/4 in. stainless steel tubes, one for bypass, and the other for reaction, which are connected through 3-way valves, also placed inside the oven. The tubing was heated by heating tape to avoid condensation of the reactants.

The feed was injected from a syringe pump, evaporated in the injection port and carried by He gas flow (He #2) into the sampling valve to fill the loop. Then, by switching the six-port valve, another He gas stream (He #1) was used to push the mixture from the sample loop into the reactor and carry it directly into the GC column for analysis. The 30 mg catalyst sample (HY, Si/Al = 40 or HZSM-5, Si/Al = 45) was mixed with 70 mg Hisil silica used as diluents and packed in the reactor tube. The catalyst bed was placed between two sections of 1 mm glass beads and fixed in place with clean glass wool. Before starting the pulse reaction experiment over the catalyst, the mixture from the sample loop was sent repeated times through the bypass line until a stable pulse size was measured in the GC. Then, the 3-way valves were switch to reactor tube. The products leaving the reactor were analyzed by the same GC-FID system mentioned above. The operating conditions for the pulse experiments can be specified as follows. Pulse: 1.0 s retention time, size: 0.0033 mmol tetralin and 0.0017 mmol anisole, atmospheric pressure, 450 ^{o}C.

5.2.3 Catalyst characterization

The coke deposited during reaction was analyzed by temperature programmed oxidation (TPO) of 30 mg samples of spent catalyst, under a gas flow of 2% O_2/He (30 mL/min). The heating ramp was 10 ^{o}C/min. The signals of H_2O (m/z = 18) and CO_2 (m/z = 44) were continuously monitored by a mass spectrometer (MKS). To get a

precise measurement of the total amount of coke deposits on the catalysts an elemental carbon analyzer was used in addition to the TPO. While the results from both techniques are essentially equivalent (±5%), those from the elemental carbon analyzer were more precise and reproducible, and those are the ones reported in this paper.

5.3 Results and discussions

5.3.1 Catalytic reactions of pure anisole over HY zeolite

The total conversion and product distribution obtained from feeding pure anisole (An) onto the HY zeolite are summarized in Table 10. The main products were phenol (Ph), cresol isomers (Cr), xylenol isomers (Xol), methylanisole isomers (MA), and trace amounts of light gases (mainly methane for pure anisole feed and C1–C5 hydrocarbons for mixture feeds).

Table 10. Product distributions from conversion of anisole and anisole-tetralin mixture (~50% tetralin) over HY zeolite. Reaction conditions: W/F = 0.42 h (wrt. anisole for co-feed reaction), T = 400 °C, P = 1 atm He

Feed	Anisole		Anisole + Tetralin	
	TOS = 0.5 h	TOS = 3.0 h	TOS = 0.5 h	TOS = 3.0 h
Conversion of Anisole	83.6	13.9	100	100
Conversion of Tetralin			98.4	96.6
Yield (wt%)				
C_1-C_5	1.2	0.2	8.8	8.2
Anisole	16.4	86.1	0.0	0.0
Phenol	35.2	6.8	28.1	29.2
Methylanisoles	3.3	4.2	0.0	0.0
Cresols	26.4	1.4	12.5	13.1
Xylenols	17.5	1.3	2.8	2.8
Benzene	0.0	0.0	2.1	1.9
Toluene	0.0	0.0	3.5	3.0
Alkylbenzene	0.0	0.0	9.7	8.8
Tetralin	0.0	0.0	0.8	1.7
Naphthalene	0.0	0.0	20.0	19.9
Alkylnaphthalene	0.0	0.0	9.9	9.5
Heavies	0.0	0.0	1.8	1.9
Selectivity of anisole products (wt%)				
Methane	1.4	1.4	2.8	1.1
Phenol	42.1	48.9	63.7	64.0
Methylanisoles	3.9	30.2	0.0	0.0
Cresols	31.6	10.1	27.4	28.7
Xylenols	20.9	9.4	6.1	6.1

In line with anisole conversion results previously observed on HZSM-5 [131, 132, 175], we find here that transalkylation is the dominant reaction over HY. The transalkylation steps involved in the anisole conversion that account for the observed products, are as follows [132]:

$$An + An \rightarrow Ph + MA$$

$$An + Ph \rightarrow Ph + Cr$$

$$An + Cr \rightarrow Ph + Xol$$

$$MA + Ph \rightarrow Cr + Cr$$

It must be noted that these steps are not necessarily elementary and may involve intermediate steps [132]. Two possible reaction pathways can be considered for the transmethylation steps involved in these reactions (see Figure 52). The first one is a dissociative pathway, in which an anisole (An) molecule generates phenol (Ph) and a methyl group, which may remain on the catalyst site as a surface methoxy. In a second step, this methoxy group can be transferred to another phenolic molecule. This phenolic molecule could be An yielding MA (as shown in Figure 52), but it also could be any of the molecules included in the secondary reactions shown above (Ph, Cr) or an aromatic molecule present in the feed, (e.g., tetralin). The second possible reaction pathway involves a non-dissociative bimolecular reaction. In this case, as shown in Figure 52, two anisole molecules directly interact on the surface, producing Ph and MA. A similar non-dissociative bimolecular reaction could in principle be operative for the other reactions mentioned above, including the reaction with tetralin, which is discussed below.

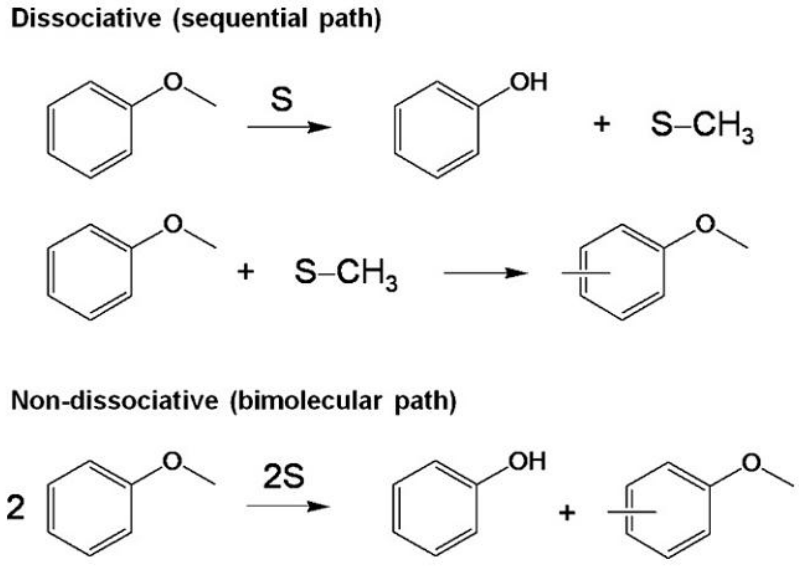

Figure 52. Possible reaction pathways for transalkylation of anisole

A rather fast catalyst deactivation was observed as a function of time on stream (TOS). That is, within 3 h of reaction, the anisole conversion dropped from more than 83% to less than 14%. Both, coke formation and strong adsorption of phenolic compounds (i.e. anisole derivatives) may be responsible for the rapid catalyst deactivation [75, 76]. An interesting trend in product distribution can be observed as the catalyst deactivates. Figure 53 shows the evolution of products (in wt.%) as a function of TOS. It is first noted that phenol (Ph) is the most abundant product at all TOS. At the beginning of the run, the yield of cresol (Cr) and xylenol isomers (Xol) is higher than that of MA; however, this trend is reversed as the catalyst deactivates (i.e. at high TOS). A previous kinetic study [132] demonstrated that Ph and MA are the two primary products arising from anisole disproportionation. By contrast, Cr and Xol appear as secondary products derived from subsequent transalkylation steps.

The evolution of MA shows a maximum as a function of TOS. MA is only produced in the primary transalkylation while the subsequent steps only consume it. The catalyst deactivation causes and initial increase in MA due to a decreased consumption, but at long enough TOS the deactivation affects the primary step as well and the overall generation of products, including MA, decreases. This maximum was not observed for Ph, which in secondary steps, is not only consumed but also produced.

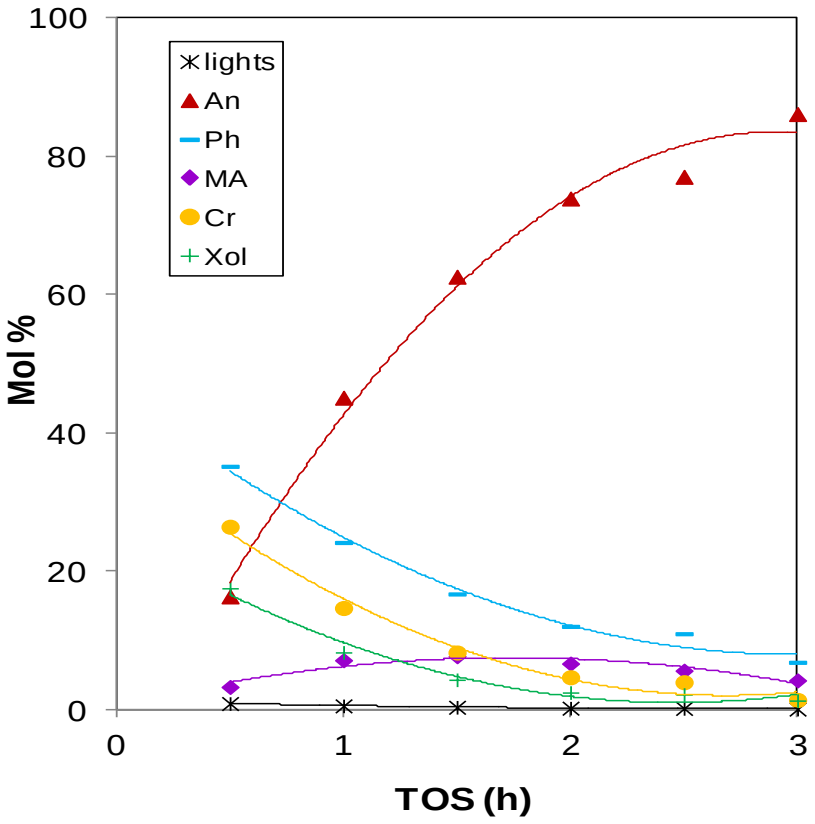

Figure 53. Product composition at the reactor outlet as a function of time on stream during anisole conversion over the HY zeolite. Reaction conditions: W/F = 0.42 h, T = 400 ^{o}C, P = 1 atm He

5.3.2 Effect of mixing anisole with different hydrocarbons over zeolites

To compare the effect of co-feeding hydrocarbons on the reaction of anisole, reactions with mixed feeds were performed at the same W/F(An) = 0.42 h with respect to the mass rate of anisole (F(An)). The total W/F was in fact lower for the mixture because the total feed rate of the mixture (F) was higher than the feed rate of anisole alone (F(An)), which was kept constant. As seen in Table 10, the anisole conversion of the feed containing 50% tetralin was enhanced dramatically to ~100% (i.e. W/F became in excess) even though the total W/F was lower and the W/F(An) was the same as in the case of pure An. We have previously reported the results obtained with pure tetralin

feeds over HY zeolite under the same conditions used in this contribution [171]. In that study, we reported that light hydrocarbons, benzene, toluene and alkylbenzenes, such as ethylbenzene and xylenes, were produced by cracking. Naphthalene, resulting from the dehydrogenation of tetralin was also observed as an important product. In the same study, we measured the H-transfer ability of different hydrocarbons by using 1-tetralone as an indicator. In that contribution, tetralin was identified as a good H-donating molecule [171].

In addition to the changes in activity and stability, significant changes in product distribution were observed with the mixed feed in comparison to the reaction with the pure anisole. For example, the amount of methylanisoles, cresols, and xylenols obtained with pure anisole were significantly higher than those obtained with the mixed feed. At the same time, no changes in product distribution were observed as a function of TOS during the reaction. As we have recently discussed [171], tetralin is an effective H-donor in H-transfer reactions, and it is conceivable that a similar effect is responsible for the enhancement observed here.

A similar set of experiments was conducted with different co-fed hydrocarbons (~50% hydrocarbon–50% anisole). The effect of the presence of different hydrocarbons in the mixture is illustrated with the different deactivation profiles shown in Figure 54 together with the profile obtained with anisole alone (dashed line). The addition of tetralin greatly increased the anisole conversion on the HY zeolite. Since the conversion was 100% during the entire reaction time it is not possible to evaluate the deactivation, but it is clear that the activity remained very high during the 3 h of the experiment. It is suggested that H-transfer from tetralin, a good H-donating compounds

[171], influences the adsorbed species in two possible ways: (1) promotes desorption of surface species; and (2) minimizes the rate of H-transfer from coke precursors. As a result, reduction of coke deposition is expected.

At the same time, tetralin itself can directly react with anisole through a bimolecular interaction. Consequently, the observed beneficial effect of tetralin the addition on anisole conversion may result of a combination of effects.

In contrast, when benzene was used in the mixture instead of tetralin, the deactivation profile followed the same trend as that observed with pure anisole. Benzene is not a H-donor molecule and therefore it is not surprising that it showed no enhancement in either anisole conversion or catalyst stability. Interestingly, as shown in Figure 54, adding only 5% of tetralin into the anisole/benzene mixture had a significant positive impact on anisole conversion. The addition of n-decane had a noticeable effect, although not as pronounced as that obtained with tetralin. Our previous study has shown that the H-transfer from n-decane is minimal [171]. Therefore, the improvement in catalytic activity upon the addition of n-decane can be ascribed to a dilution of the oxygenated aromatics (anisole or its products, phenol, cresol, etc.) on the surface, which prevents condensation of these compounds and minimizes catalyst deactivation. Finally, co-feeding propylene had a negative effect on anisole conversion; it is evident that propylene itself can participate in coke formation [176, 177] and accelerates catalyst deactivation. While to make a conclusion regarding commercial applications, much longer times on stream will need to be evaluated, the 3 h reaction period used in this comparison is long enough to illustrate the dramatic differences observed with the different co-feeds.

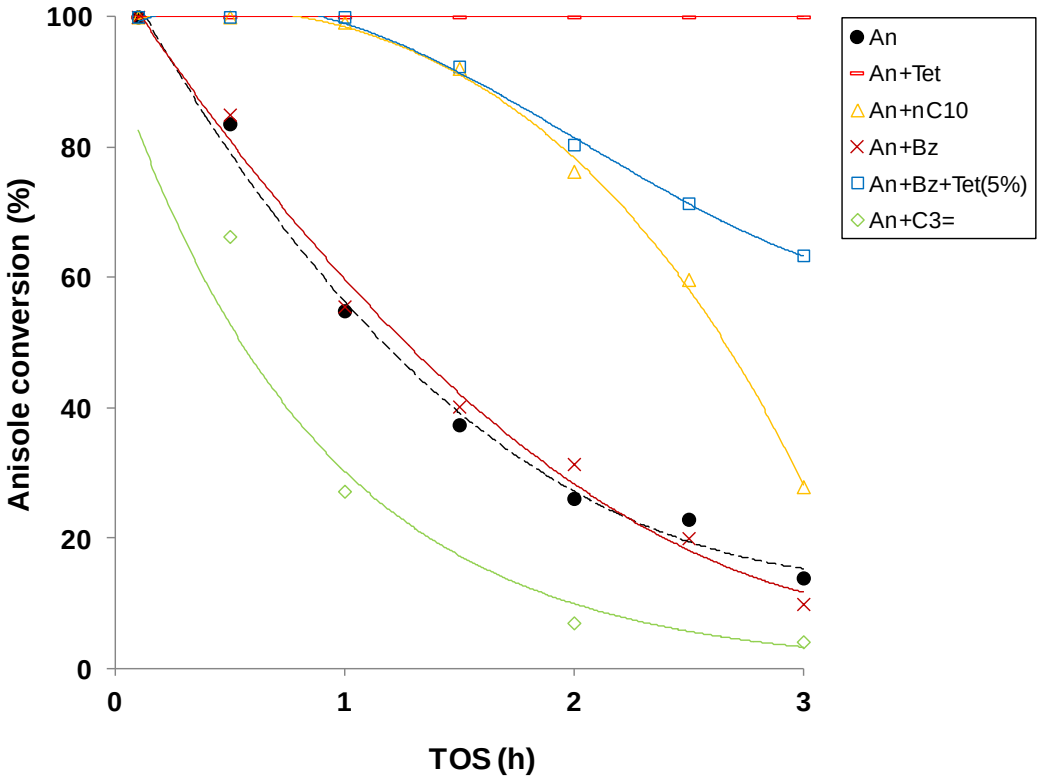

Figure 54. Anisole conversion over HY zeolite with different co-fed hydrocarbons as a function of time on stream. Pure anisole feed is indicated with a dashed line. Reaction conditions: W/F = 0.42 h (wrt. anisole for co-feed reactions), co-feed concentration = ~50%, T = 400 ^{o}C, P = 1 atm He.

The presence of tetralin not only enhanced anisole conversion, but also influenced product distribution, as shown in Figure 55. For instance, the degree of the secondary reaction of phenol alkylation can be measured by the ratio (Cr + Xol)/Ph. For the pure anisole feed, this ratio was about 1.2 at the start of the reaction and decreased to about 1.0 as the catalyst deactivated, since the contribution of the secondary reactions became less prominent (Figure 56a). Similar behavior is observed when the anisole feed was mixed with propylene, n-decane or benzene than for pure anisole (Fig. 4c and d). By contrast, the ratio was less than about 0.5 for the anisole/tetralin mixture and it remained unchanged as a function of TOS (Figure 56b). The reduced phenol alkylation in the presence of tetralin was compensated by an

increase in the alkylation of tetralin. In fact, the alkylnaphthalenes/naphthalene ratio gradually increases with the concentration of anisole in the feed as compared with that of pure tetralin (Figure 57). This trend demonstrates that anisole can transfer its methyl group from the methoxyl group to naphthalene, which is a product of tetralin dehydrogenation.

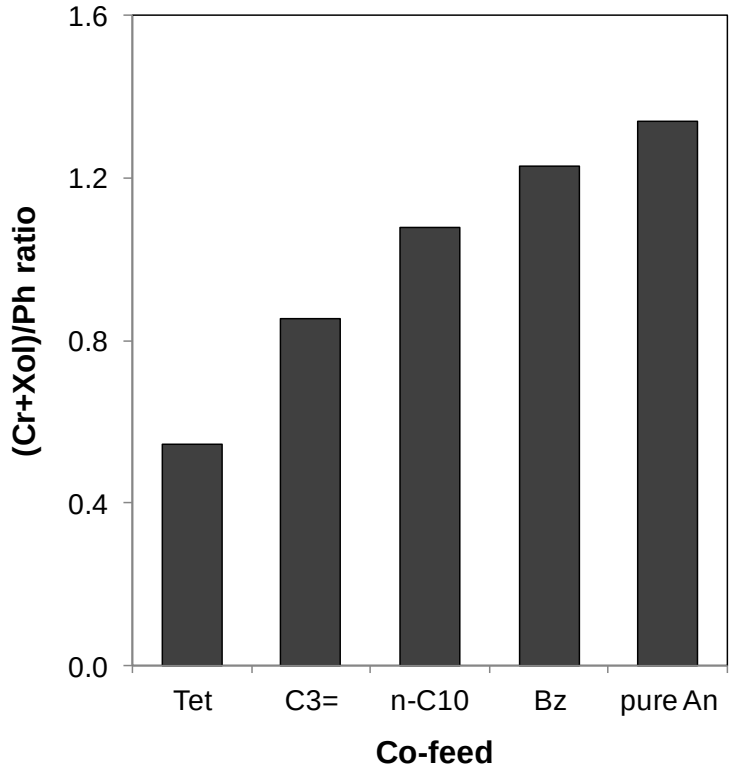

Figure 55. Degree of phenol alkylation (i.e. (Cr + Xol)/Ph yield ratio) for pure anisole and mixture feed reactions over the HY zeolite. Reaction conditions: W/F = 0.42 h (wrt. anisole), T = 400 ^{o}C, P = 1 atm He, co-feed concentration = ~50%, TOS = 0.5 h

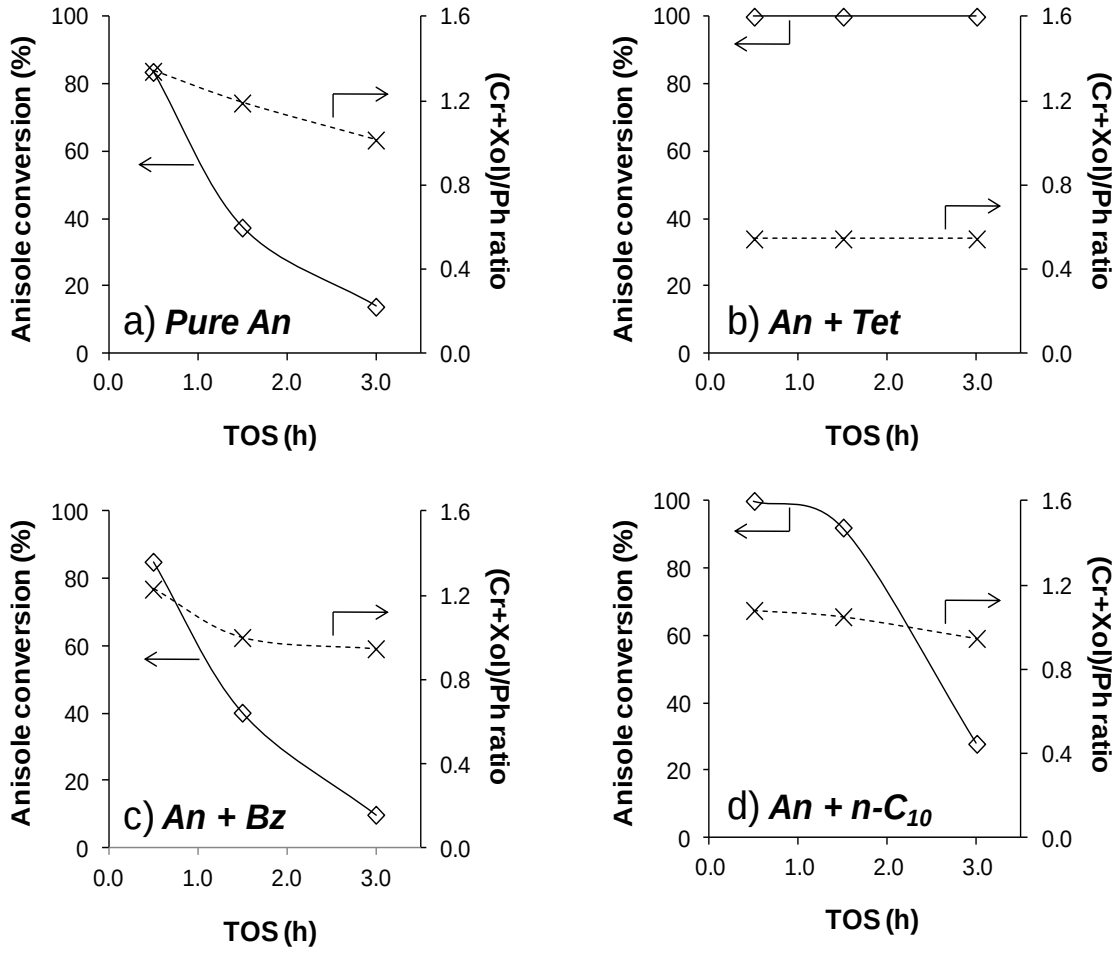

Figure 56. Relationship between conversion of anisole and degree of phenol alkylation as a function of time on stream. Reaction conditions: W/F = 0.42 h (wrt. anisole), T = 400 ^{o}C, P = 1 atm He, co-feed concentration = ~50%, TOS = 0.5 h.

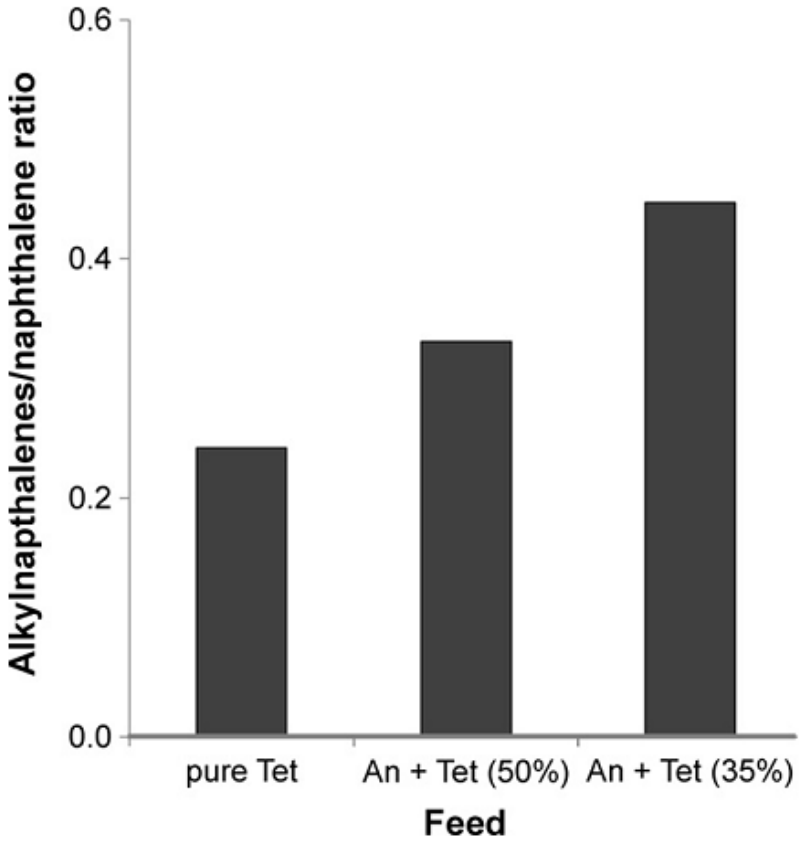

Figure 57. Alkylnapthalenes/naphthalene product ratio for pure tetralin and mixture feed reactions over the HY zeolite. Reaction conditions: W/F = 0.42 h (wrt. anisole), T = 400 ^{o}C, P = 1 atm He, TOS = 0.5 h

5.3.3 Reaction pathways

As mentioned above two possibilities can be considered for the transmethylation of aromatic molecules containing a methoxy group, a dissociative sequential pathway and a non-dissociative bimolecular pathway.

To check whether these paths occur to a significant extent the following experiment was devised. After stabilizing the reactor and the detector, a pulse of anisole was first fed to the reactor followed by a pulse of tetralin sent 4–5 s later. Since the two reactants are not simultaneously present on the catalyst, it is anticipated that only if the dissociative (sequential) pathway is operative transmethylation will be

observed. That is, the anisole from the first pulse, can dissociate and leave a methyl group on the surface, this group can subsequently react with tetralin sent in the subsequent pulse.

Methylation preferentially occurs on activated aromatic rings. The aromatic ring in tetralin is highly activated and therefore it has the tendency to accept a methyl group. At the same time, tetralin is a hydrogen donor and can easily dehydrogenate to naphthalene. Since the hydrogenation/dehydrogenation reactions can be equilibrated at the high temperature of the experiments, while alkylation involves tetralin, only alkylnaphthalene and naphthalene are observed in the products, as illustrated in Figure 58.

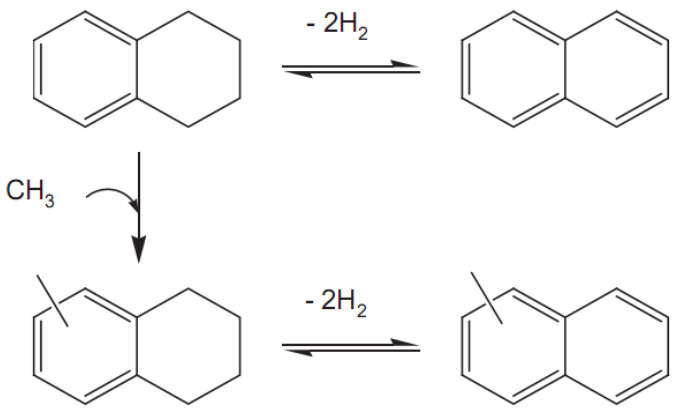

Figure 58. Alkylnaphthalene formation by methylation of tetralin

Accordingly, the ratio of methylnaphthalene-to-naphthalene represents the degree of transalkylation to tetralin. As shown in Figure 59, this ratio greatly increased with the addition of anisole since with pure tetralin, alkylation can only occur from cracking fragments. The significant increase observed during the sequential pulses (An → Tet) compared to pure tetralin supports the concept of the dissociative mechanism. It is conceivable that, while the separation time between the anisole and tetralin pulses

was very short (4 s), a significant fraction of the methyl group may leave the surface under the continuous flow of He; therefore, the degree of tetralin alkylation in the sequential pulse experiment (i.e. An → Tet) is always lower than that for the mixed pulses (i.e. An + Tet), in which the surface methyl groups can be consumed immediately, as also shown in Figure 59.

Interesting differences are observed when the results obtained on HY are compared to those obtained over an HZSM-5 zeolite of similar Si/Al ratio. When the sequential anisole/tetralin pulses were sent over the catalysts, the degree of tetralin alkylation (as measured by the alkylnaphthalene/naphthalene ratio) was almost identical for both HZSM-5 and HY. As discussed above, only the dissociative reaction pathway is operative in this case since anisole and tetralin are not simultaneously present over the catalysts. This reaction mode shows no significant differences between the two zeolites, with comparable number of acid sites. In contrast, in the mixed feed pulse experiments the extent of alkylation was much lower for HZSM-5 than for HY. Certainly, the differences in structure show a greater effect for the bimolecular path. The HZSM-5 zeolite has 10-membered ring aperture channels, with the diameter of 5.6 A , whereas HY has 12-membered ring aperture channels with the diameter of 7.4 A and much larger void spaces in the supercages [79]. The more open structure of HY is favorable for the bimolecular re-arrangements required for the non-dissociative path, which results in an extra contribution towards the alkylation rate via the non-dissociative bimolecular path. By contrast, it has been long recognized that the much more restrictive pores in HZSM-5 inhibit bimolecular encounters [178]. More recent molecular dynamics studies of aromatics in MFI structures support this concept [179].

Similarly, one can predict that tetralin and anisole can diffuse with significant hindrance into the small channel of HZSM-5 and, as a result, the bimolecular reactions would be inhibited, making the dissociative reaction pathway dominant.

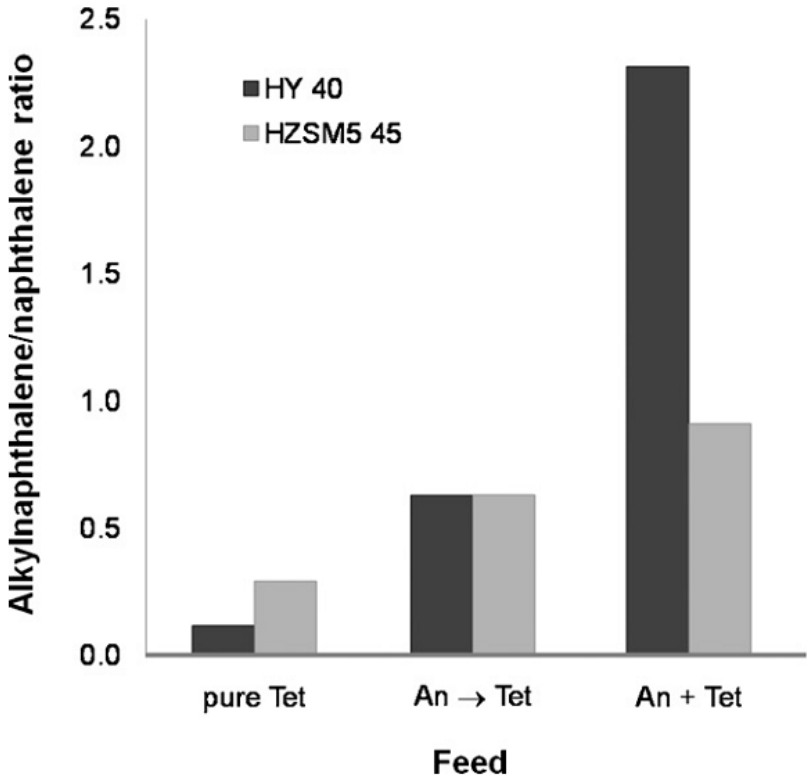

Figure 59. Alkylnapthalenes/naphthalene product ratio (at the 5th pulse) for pure tetralin and mixture feeds over the HY and HZSM5 zeolites in pulse experiment. Reaction conditions: T = 450 ^{o}C, P = 1 atm He. Pure Tet: pure tetralin, catalyst/feed ratio = 70 (g/g); An + Tet: mixture of anisole and tetralin (30 wt.% tetralin), catalyst/feed ratio = 70 (g/g tetralin); An → Tet: pulse tetralin right after anisole injection, catalyst/feed ratio = 70 (g/g tetralin) and 150 (g/g anisole).

5.3.4 Coke formation during reaction of pure anisole and mixtures

Table 11 compares the amount of C (wt.%) deposited on the HY zeolite during 3 h TOS from the different feed mixtures. The amounts deposited during this period from pure anisole and pure tetralin feeds are 11.8 and 3.0 wt.% C, respectively. Interestingly, the addition of tetralin to anisole results in a reduction in C deposits. The extent of this

reduction depends on the concentration of co-fed tetralin. That is, the amount of C deposits dropped from 11.8 to 8.8 and 6.0 wt.% C as the concentration of tetralin increased from 0% to 35% and 50%, respectively. It must be noted that, as shown in Table 11, the same trend is observed whether the amount of C deposits is compared to either the total amount of anisole or the total amount of feed passed over the catalyst.

Table 11. Comparison of amount of carbon deposited on spent catalysts from the reactions of different mixture feed over the HY zeolite. Reaction conditions: W/F = 0.42 h (wrt. anisole for co-feed reaction), T = 400 ^{o}C, P = 1 atm He. TOS = 3 h.

Feed	C (wt%)	$mg_C / g_{anisole}$	$mg_C / g_{total\ feed}$
Pure An	11.8	16.5	16.5
Pure Tet	3.0	-	4.1
An + Tet (50%)	6.0	8.4	4.2
An + Tet (35%)	8.8	12.3	8.0
An + n-C10	10.6	14.8	7.4
An + Bz	11.6	16.2	8.1
An + C3=	15.9	22.3	11.1

We rationalize the reduction in C deposits by an enhanced H-transfer, which as previously shown [166], inhibits coke formation that results in catalyst deactivation, in line with the higher stability shown in Figure 54 when tetralin is added to the feed. This concept is further supported by the almost insignificant effect on coke formation observed when other hydrocarbons with lower H-transfer capacity are used as co-feed. In fact, the amount of C deposited when incorporating n-decane and benzene to the anisole feed was about the same as that deposited when anisole was used as a pure feed. Moreover, when a coke-forming molecule such as propylene was used, the C deposits

increased to 15.9 wt.% C. That is, the trends in coke formation are consistent with the observed deactivation patterns (Figure 54).

To gain further insight about the nature of the coke deposits, the evolution of H_2O and CO_2 during the TPO of the coked catalysts was monitored and quantified in a mass spectrometer. The integrated intensity ratios between the H_2O and CO_2 signals are reported in Table 12. It is apparent that the reaction under pure anisole produced a coke richer in H compared to that obtained under either pure tetralin or the anisole/tetralin mixture. This difference suggests that, in the absence of tetralin, anisole adsorbs strongly on the HY zeolite and forms carbonaceous deposits with a much lower extent of dehydrogenation [75, 76]. So, the deactivation due to anisole can be described as a molecular condensation process on the active surface, rather than the typical formation of polyaromatic coke. By contrast, in the presence of tetralin, elimination of anisole and its surface derivatives from the surface is assisted via H-transfer from tetralin. The coke thus formed is primarily arising from tetralin and from those species, which cannot be eliminated from the surface via H-transfer. They become more dehydrogenated than the adsorbed anisole species, as suggested by the low H_2O/CO_2 ratio observed during TPO (Table 12).

Table 12. Amounts of carbon formed on the spent HY zeolite. Reaction conditions: W/F = 0.42 h (wrt. anisole for co-feed reaction), T = 400 ^{o}C, P = 1 atm He. TOS = 3 h.

Feed	C (wt%)	mg_C / $g_{total\ feed}$	$A(H_2O)/A(CO_2)$
Pure Tet	3.0	4.1	0.26
An + Tet (50%)	6.0	4.2	0.28
Pure An	11.8	16.5	0.56

5.3.5 Recovery of anisole conversion by flushing the spent catalysts with tetralin

Two additional experiments were conducted to shed further light on the role of tetralin in inhibiting deactivation by anisole (Figure 60). In the first experiment, a flow of pure anisole in He carrier was continuously fed for 2 h into the reactor at a W/F = 0.42 h and T = 400 ^{o}C. After stopping the flow of anisole (in He), pure tetralin (in He) was injected at the same W/F during 1 h. Finally, the feed of pure anisole (in He) was restarted at the same initial conditions. It is observed that during the first 2 h of reaction, the conversion of anisole dropped from ~80% to ~20%. However, after passing pure tetralin (in He) for 1 h, the anisole conversion was observed to recover to about 40%. After re-injection of the pure anisole feed, the catalyst started deactivating again. The partial recovery of the catalyst activity by passing tetralin suggests that at least some of the catalyst sites deactivated by anisole (or its derivatives) can be regenerated in the presence of tetralin. That is, unlike the typical deactivation by coke, the strong adsorption of aromatic oxygenated compounds (e.g. anisole and phenol) can be partially reversible by H-transfer from tetralin.

In the second experiment in this series, pure anisole (in He) was fed into the reactor for 2 h, under the same conditions as in the other sequence. However, in this case, after the first anisole reaction period, a 50/50 tetralin/anisole mixture was co-fed while the anisole conversion was being measured. As shown in Figure 60, a remarkable increase in anisole conversion that went from ~20% to ~100% was observed as a function of time on stream, exceeding even the initial conversion observed under pure anisole. In this case, the role of tetralin is not only helping remove fragments that

deactivate the surface, but also starting the non-dissociative bimolecular transalkylation, which is very significant on the open structure of HY zeolite.

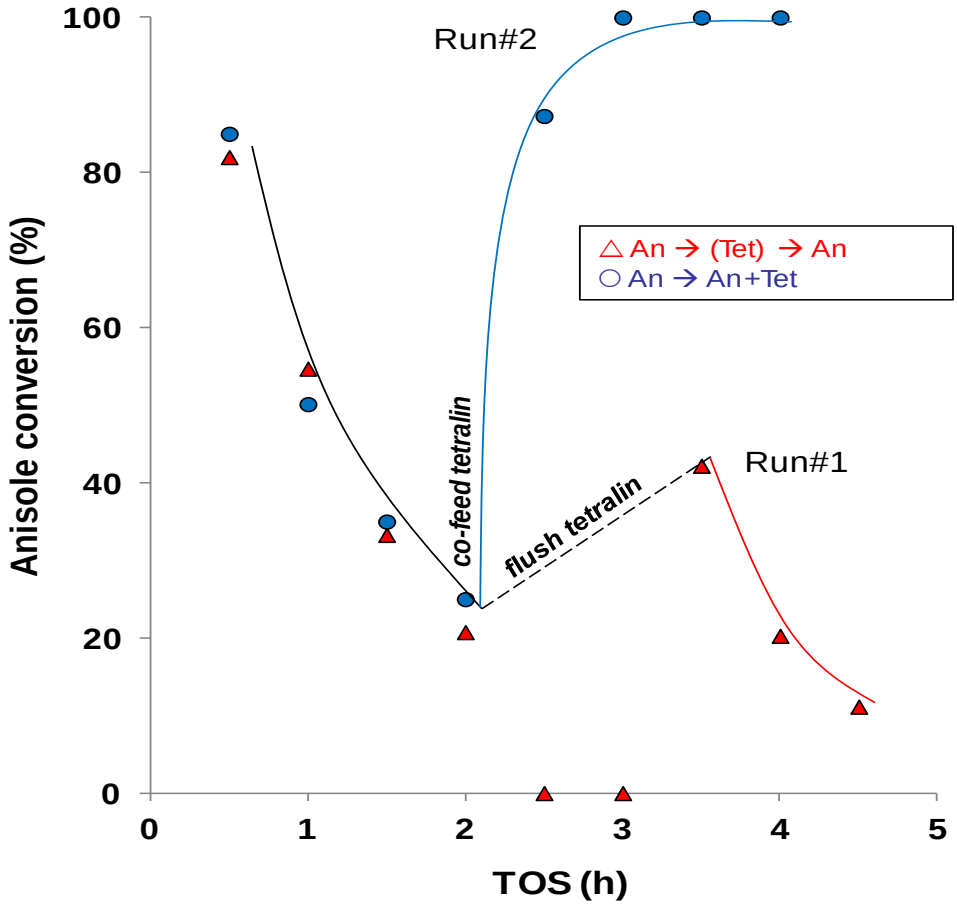

Figure 60. Effect of co-fed tetralin on anisole conversion over the HY zeolite. Reaction conditions: W/F = 0.42 h (wrt. anisole for co-feed reaction), co-feed concentration = ~50%, T = 400 ^{o}C, P = 1 atm He.

5.4 Summary

The conversion of anisole on HY zeolite produces phenol, cresols, xylenols and methylanisoles as main products during several transalkylation steps. Catalyst deactivation is significant under the reaction conditions and it is caused by strong adsorption of phenolic compounds and coke formation. The latter is an irreversible process, whereas the former is reversible and can be minimized by incorporation of molecules such as tetralin with high H-transfer capacity. Co-feeding tetralin or other H-donors has a beneficial effect on anisole conversion and reduces coke formation. Other hydrocarbons with a weaker H-transfer capacity have lower (e.g., n-decane), negligible (e.g., benzene), or even detrimental effect on activity (e.g., propylene).

Chapter 6: Conclusions and future directions

Fundamentals in the reaction of hydrocarbons, phenolic compounds and their mixture over zeolites at similar conditions to catalytic cracking process have been studied using the micropulse reaction system.

In m-cresol conversion, the zeolites capture the phenolic compounds significantly via molecular adsorption and condensation reaction forming the oligomeric phenolic species (i.e. phenolic pools), which are still active for reaction upon higher temperature to produce aromatics and light hydrocarbons. With increased reaction temperature, along with enhanced cracking to aromatics, the phenolic products were also captured less which caused less carbonaceous deposition. Small pore zeolite (i.e. HZSM-5) appears to be a better catalyst than HY in term of aromatic production and catalyst stability.

The catalytic activity of the HY zeolite is enhanced upon high temperature pretreatment due to the generation and synergism of LAS with the original BAS to form a new type of site (synergistic site) that displays enhanced activity for both, protolytic cracking and dehydrogenation reactions of paraffins. The activity enhancement caused by the synergistic sites is clearly evident for the monomolecular protolytic reaction, but it is not apparent in the conversion of olefins. Even though the synergistic sites were deactivated very quickly by strong adsorption of hydrocarbon species, but they could be regenerated by a subsequent high temperature treatment. Furthermore, the preference of reaction pathways depends on the activation entropy of the transition state for each path. With n-C6 feed, the enhancement for dehydrogenation is greater than for

protolytic cracking, but the opposite trend was observed in the conversion of 23DMB. Contribution of different reaction pathways of paraffin also depend on the reaction parameters, i.e. monomolecular reaction is more favored at high reaction temperature, at low paraffin concentration and low conversion, where olefinic product's concentration is low; while bimolecular hydride transfer reaction is more favored at high reaction temperature with high paraffin and olefinic product's concentration. Besides, the branched paraffin having tertiary carbons is also a better hydride donor than a linear one.

Co-feeding small amount of m-cresol caused severed deactivation to the synergistic sites, while slightly deactivated the reaction over normal BAS due to competitive adsorption at low reactant's concentration. Interestingly, when reactant's concentration was increased or a better hydride donor reactant was used, deactivation effect of m-cresol diminished. Enhanced hydride transfer from the paraffin at higher reactant's concentration was used to explain for the less deactivation. Co-feeding m-cresol also affected contribution of different reaction pathways of paraffins. Competitive adsorption deactivated protolytic cracking and protolytic dehydrogenation paths. While the phenolic pool formed by condensation of phenolic compounds acted as hydride acceptors that compete with hydride transfer between hydrocarbons. In reverse, hydride transfer from hydrocarbons also promoted desorption of the phenolic compounds, suppressed the formation of the phenolic pool which then resulted in less aromatic and coke formation.

Positive effect of hydride transfer to catalyst deactivation was confirmed in the reaction of anisole with tetralin, a good hydride donor agent. In anisole conversion,

catalyst deactivation is significant due to strong adsorption of phenolic compounds and coke formation. The latter is an irreversible process, whereas the former is reversible and can be minimized by incorporation of molecules such as tetralin with high H-transfer capacity. Co-feeding tetralin or other H-donors has a beneficial effect on anisole conversion and reduces coke formation. Other hydrocarbons with a weaker H-transfer capacity have lower (e.g., n-decane), negligible (e.g., benzene), or even detrimental effect on activity (e.g., propylene).

The formation and reaction of the phenolic pool during conversion of m-cresol over zeolites is an important results explaining for the aromatic production. This will be very valuable for fuels production when phenolic compounds are co-fed with hydrocarbon in the FCC process, especially at the condition where deactivation was inconsiderable. Therefore, further study in order to shed light into the structure of the phenolic pool will be an interesting research area. For instance, when the phenolic compounds having different functional group, such as methoxy, hydroxyl or aldehyde, were used, will the mechanism of the pool formation be similar? Will the structure of the phenolic pool be affected by the type of reactant or when there was hydride transfer from the hydrocarbons? And how does aromatic production depend on structure of the phenolic pool. Application of in-situ analysis techniques, such as FT-IR, will be very useful to study the structure of the phenolic pool during its formation and transformation at elevated temperatures.

References

[1] U.S., Energy Information Administration, International Energy Outlook 2010, (2010).

[2] U.S., Energy Information Administration, Annual Energy Outlook 2014, (2014).

[3] U.S., Energy Information Administration, International Energy Outlook 2013, (2013).

[4] R.H. Venderbosch, W. Prins, Biofuels, Bioproducts and Biorefining, 4 (2010) 178.

[5] B.V. Babu, Biofuels, Bioproducts and Biorefining, 2 (2008) 393.

[6] G.W. Huber, S. Iborra, A. Corma, Chem. Rev., 106 (2006) 4044.

[7] J.N. Chheda, G.W. Huber, J.A. Dumesic, Angew. Chem. Int. Ed., 46 (2007) 7164.

[8] S.K. Hoekman, Renewable Energy, 34 (2009) 14.

[9] Official Journal of the European Union, Directive 2009/29/EC, (2009).

[10] U.S. Congress, Energy Independence and Security Act of 2007, (2007) 1491.

[11] D.L. Klass, Chapter 2 - Biomass as an Energy Resource: Concept and Markets, in: D.L. Klass (Ed.) Biomass for Renewable Energy, Fuels, and Chemicals, Academic Press, San Diego, 1998, pp. 29.

[12] R.D. Perlack, in: Biomass as feedstock for a bioenergy and bioproducts industry the technical feasibility of a billion-ton annual supply, United States Department of Energy, United States Department of Agriculture, Oak Ridge National Laboratory, Oak Ridge, Tennessee, 2005.

[13] Q. Zhang, J. Chang, T. Wang, Y. Xu, Energy Convers. Manage., 48 (2007) 87.

[14] R.P. Anex, A. Aden, F.K. Kazi, J. Fortman, R.M. Swanson, M.M. Wright, J.A. Satrio, R.C. Brown, D.E. Daugaard, A. Platon, G. Kothandaraman, D.D. Hsu, A. Dutta, Fuel, 89, Supplement 1 (2010) S29.

[15] C.A. Mullen, A.A. Boateng, Energy Fuels, 22 (2008) 2104.

[16] W.T. Tsai, M.K. Lee, Y.M. Chang, Bioresour. Technol., 98 (2007) 22.

[17] S. Wan, T. Pham, S. Zhang, L. Lobban, D. Resasco, R. Mallinson, AlChE J., 59 (2013) 2275.

[18] A.V. Bridgwater, G.V.C. Peacocke, Renewable and Sustainable Energy Reviews, 4 (2000) 1.

[19] D.L. Klass, Chapter 8 - Thermal Conversion: Pyrolysis and Liquefaction, in: D.L. Klass (Ed.) Biomass for Renewable Energy, Fuels, and Chemicals, Academic Press, San Diego, 1998, pp. 225.

[20] D. Mohan, C.U. Pittman, P.H. Steele, Energy Fuels, 20 (2006) 848.

[21] P. Basu, Chapter 5 - Pyrolysis, in: P. Basu (Ed.) Biomass Gasification, Pyrolysis and Torrefaction (Second Edition), Academic Press, Boston, 2013, pp. 147.

[22] S. Czernik, A.V. Bridgwater, Energy Fuels, 18 (2004) 590.

[23] J.P. Diebold, Report No. NREL/SR-570-27613; National Renewable Energy Laboratory, (2000).

[24] C. Branca, P. Giudicianni, C. Di Blasi, Ind. Eng. Chem. Res., 42 (2003) 3190.

[25] P. Basu, Chapter 4 - Torrefaction, in: P. Basu (Ed.) Biomass Gasification, Pyrolysis and Torrefaction (Second Edition), Academic Press, Boston, 2013, pp. 87.

[26] M.J.C. van der Stelt, H. Gerhauser, J.H.A. Kiel, K.J. Ptasinski, Biomass Bioenergy, 35 (2011) 3748.

[27] J.J. Chew, V. Doshi, Renewable and Sustainable Energy Reviews, 15 (2011) 4212.

[28] M.J. Prins, K.J. Ptasinski, F.J.J.G. Janssen, J. Anal. Appl. Pyrolysis, 77 (2006) 35.

[29] H. Yang, R. Yan, H. Chen, D.H. Lee, C. Zheng, Fuel, 86 (2007) 1781.

[30] H. Yang, R. Yan, H. Chen, C. Zheng, D.H. Lee, D.T. Liang, Energy Fuels, 20 (2005) 388.

[31] R.J. Evans, T.A. Milne, Energy Fuels, 1 (1987) 123.

[32] R.J. Evans, T.A. Milne, M.N. Soltys, J. Anal. Appl. Pyrolysis, 9 (1986) 207.

[33] T.T. Pham, L.L. Lobban, D.E. Resasco, R.G. Mallinson, J. Catal., 266 (2009) 9.

[34] S. Sitthisa, T. Pham, T. Prasomsri, T. Sooknoi, R.G. Mallinson, D.E. Resasco, J. Catal., 280 (2011) 17.

[35] S. Sitthisa, W. An, D.E. Resasco, J. Catal., 284 (2011) 90.

[36] V.N. Bui, D. Laurenti, P. Afanasiev, C. Geantet, Appl. Catal., B: Environ., 101 (2011) 239.

[37] V.N. Bui, D. Laurenti, P. Delichère, C. Geantet, Appl. Catal., B: Environ., 101 (2011) 246.

[38] E. Furimsky, Appl. Catal., A: Gen., 199 (2000) 147.

[39] F. de Miguel Mercader, M.J. Groeneveld, S.R.A. Kersten, C. Geantet, G. Toussaint, N.W.J. Way, C.J. Schaverien, K.J.A. Hogendoorn, Energy & Environmental Science, 4 (2011) 985.

[40] N. Joshi, A. Lawal, Chem. Eng. Sci., 74 (2012) 1.

[41] X. Xu, C. Zhang, Y. Liu, Y. Zhai, R. Zhang, Chemosphere, 93 (2013) 652.

[42] F. de Miguel Mercader, M.J. Groeneveld, S.R.A. Kersten, N.W.J. Way, C.J. Schaverien, J.A. Hogendoorn, Appl. Catal., B: Environ., 96 (2010) 57.

[43] A. Gangadharan, M. Shen, T. Sooknoi, D.E. Resasco, R.G. Mallinson, Appl. Catal., A: Gen., 385 (2010) 80.

[44] T. Pham, D. Shi, D. Resasco, Top. Catal., 57 (2014) 706.

[45] T.N. Pham, T. Sooknoi, S.P. Crossley, D.E. Resasco, ACS Catal., 3 (2013) 2456.

[46] R.W. Snell, B.H. Shanks, ACS Catal., 3 (2013) 783.

[47] M. Vervecken, Y. Servotte, M. Wydoodt, L. Jacobs, J.A. Martens, P.A. Jacobs, Zeolite-Induced Selectivity in the Conversion of the Lower Aliphatic Carboxylic Acids, in: R. Setton (Ed.) Chemical Reactions in Organic and Inorganic Constrained Systems, Springer Netherlands, 1986, pp. 95.

[48] T.T. Pham, S.P. Crossley, T. Sooknoi, L.L. Lobban, D.E. Resasco, R.G. Mallinson, Appl. Catal., A: Gen., 379 (2010) 135.

[49] L. Nie, D.E. Resasco, Appl. Catal., A: Gen., 447–448 (2012) 14.

[50] A.G. Gayubo, A.T. Aguayo, A. Atutxa, R. Aguado, J. Bilbao, Ind. Eng. Chem. Res., 43 (2004) 2610.

[51] A.G. Gayubo, A.T. Aguayo, A. Atutxa, R. Aguado, M. Olazar, J. Bilbao, Ind. Eng. Chem. Res., 43 (2004) 2619.

[52] A.G. Gayubo, A.T. Aguayo, A. Atutxa, B. Valle, J. Bilbao, Journal of Chemical Technology & Biotechnology, 80 (2005) 1244.

[53] J.D. Adjaye, N.N. Bakhshi, Biomass Bioenergy, 8 (1995) 131.

[54] J.D. Adjaye, N.N. Bakhshi, Biomass Bioenergy, 8 (1995) 265.

[55] A.G. Gayubo, A.T. Aguayo, A. Atutxa, R. Prieto, J. Bilbao, Energy Fuels, 18 (2004) 1640.

[56] J.D. Adjaye, N.N. Bakhshi, Fuel Process. Technol., 45 (1995) 161.

[57] J.D. Adjaye, N.N. Bakhshi, Fuel Process. Technol., 45 (1995) 185.

[58] J.D. Adjaye, S.P.R. Katikaneni, N.N. Bakhshi, Fuel Process. Technol., 48 (1996) 115.

[59] G. Fogassy, N. Thegarid, G. Toussaint, A.C. van Veen, Y. Schuurman, C. Mirodatos, Appl. Catal., B: Environ., 96 (2010) 476.

[60] J. Chang, T. Danuthai, S. Dewiyanti, C. Wang, A. Borgna, ChemCatChem, 5 (2013) 3041.

[61] A.A. Lappas, S. Bezergianni, I.A. Vasalos, Catal. Today, 145 (2009) 55.

[62] T.L. Marker, in: Opportunities for Biorenewables in Oil Refineries, UOP LLC, 2005, pp. 60.

[63] I. Graça, F.R. Ribeiro, H.S. Cerqueira, Y.L. Lam, M.B.B. de Almeida, Appl. Catal., B: Environ., 90 (2009) 556.

[64] G.W. Huber, A. Corma, Angew. Chem. Int. Ed., 46 (2007) 7184.

[65] V.N. Bui, G. Toussaint, D. Laurenti, C. Mirodatos, C. Geantet, Catal. Today, 143 (2009) 172.

[66] A. Pinheiro, D. Hudebine, N. Dupassieux, C. Geantet, Energy Fuels, 23 (2009) 1007.

[67] J.G. Speight, B. Ozum, Petroleum refining processes, Marcel Dekker, Inc., 2002.

[68] R. Sadeghbeigi, Fluid catalytic cracking handbook, 2 ed., Gulf Professional Publishing, 1993.

[69] W.O. Haag, R.M. Dessau, "Proceedings, 8th International Congress on Catalysis, Berlin, 1984", Vol. 2 (1984) 305.

[70] J.S. Buchanan, J.G. Santiesteban, W.O. Haag, J. Catal., 158 (1996) 279.

[71] R.D. Cortright, J.A. Dumesic, R.J. Madon, Top. Catal., 4 (1997) 15.

[72] A. Corma, A.V. Orchillés, Microporous Mesoporous Mater., 35–36 (2000) 21.

[73] A. Humphries, D.H. Harris, P. O'Connor, Chapter 2 The Nature of Active Sites in Zeolites: Influence on Catalyst Performance, in: S.M. John, M.M. Maurice (Eds.) Stud. Surf. Sci. Catal., Elsevier, 1993, pp. 41.

[74] A. Corma, G.W. Huber, L. Sauvanaud, P. O'Connor, J. Catal., 247 (2007) 307.

[75] I. Graça, J.D. Comparot, S. Laforge, P. Magnoux, J.M. Lopes, M.F. Ribeiro, F.R. Ribeiro, Appl. Catal., A: Gen., 353 (2009) 123.

[76] I.s. Graça, J.-D. Comparot, S.b. Laforge, P. Magnoux, J.M. Lopes, M.F. Ribeiro, F. Ramôa Ribeiro, Energy Fuels, 23 (2009) 4224.

[77] I. Graça, A. Fernandes, J.M. Lopes, M.F. Ribeiro, S. Laforge, P. Magnoux, F. Ramôa Ribeiro, Appl. Catal., A: Gen., 385 (2010) 178.

[78] I. Graça, J.M. Lopes, M.F. Ribeiro, F. Ramôa Ribeiro, H.S. Cerqueira, M.B.B. de Almeida, Appl. Catal., B: Environ., 101 (2011) 613.

[79] R.T. Yang, Adsorbents: Fundamentals and Applications, John Wiley & Sons, Inc., USA, 2003.

[80] F.L. Raúl, Introduction to the Structural Chemistry of Zeolites, in: Handbook of Zeolite Science and Technology, CRC Press, 2003.

[81] R. Xavier, A.v.S. Rutger, Reaction Mechanisms in Zeolite Catalysis, in: Handbook of Zeolite Science and Technology, CRC Press, 2003.

[82] W.E. Farneth, R.J. Gorte, Chem. Rev., 95 (1995) 615.

[83] A. Corma, P.J. Miguel, A.V. Orchilles, J. Catal., 145 (1994) 171.

[84] S. Kotrel, H. Knözinger, B.C. Gates, Microporous Mesoporous Mater., 35–36 (2000) 11.

[85] W.O. Haag, R.M. Dessau, R.M. Lago, Kinetics and Mechanism of Paraffin Cracking with Zeolite Catalysts, in: S.N. Tomoyuki lnui, T. Takashi (Eds.) Stud. Surf. Sci. Catal., Elsevier, 1991, pp. 255.

[86] D.H. Olson, W.O. Haag, R.M. Lago, J. Catal., 61 (1980) 390.

[87] W.O. Haag, R.M. Lago, P.B. Weisz, Nature (London), 309 (1984) 589.

[88] Y. Sendoda, Y. Ono, Zeolites, 8 (1988) 101.

[89] K.A. Al-majnouni, J.H. Yun, R.F. Lobo, ChemCatChem, 3 (2011) 1333.

[90] J.H. Yun, Structure and reactivity of dehydroxylated Brønsted acid sites in H-ZSM-5 zeolite: Generation of stable organic radical cation and catalytic activity for isobutane conversion, MS Thesis, University of Delaware, 2011.

[91] J.A. van Bokhoven, M. Tromp, D.C. Koningsberger, J.T. Miller, J.A.Z. Pieterse, J.A. Lercher, B.A. Williams, H.H. Kung, J. Catal., 202 (2001) 129.

[92] S.M. Babitz, B.A. Williams, J.T. Miller, R.Q. Snurr, W.O. Haag, H.H. Kung, Appl. Catal., A: Gen., 179 (1999) 71.

[93] C. Mirodatos, D. Barthomeuf, J. Chem. Soc., Chem. Commun., 0 (1981) 39.

[94] R.M. Lago, W.O. Haag, R.J. Mikovsky, D.H. Olson, S.D. Hellring, K.D. Schmitt, G.T. Kerr, The Nature of the Catalytic Sites in HZSM-5- Activity Enhancement, in: A.I. Y. Murakami, J.W. Ward (Eds.) Stud. Surf. Sci. Catal., Elsevier, 1986, pp. 677.

[95] R.A. Beyerlein, G.B. McVicker, L.N. Yacullo, J.J. Ziemiak, The Journal of Physical Chemistry, 92 (1988) 1967.

[96] N.O. Gonzales, A.T. Bell, A.K. Chakraborty, The Journal of Physical Chemistry B, 101 (1997) 10058.

[97] S. Li, A. Zheng, Y. Su, H. Zhang, L. Chen, J. Yang, C. Ye, F. Deng, J. Am. Chem. Soc., 129 (2007) 11161.

[98] D. Freude, T. Fröhlich, H. Pfeifer, G. Scheler, Zeolites, 3 (1983) 171.

[99] V.B. Kazansky, Catal. Today, 3 (1988) 367.

[100] C. Pereira, R.J. Gorte, Appl. Catal., A: Gen., 90 (1992) 145.

[101] A.I. Biaglow, D.J. Parrillo, R.J. Gorte, J. Catal., 144 (1993) 193.

[102] J. Engelhardt, W.K. Hall, J. Catal., 151 (1995) 1.

[103] H.G. Karge, E. Boldingh, Catal. Today, 3 (1988) 379.

[104] J.P. Lange, A. Gutsze, H.G. Karge, J. Catal., 114 (1988) 136.

[105] A. Corma, P.J. Miguel, A.V. Orchilles, J. Catal., 145 (1994) 171.

[106] T.F. Narbeshuber, A. Brait, K. Seshan, J.A. Lercher, Appl. Catal., A: Gen., 146 (1996) 119.

[107] T.F. Narbeshuber, A. Brait, K. Seshan, J.A. Lercher, J. Catal., 172 (1997) 127.

[108] M.H.W. Sonnemans, C. Den Heijer, M. Crocker, The Journal of Physical Chemistry, 97 (1993) 440.

[109] R.D. Shannon, K.H. Gardner, R.H. Staley, G. Bergeret, P. Gallezot, A. Auroux, The Journal of Physical Chemistry, 89 (1985) 4778.

[110] V.B. Kazansky, M.V. Frash, R.A. van Santen, Appl. Catal., A: Gen., 146 (1996) 225.

[111] J. Abbot, B.W. Wojciechowski, J. Catal., 113 (1988) 353.

[112] J. Abbot, B.W. Wojclechowski, The Canadian Journal of Chemical Engineering, 66 (1988) 825.

[113] J. Abbot, B.W. Wojciechowski, J. Catal., 115 (1989) 1.

[114] M.V. Frash, R.A. van Santen, Top. Catal., 9 (1999) 191.

[115] S. Mallikarjun Sharada, P.M. Zimmerman, A.T. Bell, M. Head-Gordon, The Journal of Physical Chemistry C, (2013).

[116] S.J. Collins, P.J. O'Malley, Chem. Phys. Lett., 246 (1995) 555.

[117] I. Milas, M.A.C. Nascimento, Chem. Phys. Lett., 373 (2003) 379.

[118] I. Milas, M.A. Chaer Nascimento, Chem. Phys. Lett., 418 (2006) 368.

[119] R. Gounder, E. Iglesia, J. Am. Chem. Soc., 131 (2009) 1958.

[120] R. Gounder, E. Iglesia, Angew. Chem. Int. Ed., 49 (2010) 808.

[121] R. Gounder, A.J. Jones, R.T. Carr, E. Iglesia, J. Catal., 286 (2012) 214.

[122] Y. Ono, K. Kanae, J. Chem. Soc., Faraday Trans., 87 (1991) 663.

[123] H. Krannila, W.O. Haag, B.C. Gates, J. Catal., 135 (1992) 115.

[124] D.E. Resasco, S. Crossley, AlChE J., 55 (2009) 1082.

[125] M.C. Samolada, A. Papafotica, I.A. Vasalos, Energy Fuels, 14 (2000) 1161.

[126] P.T. Williams, N. Nugranad, Energy, 25 (2000) 493.

[127] T.S. Nguyen, M. Zabeti, L. Lefferts, G. Brem, K. Seshan, Biomass Bioenergy, 48 (2013) 100.

[128] P.T. Williams, P.A. Horne, Fuel, 74 (1995) 1839.

[129] P.M. Mortensen, J.D. Grunwaldt, P.A. Jensen, K.G. Knudsen, A.D. Jensen, Appl. Catal., A: Gen., 407 (2011) 1.

[130] J. Jae, G.A. Tompsett, A.J. Foster, K.D. Hammond, S.M. Auerbach, R.F. Lobo, G.W. Huber, J. Catal., 279 (2011) 257.

[131] P.D. Chantal, S. Kaliaguine, J.L. Grandmaison, Appl. Catal., 18 (1985) 133.

[132] X. Zhu, R.G. Mallinson, D.E. Resasco, Appl. Catal., A: Gen., 379 (2010) 172.

[133] A. Ausavasukhi, Y. Huang, A.T. To, T. Sooknoi, D.E. Resasco, J. Catal., 290 (2012) 90.

[134] F.E. Imbert, N. Gnep, M. Guisnet, J. Catal., 172 (1997) 307.

[135] F.E. Imbert, S. Gnep, M. Guisnet, Catal. Lett., 49 (1997) 121.

[136] P. Beltrame, P.L. Beltrame, P. Carniti, L. Forni, G. Zuretti, Zeolites, 5 (1985) 400.

[137] C.L. Thomas, J. Hoekstra, J.T. Pinkston, J. Am. Chem. Soc., 66 (1944) 1694.

[138] R.F.d. SANTOS, E.A. URQUIETA-GONZÁLEZ, Brazilian Journal of Chemical Engineering, 15 (1998).

[139] Y.X. Zhao, G.R. Bamwenda, W.A. Groten, B.W. Wojciechowski, J. Catal., 140 (1993) 243.

[140] S. Al-Khattaf, Energy Fuels, 20 (2006) 946.

[141] Y.-T. Cheng, G.W. Huber, ACS Catal., 1 (2011) 611.

[142] M. Guisnet, P. Magnoux, C. Canaff, Formation and Nature of Coke Deposits on Zeolites HY and HZSM-5, in: A.I. Y. Murakami, J.W. Ward (Eds.) Stud. Surf. Sci. Catal., Elsevier, 1986, pp. 701.

[143] W. Wang, Y. Jiang, M. Hunger, Catal. Today, 113 (2006) 102.

[144] S. Ilias, A. Bhan, ACS Catal., 3 (2012) 18.

[145] S. Ilias, A. Bhan, J. Catal., 290 (2012) 186.

[146] G.V. Echevskii, K.G. Ione, G.N. Nosyreva, G.S. Litvak, Appl. Catal., 43 (1988) 85.

[147] T.R. Carlson, J. Jae, G.W. Huber, ChemCatChem, 1 (2009) 107.

[148] S.E. Shull, A.N. Hixson, Industrial & Engineering Chemistry Process Design and Development, 5 (1966) 146.

[149] T. Doumani, Ind. Eng. Chem., 50 (1958) 1677.

[150] J. Haber, E. Zienkiewicz, Appl. Catal., 10 (1984) 267.

[151] Y. Xiong, P.G. Rodewald, C.D. Chang, J. Am. Chem. Soc., 117 (1995) 9427.

[152] F. Chen, G. Coudurier, C. Naccache, The Formation of Toluene Disproportionation Intermediates on Zeolite Catalysts, in: P.A. Jacobs, R.A.v. Santen (Eds.) Stud. Surf. Sci. Catal., Elsevier, 1989, pp. 1387.

[153] M. Guisnet, N.S. Gnep, S. Morin, Microporous Mesoporous Mater., 35–36 (2000) 47.

[154] A. Iliyas, S. Al-Khattaf, Appl. Catal., A: Gen., 269 (2004) 225.

[155] M. Guisnet, P. Magnoux, Appl. Catal., 54 (1989) 1.

[156] M. Guisnet, P. Magnoux, D. Martin, Roles of acidity and pore structure in the deactivation of zeolites by carbonaceous deposits, in: C.H. Bartholomew, G.A. Fuentes (Eds.) Stud. Surf. Sci. Catal., Elsevier, 1997, pp. 1.

[157] F.E. Imbert, M. Guisnet, S. Gnep, J. Catal., 195 (2000) 279.

[158] E. Antonakou, A. Lappas, M.H. Nilsen, A. Bouzga, M. Stöcker, Fuel, 85 (2006) 2202.

[159] A. Oasmaa, S. Czernik, Energy Fuels, 13 (1999) 914.

[160] A.V. Bridgwater, Chem. Eng. J., 91 (2003) 87.

[161] D. Meier, A. Oasmaa, G.V.C. Peacocke, Properties of Fast Pyrolysis Liquids: Status of Test Methods, in: A.V. Bridgwater, D.G.B. Boocock (Eds.) Developments in Thermochemical Biomass Conversion, Springer Netherlands, 1997, pp. 391.

[162] T. Prasomsri, A.T. To, S. Crossley, W.E. Alvarez, D.E. Resasco, Appl. Catal., B: Environ., 106 (2011) 204.

[163] J. Abbot, J. Catal., 126 (1990) 628.

[164] P.V. Shertukde, G. Marcelin, G.A. Sill, W. Keith Hall, J. Catal., 136 (1992) 446.

[165] F.C. Jentoft, B.C. Gates, Top. Catal., 4 (1997) 1.

[166] K.A. Cumming, B.W. Wojciechowski, Catalysis Reviews, 38 (1996) 101.

[167] A. Corma, V. González-Alfaro, A.V. Orchillés, Appl. Catal., A: Gen., 187 (1999) 245.

[168] A.F.H. Wielers, M. Vaarkamp, M.F.M. Post, J. Catal., 127 (1991) 51.

[169] Y.X. Zhao, B.W. Wojciechowski, J. Catal., 142 (1993) 499.

[170] M. Guisnet, P. Magnoux, Appl. Catal., A: Gen., 212 (2001) 83.

[171] T. Prasomsri, R.E. Galiasso Tailleur, W.E. Alvarez, T. Sooknoi, D.E. Resasco, Appl. Catal., A: Gen., 389 (2010) 140.

[172] B.J.M. de Vries, D.P. van Vuuren, M.M. Hoogwijk, Energy Policy, 35 (2007) 2590.

[173] F. McGowan, Energy Policy, 19 (1991) 110.

[174] A. Corma, J. Catal., 216 (2003) 298.

[175] P.A. Horne, P.T. Williams, Renewable Energy, 7 (1996) 131.

[176] B.E. Langner, Industrial & Engineering Chemistry Process Design and Development, 20 (1981) 326.

[177] G.F. Froment, J.D. Meyer, E.G. Derouane, J. Catal., 124 (1990) 391.

[178] J. Kärger, M. Petzold, H. Pfeifer, S. Ernst, J. Weitkamp, J. Catal., 136 (1992) 283.

[179] R. Rungsirisakun, T. Nanok, M. Probst, J. Limtrakul, J. Mol. Graphics Modell., 24 (2006) 373.